AFML-TR-71-70

AD 725761

MECHANICS OF BRITTLE MATERIALS UNDER LINEAR TEMPERATURE INCREASES

H. NEUBER

A. WIMMER

INSTITUT FUR TECHNISCHE MECHANIK

TECHNISCHE UNIVERSITAT

MUNICH, W. GERMANY

TECHNICAL REPORT AFML-TR-71-70

APRIL 1971

D D C
RECEIVED
MAR 23 1971
B

This document has been approved for public release and sale; its distribution is unlimited.

Reproduced by
NATIONAL TECHNICAL
INFORMATION SERVICE
Springfield, Va. 22151

AIR FORCE MATERIALS LABORATORY
AIR FORCE SYSTEMS COMMAND
WRIGHT-PATTERSON AIR FORCE BASE, OHIO

DISCLAIMER NOTICE

THIS DOCUMENT IS BEST QUALITY PRACTICABLE. THE COPY FURNISHED TO DTIC CONTAINED A SIGNIFICANT NUMBER OF PAGES WHICH DO NOT REPRODUCE LEGIBLY.

NOTICE

When Government drawings, specifications, or other data are used for any purpose other than in connection with a definitely related Government procurement operation, the United States Government thereby incurs no responsibility nor any obligation whatsoever; and the fact that the government may have formulated, furnished, or in any way supplied the said drawings, specifications, or other data, is not to be regarded by implication or otherwise as in any manner licensing the holder or any other person or corporation, or conveying any rights or permission to manufacture, use, or sell any patented invention that may in any way be related thereto.

ACCESSION for

CFSTI WHITE SECTION ☐

DDC BUFF SECTION ☐

UNANNOUNCED ☐

JUSTIFICATION .....

BY .....

DISTRIBUTION/AVAILABILITY CODES

DIST.	AVAIL. and/or SPECIAL	
A		

Copies of this report should not be returned unless return is required by security considerations, contractual obligations, or notice on a specific document.

300-June 1971-CO305-40-71-676

AFML-TR-71-70

MECHANICS OF BRITTLE MATERIALS UNDER LINEAR TEMPERATURE INCREASES

H. NEUBER
A. WIMMER

This document has been approved for public release
and sale; its distribution is unlimited.

FOREWORD

The research described in this report was performed by the Institut fur Technische Mechanik, Technische Universitat Munchen, Germany under USAF Contract AF 61 (052) -875. The contract was initiated under Project No. 7350 "Refractory Inorganic Nonmetallic Materials," Task No. 735005, "Theory and Mechanical Phenomena." The work was technically administered by the Air Force Materials Laboratory, Air Force Systems Command, Wright-Patterson Air Force Base, Ohio, with Dr. A.J. Herzog and Mr. James W. Poynter acting as Project Engineers.

This report summarizes the results of research conducted between 1 October 1966 and 31 October 1969. The results of a related aspect of this overall program are reported in AFML-TR-68-23 dated March 1968. The manuscript of this report was released by the authors in September 1970 for publication as a technical report.

The authors wish to express their thanks to Dr. A.J. Herzog (now retired) and Mr. W.J. Trapp of the Air Force Materials Laboratory as well as to the officers of the European Office of Aerospace Research in Brussels for their cooperation. The advice and suggestions of Dr. Hahn and Dr. Heckel from the Institut fur Technische Mechanik, Technische Universitat Munchen, are greatly appreciated.

This report has been reviewed and is approved.

C.T. Lynch

C.T. LYNCH
Chief, Advanced Metallurgical Studies Br.
Metals and Ceramics Division
Air Force Materials Laboratory

UNCLASSIFIED
Security Classification

DOCUMENT CONTROL DATA - R&D

(Security classification of title, body of abstract and indexing annotation must be entered when the overall report is classified)

1 ORIGINATING ACTIVITY *(Corporate author)*
Institut fur Technische Mechanik
Technische Universitat
Munich, W. Germany

2a REPORT SECURITY CLASSIFICATION
Unclassified

2b GROUP

3 REPORT TITLE
Mechanics of Brittle Materials Under Linear Temperature Increases.

4 DESCRIPTIVE NOTES *(Type of report and inclusive dates)*

5. AUTHOR(S)
H. Neuber and A. Wimmer

6. REPORT DATE
Apr 1971

7a. TOTAL NO. OF PAGES
115

7b. NO. OF REFS
14

8a CONTRACT OR GRANT NO.
AF6(052)-875

b. PROJECT NO. 7350

c. Task 735005

d.

9a. ORIGINATOR'S REPORT NUMBER(S)

9b. OTHER REPORT NO(S) *(Any other numbers that may be assigned this report)*
AFML-TR-71-70

10. AVAILABILITY/LIMITATION NOTICES
This document has been approved for public release and sale; its distribution is unlimited.

11. SUPPLEMENTARY NOTES

12. SPONSORING MILITARY ACTIVITY
Air Force Materials Laboratory (LLS)
Air Force Systems Command
Wright-Patterson AFB OH 45433

13. ABSTRACT

~~This~~ results of work done to show the effects of surface roughness, residual stresses, strain rate, microstructure, alternating bending fatigue loading and a non-uniform stress field on the strength of small (2.-8.mm diameter) alumina rods are given. The rods used in the work were characterized by determinations of grain size, porosity, hardness, surface roughness and damping factor. Static bend tests at room temperature are used to determine the Young's modulus, the fracture stress, and the strain at fracture and to show the influence of specimen volume on the fracture stress. The effects of grain size and of porosity on these characteristics are shown. A new tensile test specimen is designed which achieves an almost uniform stress field in the test area. Some test results are given to show the validity of this procedure for brittle specimens.

DD FORM 1 JAN 64 1473

Unclassified
Security Classification

UNCLASSIFIED
Security Classification

14. KEY WORDS	LINK A ROLE	LINK A WT	LINK B ROLE	LINK B WT	LINK C ROLE	LINK C WT
Mechanical Properties - Alumina						
New Design Tensile Test Specimen						
Microstructure - Alumina						
Porosity - Property Relationships						
Residual Stresses in Alumina Rods						
Damping Characteristics - Alumina						

INSTRUCTIONS

1. ORIGINATING ACTIVITY. Enter the name and address of the contractor, subcontractor, grantee, Department of Defense activity or other organization *(corporate author)* issuing the report.

2a. REPORT SECURITY CLASSIFICATION: Enter the overall security classification of the report. Indicate whether "Restricted Data" is included. Marking is to be in accordance with approoriate security regulations.

2b. GROUP: Automatic downgrading is specified in DoD Directive 5200.10 and Armed Forces Industrial Manual. Enter the group number. Also, when applicable, show that optional markings have been used for Group 3 and Group 4 as authorized.

3. REPORT TITLE: Enter the complete report title in all capital letters. Titles in all cases should be unclassified. If a meaningful title cannot be selected without classification, show title classification in all capitals in parenthesis immediately following the title.

4. DESCRIPTIVE NOTES: If appropriate, enter the type of report, e.g., interim, progress, summary, annual, or final. Give the inclusive dates when a specific reporting period is covered.

5. AUTHOR(S): Enter the name(s) of author(s) as shown on or in the report. Enter last name, first name, middle initial. If military, show rank and branch of service. The name of the principal author is an absolute minimum requirement.

6. REPORT DATE: Enter the date of the report as day, month, year, or month, year. If more than one date appears on the report, use date of publication.

7a TOTAL NUMBER OF PAGES: The total page count should follow normal pagination procedures, i.e., enter the number of pages containing information.

7b NUMBER OF REFERENCES: Enter the total number of references cited in the report.

8a. CONTRACT OR GRANT NUMBER. If appropriate, enter the applicable number of the contract or grant under which the report was written.

8b, 8c, & 8d. PROJECT NUMBER: Enter the appropriate military department identification, such as project number, subproject number, system numbers, task number, etc.

9a. ORIGINATOR'S REPORT NUMBER(S) Enter the official report number by which the document will be identified and controlled by the originating activity. This number must be unique to this report.

9b OTHER REPORT NUMBER(S): If the report has been assigned any other report numbers *(either by the originator or by the sponsor)*, also enter this number(s).

10. AVAILABILITY/LIMITATION NOTICES: Enter any limitations on further dissemination of the report, other than those imposed by security classification, using standard statements such as:

(1) "Qualified requesters may obtain copies of this report from DDC."

(2) "Foreign announcement and dissemination of this report by DDC is not authorized."

(3) "U. S. Government agencies may obtain copies of this report directly from DDC. Other qualified DDC users shall request through _____."

(4) "U. S. military agencies may obtain copies of this report directly from DDC. Other qualified users shall request through _____."

(5) "All distribution of this report is controlled. Qualified DDC users shall request through _____."

If the report has been furnished to the Office of Technical Services, Department of Commerce, for sale to the public, indicate this fact and enter the price, if known.

11. SUPPLEMENTARY NOTES: Use for additional explanatory notes.

12. SPONSORING MILITARY ACTIVITY: Enter the name of the departmental project office or laboratory sponsoring *(paying for)* the research and development. Include address.

13. ABSTRACT: Enter an abstract giving a brief and factual summary of the document indicative of the report, even though it may also appear elsewhere in the body of the technical report. If additional space is required, a continuation sheet shall be attached.

It is highly desirable that the abstract of classified reports be unclassified. Each paragraph of the abstract shall end with an indication of the military security classification of the information in the paragraph, represented as *(TS)*, *(S)*, *(C)*, or *(U)*.

There is no limitation on the length of the abstract. However, the suggested length is from 150 to 225 words.

14 KEY WORDS: Key words are technically meaningful terms or short phrases that characterize a report and may be used as index entries for cataloging the report. Key words must be selected so that no security classification is required. Identifiers, such as equipment model designation, trade name, military project code name, geographic location, may be used as key words but will be followed by an indication of technical context. The assignment of links, rules, and weights is optional.

ABSTRACT

The results of work done to show the effects of surface roughness, residual stresses, strain rate, microstructure, alternating bending fatigue loading and a non-uniform stress field on the strength of small (2.-8.mm diameter) alumina rods are given. The rods used in the work were characterized by determinations of grain size, porosity, hardness, surface roughness and damping factor. Static bend tests at room temperature are used to determine the Young's modulus, the fracture stress, and the strain at fracture and to show the influence of specimen volume on the fracture stress. The effects of grain size and of porosity on these characteristics are shown. A new tensile test specimen is designed which achieves an almost uniform stress field in the test area. Some test results are given to show the validity of this procedure for brittle specimens.

TABLE OF CONTENTS

		Page No.
1.	Introduction	1
2.	Experimental Investigation of Alumina	2
2.1.	Test Material	2
2.1.1.	Chemical Analysis	2
2.1.2.	Grain Size and Porosity	5
2.1.3.	Surface Roughness	8
2.1.4.	Hardness	9
2.1.5.	Damping	11
2.2.	Performance of Strength Tests	12
2.2.1.	Influence of the Surface Roughness on the Fracture Stress, Young's Modulus and the Fracture Strain of Alumina	12
2.2.2.	Residual Stresses in Alumina Rods	13
2.2.3.	Influence of the Loading Speed on the Fracture Stress, Young's Modulus and the Fracture Strain of Alumina	15
2.2.4.	Alternating Bending Fatigue Tests	16
2.2.5.	Dependency of Fracture Stress, Young's Modulus and Fracture Strain from Grain Size and Porosity	20
2.2.6.	Influence of the Specimen Volume and the Stress Distribution on the Fracture Stress of Alumina at Various Grain Sizes and Porosities	23
2.2.7.	Tension Tests	30
3.	References	33
4.	Tables and Illustrations	35

LIST OF TABLES

Table		Page
1	Chemical analysis of Degussit Al 23, Al 23 PT, Degussit Al 24 and Degussit test substance 2461	35
2	Distribution of the grainsize and the porosity over the length of Alumina rods	36
3	Dependency of the "Rauhtiefe" R_t, "Glättungstiefe" R_p and the Center-Line-Average CLA from the grainsize and the porosity of Degussit Al_2O_3 round bar specimens	39
4	Dependency of the Vickers-micro-hardness from the grainsize and the porosity of 4 mm Ø Degussit Al_2O_3 round bar specimens	40
5	Vickers-micro-hardness measurements on single grains of different sizes. Determined on a Wesgo Al 995 rod 6 mm Ø, porosity p = 3.70%	41
6	Variation of the damping factor of 4 mm Ø Degussit Al_2O_3 specimens with the porosity and the grainsize	42
7	Dependency of the fracture stress, Young's modulus and the fracture strain from the surface condition of 6 mm Ø Degussit Al_2O_3 specimens determined from a bending test at room temperature	43
8	Residual stresses of a 6 mm Ø Wesgo Al 995 specimen, grainsize G = 17.2 μm porosity p = 3.99%	44
9	Residual stresses of a 6 mm Ø Wesgo Al 995 specimen, grainsize G = 16.5 μm porosity p = 4.08%	45

List of Tables (Continuation)

Table		Page
10	Residual stresses of a 6 mm Ø Wesgo Al 995 specimen, grainsize G = 16.4 μm porosity p = 4.09%	46
11	Dependency of the fracture stress, Young's modulus and the strain at fracture from the strain rate of 6 mm Ø Wesgo Al 995 specimens at room temperature determined from a bending test	47
12	Dependency of the fracture stress of 5 mm Ø smooth Wesgo Al 995 specimens from the numbers of cycles to fracture determined from alternating bend fatigue tests at room temperature	49
13	Dependency of the fracture stress of notched round bar Wesgo Al 995 specimens (nominal diameter 5 mm) from the numbers of cycles to fracture determined from alternating bend fatigue tests at room temperature	50
14	Dependency of the fracture stress of 5 mm Ø smooth Degussit Al 23 specimens from the numbers of cycles to fracture determined from alternating bend fatigue tests at room temperature	51
15	Dependency of the fracture stress of notched round bar Degussit Al 23 specimens (nominal diameter 5 mm) from the numbers of cycles to fracture determined from alternating bend fatigue tests at room temperature	52
16	Dependency of the fracture stress, Young's modulus and the fracture strain from the porosity and grainsize of 4 mm Ø Degussit Al_2O_3 specimens determined from a bending test at room temperature	53

List of Tables (Continuation)

Table		Page
17	Dependency of the fracture stress from the specimen volume, the porosity and the grainsize, determined from a bending test at room temperature	63
18	Dependency of the exponent $\frac{1}{m}$ from the porosity and grainsize, determined at room temperature	75

List of Figures

Fig.		Page
1	Polished and etched Alumina specimens	77
2	Distribution of the grainsize and the porosity of the round bar Alumina specimens delivered by Degussa	78
3	Distribution of the porosity and the grainsize over the length of a 4 mm diameter Degussit Al 23 specimen	79
4	Distribution of the porosity and the grainsize over the length of a 4 mm diameter Degussit Al 23 PT specimen	80
5	Distribution of the porosity and the grainsize over the length of a 4 mm diameter Degussit Al 24 specimen	81
6	Distribution of the porosity and the grainsize over the length of a 6 mm diameter Wesgo Al 995 specimen	82
7	Dependency of the poresize and pore-distance from the porosity at constant grainsize $G \sim 6.1\,\mu m$	83
8	Dependency of the poresize and pore-distance from the grainsize at constant porosity $p \sim 5.6\%$	84
9	Dependency of the "Rauhtiefe" R_t, "Glättungstiefe" R_p and the Center-Line-Average CLA from the grainsize and the porosity of 4 mm diameter Degussit Al_2O_3 specimens	85
10	Dependency of the Vickers-micro-hardness on the grainsize and the porosity of 4 mm Ø Degussit Al_2O_3 round bar specimens	86
11	Dependency of the Vickers-hardness from the size of single grains of a Wesgo Al 995 rod 6 mm Ø, porosity 3.7%	87

List of Figures (Continuation)

Fig.		Page
12	Vickers-impression on an Alumina specimen. Pressure of the diamond pyramid 94 p. Magnification 1400 x	87
13	Broken pieces of an Alumina rod photographed shortly after a bending test with a Hitachi high speed motion camera	88
14	Förster elastomat for the determination of the damping constant δ	88
15	Variation of the damping factor of 4 mm diameter Degussit Al_2O_3 specimens with the porosity and the grainsize	89
16	Bending test equipment for the determination of the fracture stress, Young's modulus and the fracture strain of Alumina at room temperature	90
17	Dependency of the fracture stress, Young's modulus and the fracture strain from the Rauhtiefe R_t of 6 mm diameter Degussit Al_2O_3 specimens determined from a bending test	91
18	Dependency of the fracture stress, Young's modulus and the fracture strain from the Glättungstiefe R_p of a 6 mm diameter Degussit Al_2O_3 specimens determined from a bending test	92
19	Dependency of the fracture stress, Young's modulus and the fracture strain from the Center-Line-Average CLA of 6 mm diameter Degussit Al_2O_3 specimens determined from a bending test	93
20	Measuring equipment for the determination of the residual stresses on 6 mm diameter Wesgo Al 995 specimens	94

List of Figures (Continuation

Fig.		Page
21	Strains ε plotted versus the remaining area received from the grinding off process of a 6 mm diameter Wesgo Al 995 specimen and distribution of the residual stress over the cross-section determined from the above diagram	95
22	Strains ε plotted versus the remaining area received from the grinding off process of a 6 mm diameter Wesgo Al 995 specimen and distribution of the residual stress over the cross-section determined from the above diagram	96
23	Strains ε plotted versus the remaining area received from the grinding off process of a 6 mm diameter Wesgo Al 995 specimen and distribution of the residual stress over the cross-section determined from the above diagram	97
24	Test equipment for the determination of the influence of the loading speed on the fracture stress, Young's modulus and the strain at fracture	98
25	Bending test equipment for the determination of the influence of the loading speed on the fracture stress, Young's modulus and the strain of fracture	99
26	Photographs of a bending test taken on Tektronix cathode ray oscillographs. Crosshead speed of the Zwick electronic tension test machine 600 mm/minute.	100
27	Dependency of the fracture stress, Young's modulus and the strain at fracture from the strain rate of 6 mm diameter Wesgo Al 995 specimens determined from a bending test at room temperature	101

List of Figures (Continuation)

Fig.		Page
28	Degussit Al_2O_3 specimen for alternating bend fatigue tests	102
29	Schenck-Webi fatigue test machine and Tektronix cathode ray odcilloscope	102
30	Scheme of the Schenck-Webi test machine	103
31	Clamping device for alternating bend fatigue tests	104
32	Vibration of a specimen mounted in a Schenck-Webi fatigue test machine	104
33	Dependency of the fracture stress of smooth and notched Wesgo Al 995 specimens from the numbers of cycles to fracture, determined from an alternating bend fatigue test at room temperature	105
34	Dependency of the fracture stress of smooth and notched Degussit Al 23 specimens from the numbers of cycles to fracture, determined from an alternating bend fatigue test at room temperature	106
35	Fracture shapes of smooth Wesgo Al 995 specimens broken under static and cyclic loads	107
36	Fracture shapes of notched Wesgo Al 995 specimens broken under static and cyclic loads	107
37	Dependency of the fracture stress, Young's modulus and the fracture strain from the grainsize of 4 mm diameter Degussit Al_2O_3 specimens determined from a bending test at room temperature	108

List of Figures (Continuation)

Fig.		Page
38	Dependency of the fracture stress, Young's modulus and the fracture strain from the porosity of 4 mm diameter Degussit Al_2O_3 specimens determined from a bending test at room temperature	109
39	Dependency of the fracture stress of round bar Alumina specimens from the specimen volume, determined from a bending test at room temperature	110
40	Dependency of the fracture stress of 4 mm Ø round bar Degussit Al_2O_3 specimens from the porosity with the grainsize as parameter. The values were determined from bending tests at room temperature	111
41	Dependency of the Weibull exponent $\frac{1}{m}$ from the porosity for various grain-sizes	112
42	Specimen shape for tension tests with Alumina	113
43	Tension test specimen of Alumina	114
44	Complete test setup for a tension test on Alumina	115

1. Introduction

For an understanding of the fundamental properties of polycrystalline brittle materials the study of the mechanical behavior of such solids is very important.

In former times there was little interest in brittle materials, mostly due to their irregular behavior. Only in recent years a gradual realization of the importance of brittle materials exists as they provide a very high temperature strength. The need of such materials in high temperature engines leads to an intensified attention focused on factores affecting the strength of brittle solids. This resulted in an increased research effort in order to understand the phenomenological properties and the behavior of these materials.

Today the initiation of cracks is generally accepted as being due to the mobilization of dislocations, which are rather uniformly dispersed. Once the dislocations are activated, either by temperature or by applied stress, they continue to move until an obstacle is encountered. This is most often provided by a grain boundary or some other barrier, where the dislocations pile up.

If this occurs for sufficient numbers of dislocations a microcrack will form, which then leads to crack initiation in the material.

In many cases the materials contain numerous finely dispersed flaws, inclusions or vacancies in the form of pores, which became operative at crack initiation mechanisms long before dislocation activation can act. Under these circumstances the material may fail at

stresses far lower than those required to mobilize the dislocation movement.

Brittle crack propagation can be described with the theory derived by Griffith /1/. He postulates, that a flaw can propagate, provided its extension is accompanied by a surplus of strain energy in the material. The Griffith criterion entails only one constant, the crack depth. The energy required to create new surfaces is based upon the theoretical surface energy of the substance. This concept was proved to hold for completely brittle materials like glass in numerous investigations.

Subsequent work extended the utility of the Griffith criterion to the case of multiaxial stresses and non-uniform stress fields and it has been applied with some success to explain the influence of the grainsize on the fracture stress or for strain rate effects. At the same time, the Griffith theory cannot explain size effects and different strengths corresponding to various loading conditions.

Another theory, proposed by Weibull /2/, considers, that a random distribution of flaws exists in the material, assigning a certain probability of failure which depends upon the size and the state of stress of the body. This statistical approach to fracture can account for the variation in strength with volume, state of stress or type of loading. Regarding, however, such parameters as grainsize, porosity, surface effects or stress gradients the theory is reduced to a condition requiring arbitrary adjustments in the empirical constants contained in it. The Weibull theory, however, is incapable to consider strain rate effects or delayed

fracture for instance.

In performing the research brittle materials had to be chosen which allow a well-planned approach to fundamental investigations of the parameters influencing the strength and failure characteristics. Oxide ceramics are very suitable for this purpose. Therefore studies have already been done for several years (see former report /3/ and /4/) on Alumina, Zirconia, Magnesia and Spinell. The first year's effort consisted essentially in the performance of compression, bending and some not very accurate tension tests. As the results from the bending tests turned out to be most reliable this method was maintained for the determination of the fracture stress, Young's modulus and the fracture strain (strain of fracture) of the above mentioned oxide ceramics in the temperature range from -195°C to 1200°C or 1400°C. Alumina showed the most promising material properties and was therefore selected for further research work.

This report deals mainly with a study of such factors affecting the strength of Alumina as effect of surface roughness, residual stresses, influence of strain rate, fatigue, effect of microstructure, size effect and non-uniform stress field.

The decision for these initial investigations was largely based on the importance of information for the designing engineer, who must be able to predict the failure of construction elements by knowing the constitution of the material and the loading conditions.

2. Experimental Investigation of Alumina

2.1. Test material

For the conduction of the planned tests round bar Alumina specimens with diameters of 2, 4, 6 and 8 mm and with different lengths of 60, 110 and 250 mm were obtained from the companies "Degussa", Frankfurt/Main, Western Gold and Platinum Co., Berkley, Calif., USA and Hrand Djevahirdjian, Monthey, Switzerland. The obtained Alumina rods were denoted as Degussit Al 23, Degussit Al 23 PT, Degussit Al 24, Degussit test substance 2461, Wesgo Al 995 and Djevax Korund.

2.1.1. Chemical analysis

All above mentioned Alumina specimens had a chemical purity of at least 99,5%. An analysis of the Degussit rods, given by Degussa is presented in Table 1. Al 23 and Al 23 PT are equal. Al 24 differs from both materials only by the content of MgO. Investigations performed by the manufacturer in order to determine the effect of the contents of MgO on the compression strength exhibit, that the influence up to a content of 3% of MgO is below 3,5% in a temperature range from 20°C to 1100°C. From Wesgo Al 995 specimens it is only known, that the purity level is beyond 99,5%. With the specimens of extreme purity like Degussit test substance 2461 and synthetic corundum it is intended to compare the coincidence of their test results with the others.

2.1.2. Grainsize and porosity

The microstructure of Alumina plays an important part for the mechanical properties, therefore the grainsize and the porosity was determined of each specimen.

For the determination of the grainsize the specimens had to be polished and etched. For this reason small parts were cut with a diamand saw close to the fracture surface form the tested specimens. Then the parts were ground with silicon carbide on cast-iron disks and polished with diamond compound of a particle size of 3 μm. After these preparations the specimens were etched for two minutes in melted Borax at 1100°C and then boiled for about half an hour in a 50% hydrochlorid acid solution and for neutralisation another half an hour in water with little Amonia. The measurements of the grainsize of Al_2O_3 which is an irregular and multifarious product can be carried out in several ways. In accordance to other works we used the Rosival method, which consists at drawing a straight line of known length across many grains and counting the number of grains, crossed by the line. For a more exact determination 2 lines in perpendicular directions were drawn on 7 arbitrary spots. The average "graindiameter G" can then be received from the equation

$$G = \frac{14 \cdot t}{\sum_{i=1}^{14} z_i} \qquad (1)$$

where z_i is the number of grains counted in one line of length L . Fig.1 exhibits photographs of a polished and etched Alumina specimen magnified 500 times.

The porosity is a measure of the gaseous inclosures in the material and is usually expressed in percent as the ratio of the pore-volume to the total volume of the specimen. The pore-volume can easily be calculated from the difference of the specific weight of the testmaterial to the theoretical density of a pore-free Alumina body. The theoretical density γ_0 was determined to be 4,00 p/cm^3 by X - ray examinations of pure α -Aluminumoxide. The same value could also be achieved asymtotically by the method of the buoyant force.

Thus, the value of the porosity can be expressed in percent by

$$p = (1 - \frac{\gamma}{\gamma_0}) \, 100 \quad [\%] \qquad (2)$$

where p = porosity $[\%]$

γ_0 = 4,00 $[p/cm]$ the theoretical density of Al_2O_3

$\gamma = \frac{G}{V}$ the specific weigth of the Alumina test specimen

The grainsize and the porosity of the Alumina rods delivered from Degussa for the conduction of the tests varied from 1,5 μm to 60 μm for the grain-size and from 1% to 20% for the porosity. Unfortunately the values were not distributed uniformly over the whole range. Fig.2 shows, that especially for small values of the porosities large grainsizes are lacking

and that for porosities from 10% to 15% only grain-sizes from 5 μm to 7 μm are present.

In order to determine the influence of the grainsize and the porosity on the fracture stress it would be valuable to know both quantities exactly at the fracture area. As the porosity is a mean value of the whole specimen and as the grainsize was determined only close to the fracture surface their distributions over the length and the diameter of each group of the Alumina specimens were measured. For this purpose the specimens were cut into 16 pieces and the grainsize and the porosity were determined from each piece. While the grainsize and the porosity were almost constant over the whole cross-section, the distribution over the length showed considerable variation.

The results are exhibited in Table 2 and in Fig.3, 4, 5 and 6. It can be seen from the diagrams that especially with the Al 23 PT and Al 24 specimen the grainsize and porosity change over the specimen length and that this fact requires to determine both values right on the fracture surface. However, it is not possible to measure the porosity on the fracture surface. The simplest method is to photograph a polished specimen and measure the area of the dark spots, then calculate the ratio of the area of the dark spots to the whole area. But this method is unreliable as always pieces of grains will be torn out during the process of cutting, grinding and polishing. The fact, that we only can take an average porosity of each specimen partially can explain the scatter of the fracture stress if the scatter of the porosity over the specimen length is taken into account.

The stress concentrations at the pores are mostly affected by the pore-shape and the pore-distance. Therefore the relation between both parameters and their dependence on the grainsize and the porosity was investigated. For this reason two groups of specimens were selected, one with constant porosity of 5,6% and varying grainsize, the other with constant grainsize of 6,1 μm and varying porosity. In Figs.7 and 8 the photographs of the carefully polished specimen are presented and they show clearly, that with constant porosity and changing grainsize the size of the pores grows with increasing grainsize. Consequently the number of pores diminishes by the same amount. At constant grainsize the number of pores increase with increasing porosity whereas the poresize remains unchanged. These facts make it possible that with changing grainsize not only the dislocation mechanism, but also the varying pore-shape and -distance is responsible for altering the fracture stress.

2.1.3. Surface roughness

The surface roughness may influence the fracture stress of Alumina, therefore the variation of the surface roughness with changing grainsize and porosity is of high interest. For these investigations Degussit Alumina specimens with changing grainsize at constant porosity or changing porosity at constant grainsize were examined in the as received condition of the material. The surface texture was measured on several spots by means of a Perth-O-Meter, a surface measuring instrument, equipped with surface tracers which explore the fine surface and transmit the oscillation caused by the peaks and valleys to an electro-mechanical converter.

Three characteristic values were measured by the Perth-O-Meter, the "Rauhtiefe" R_t, which is the total height from the highest peak to the lowest valley, the "Glättungstiefe" R_p, which is the maximum peak height above the centerline of the modified profile and the Center-Line-Average CLA, which represents the arithmetic mean value received from the absolute amounts of the distances of the surface profile to the centerline.

Generally one of the characteristic data is not sufficient as the surface might, for example, exist of many small peaks or of wide hills. In both cases the values of R_t could be the same, in spite of the different surface profiles which affect the fracture stress.

It turned out from the measurements, that all characteristic surface data decreased with increasing grainsize, that means the surface becomes smoother with larger grains, whereas with growing porosity the roughness of the surface increases (see Fig.9 and Table 3).

2.1.4. Hardness

According to the hardness scale of F. Mohs which extends from 1 to 10, where number 10 is assigned to diamond as the hardest material, Alumina has the hardness 9. However not the degree of hardness is of main interest, but the possibility to measure the plastic deformability of Alumina by micro-hardness tests with little effort. Therefore hardness tests according to the Vickers method were conducted on Alumina specimens with varying grain-size and porosity.

Throughout the whole test series the Vickers pyramide was pressed upon the specimens with constant load P

A measure for the size of the impression is then the diagonal d_H and the micro-hardness can be calculated according to

$$HV = 1{,}854 \cdot \frac{P}{d_H} \quad \cdot \left[kp/mm^2\right] \qquad (3)$$

On each specimen 10 impressions were arbitrarily distributed and evaluated. In Table 4 the arithmetic mean values of the Vickers-hardness are given with respect to the grainsize and the porosity of each specimen. The results are also plotted in Fig.10. They show at small grains an increasing hardness. There is a maximum at a grainsize of about 18 μm and from there on the hardness decreases with growing grainsize. With increasing porosity however the Vickers-hardness decreases monotonously. The low values for specimens with high porosities are in good agreement with the observations made by E. Ryshkewitch /5/, who states that the brittleness of Alumina decreases with increasing porosity.

The mentioned hardness tests were distributed arbitrarily over the cross-section. The grainsize however, as Fig.10 shows, exerts a considerable influence, therefore it was necessary to measure the Vickers-hardness individually on single grains of certain sizes. For these tests a Wesgo Al 995 rod, 6 mm diameter was taken which scattered in the grainsize from 12 μm to 50 μm . 10 grains of almost equal sizes were selected in certain intervals for hardness tests. The results are assorted in Table 5 and plotted in Fig.11. The dependency of the hardness on the grainsize was similar to that shown in Fig.10. One of the Vickers impressions in the polished and

etched Wesgo specimens is demonstrated in Fig.12.

2.1.5. Damping

The fracture face of the tested Alumina rods like the fracture surface or the number of broken pieces of an Alumina rod after a bending test (see Fig.13) is partly determined by the interior damping of the material. Therefore damping measurements were performed at room temperature with Degussit Al_2O_3 round bar specimens having a diameter of 4 mm and a length of 100 mm.

The damping constant δ , also called the logarithmic decrement, is a measure for the amount of damping which the specimen possesses. If the amplitude of a vibrating specimen decreases during N cycles from a value A_2 to a value $A_1 = A_2/e$ (where e is the basis of the natural logarithms) it follows

$$\delta = \frac{1}{N} \qquad (4)$$

For these tests we used "Förster's Elastomat" (see Fig.14). In this apparatus the specimens are excited to a certain resonance vibration (torsional, longitudinal, transversal) and the N cycles of a given amplitude range during the natural diminution are counted.

The excitation can be done by means of piezoelectric or magnetic systems. The magnetic systems are only applicable to ferromagnetic materials, whereas the piezoelectric ones are applicable to all oscillatory materials.

In order to be able to apply the magnetic system, small metal sheets were glued to the specimens in a

way, that the specimens were excited to transversal vibrations.

The test results are presented in Table 6 and plotted in Fig.15. The damping constant shows an enormous increase with increasing porosity and a slight decrease with increasing grainsize. This result coincides with the observations that specimens with a low porosity break into more pieces than specimens with a high porosity.

2.2. Performance of strength tests

2.2.1. Influence of the surface roughness on the fracture stress, Young's modulus and the fracture strain

The influence of the surface condition on the fracture stress, Young's modulus and the fracture strain was investigated at room temperature with Degussit Al_2O_3 specimens fired in one kiln under equal conditions in order to achieve constant grainsize and porosity for all specimens.

For the test series specimens with a diameter of 6 mm and a length of 250 mm were chosen. The average grainsize was 9,0 μm and the average porosity 5,37%.

The surface condition of the specimens was varied by grinding with Silicon carbide of different grainsize or polishing with fine grained diamond compound. Three characteristic values, as described in chapter 2.1.3., were measured by a Perth-O-Meter, the "Rauhtiefe" R_t, the "Glättungstiefe" R_p and the Center-Line-Average CLA.

For determining the fracture stress, Young's modulus and fracture strain in dependence from the surface condition, the prepared specimens were tested in bending. The bending test equipment is shown in Fig.16.

It is in principal the same as described in /3/ and /4/. The evaluation of the fracture stress, Young's modulus and the fracture strain remained unchanged. The test results are presented in Table 7 and in Figs.17 to 19. They show, that the decrease rate of the fracture stress and fracture strain with increasing roughness is almost negligible. Furthermore, Young's modulus remains constant. These data reveal that fracture originates primarily on the flaws. It is suspected that only at low porosities the groves of the surface texture influence the fracture stress evidently. However, only a test series covering the whole range of grainsize and porosity can give a complete answer.

2.2.2. Residual stresses in Alumina rods

As the residual stresses of a material affect the fracture stress and fracture strain their determination was attempted on our common Alumina specimens. For this purpose 20 Wesgo Al 995 specimens with a length of 250 mm, a diameter of 6 mm and little variation of grainsize and porosity were selected. By this specimen shape, which corresponds to our bending test specimens, only the grinding off method which was elaborated by G. Sachs /6/ could be applied. With this method the diameter of the specimen has to be ground off stepwise and the change of length must be measured after each step. As only longitudinal strains can be measured a simplificating assumption has to be made, that there exists only a uniaxial stress state. According to G. Sachs this leads to the following equation

$$\sigma_L = -E \cdot \left[\rho \cdot \frac{d\varepsilon_L}{d\rho} + \varepsilon_L \right] \qquad (5)$$

where E is Young's modulus
ρ the remaining cross-section
ε_L the axial strain of the specimen

from which the distribution of the residual stresses over the cross-section of the specimen can be determined.

Much care was taken for the grinding process in order not to produce additional stresses. The surface was ground off stepwise from 6 to 3,5 mm, however, only over a part of the length in order to have the specimen always fixed in the same position of the measuring equipment. After each step the specimen was stored for about one hour in a room with almost constant temperature, then the change of the specimen length was measured by means of a Huggenberger Optimeter with an accuray of ± 0,0003 mm. The maximum variation of the temperature was approximately ± 1°C. The elongations resulting from this change of temperature were eliminated by comparison with a gaging rod. Fig.20 shows a measuring equipment which was mounted on a heavy steel plate in order to exclude the deformations between the supports and the optimeter. The test results of three specimens are presented in Tables 8 to 10 and plotted in Figs.21 to 23. The tests show, that all kinds of distributions are possible, the stresses however are negligible small. It also follows, if the arithmetic mean value of the elongations of all 20 tests is taken that the corresponding residual stress is zero throughout the whole cross-section.

2.2.3. Influence of the loading speed on the fracture stress, Young's modulus and fracture strain of Alumina

One can imagine that the strain rate, as long as dislocation movements take place, affects the fracture stress and fracture strain. Therefore a test series for the determination of the influence of the loading speed at our bending tests on the fracture stress, Young's modulus and the strain at fracture was conducted at room temperature. For the bending tests Wesgo Al 995 specimens with a diameter of 6 mm and only slightly differing porosity and grainsize were taken. All specimens were fired in one kiln, they had an average porosity of 3.7% and an average grainsize of 12 μm .

The bending test setup which was built in into our Zwick electronic tension test equipment is shown in Figs.24 and 25. One can see the arrangement of the electric strain gages which measure the load applied to the leverarms (1) and the strains of the specimen (2). The electric signals of the strain gages were given into two Tektronix cathode ray oscillographs which recorded a load-strain and a strain-time diagram. Figs.26a and 26b show examples of a test. Prior to the tests the load, strain and time signals were gaged for analysing the photographed diagram. The straight line from Fig.26a results from the superimposition of the load and strain signals, the inclination of which is in connection with the length of the leverarm and the moment of resistance a measure of Young's modulus. The end of the line which shows the maximum load and strain is a measure for the fracture stress and strain. The curved line of Fig.26b is a superimposition of time and strain. The inclination is a measure of the

strain rate. The tests were performed at four cross-head speeds of the Zwick tension test machine, namely 0.6, 6.0, 60 and 600 mm per minute. It can be seen from the photograph that the strain rate becomes constant at the end even at the maximum speed of 600 mm per minute, therefore inertia influences can be neglected for the determination of the fracture stress, fracture strain and for Young's modulus if the measurements will be done in the region of the constant strain rate.

The errors which are caused by the inclined and displaced glueing of the strain gages on the tension and compression side of the specimens are kept small because of the special form of the metal film strain gages, which had a width of 0.75 mm and a length of 15 mm.

The test results of this series are given in Table 11. This table contains also the porosity and the grain-size of each specimen in order to eliminate their influence. The values of the fracture stress, Young's modulus and the strain at fracture are reduced to an uniform porosity of 4% and a grainsize of 12 μm . The test results are also plotted in Fig.27. The diagrams exhibit, that the fracture stress and the strain at fracture increase slightly with increasing strain rate, whereas Young's modulus remains constant.

2.2.4. Alternating bending fatigue tests

An important reason for investigating fatigue phenomena in Alumina is that very little experimental work under fatigue conditions has been done with materials which approach the ideal concept of brittleness. Thus a knowledge of the fatigue behavior of ceramics in general should benefit a far wider field.

Alternating bending fatigue tests were started with Wesgo Al 995 and Degussit Al 23 Alumina rods. For the tests cylindrical smooth and circumferentially notched specimens were selected which are shown in Fig.28. The manufacturing of the smooth and notched specimens was done with diamond tools of equal grainsize. The specimen was rotating and the diamond disks of 175 mm and 2 mm diameter were grinding parallel to the direction of the centeraxis in order to achieve similar surface conditions. At first it was intended to determine the familiar SN curve with the stress plotted on a linear or logarithmic scale versus the numbers of cycles to fracture shown logarithmically.

The tests were carried out on two Schenck-Webi fatigue test machines (Fig.29) which were developed for bending and torsion fatigue tests on all kinds of materials. It is possible to superimpose the dynamic loads with a static preload. For the momentary tests, however, the static preload (bending moment) was kept zero.

The "Webi" is a mechanically driven machine with a steady adjustable lift which is necessarily constant during the operation. The frequency is 1495 cpm. Fig.30 shows schematically the method of operation and the measuring equipment. The double eccentric (8) can be adjusted to each permissable lift. With the help of the connecting rod (7) the lift can be transmitted to the loading lever (6). The specimen (5) will be fastened with a special clamping device (see Fig.31) on the loading and measuring lever (2). The clamping device had to be equipped with roller bearings in order to avoid torsional stresses which otherwise would originate by tightening the screws

of the clamps. In addition it is necessary that the specimen is clamped in such a way that the neutral axis is in the same level as the center of the axis of rotation (4). The measuring level is mounted on leaf-springs (3) which enable a motion in the longitudinal direction of the specimen so that tension and compression stresses which arise from the contraction of the specimen under bending load are excluded. The bending moment is generated by the lift of the loading lever and by the resistance of the spring (10) which can be installed with different strengths. The measuring lever enlarges the motions of the spring and with the help of the two dial gages the amplitude of oscillation can be determined. The mounted spring and the indication of the dial gages are a measure for the applied load which can be determined from the diagram of the characteristic curves.

If a specimen is broken, an automatic switch turns the motor off. The numbers of cycles of the test can be read from a counter. Before starting the test series several possibilities of error of the fatigue machine were investigated.

For instance, the upper and lower bending stress and the preload which can be adjusted statically with the two dial gages were checked by means of electrical strain gages and the diagrams of the characteristic curves of the springs were improved according to our measurements. The already mentioned torsional stresses were also measured and it turned out that they are negligible small because of the installed roller bearings in the clamping device (Fig.31). Further,

it was assumed that the weight of the measuring lever varies the statically applied load during cycling and disturbes the sinusoidal vibration more and more with decreasing flexural rigidity EJ. For this reason tests were performed with specimens of different materials and diameters in order to vary Young's modulus E and the ratio of inertia J. The electric signals of the applied strain gages were given into a Tektronix cathode ray oscilloscope which recorded a strain-time diagram. No disturbance of the measuring lever on the bending stress or the vibration was noticed. This test was not interrupted for five days and we found that the stresses and the sinusoidal vibration remained unchanged. Fig.32 shows an example of one vibration cycle.

The test program was started with 30 Wesgo Al 995 and 20 Degussit Al 23 smooth and notched bending specimens at room temperature. The test results are presented in Tables 12 to 15 and plotted in Figs.33 and 34. It can be seen that the fracture stress of the smooth and notched specimens decreases with increasing numbers of cycles. It seams however that the decrease rate of the notched specimens is less than that of the smooth specimens, so that for the Degussit Al 23 specimens the stress of the nonruptured specimens which have passed the fatigue test is the same for the notched and the smooth specimens and for the Wesgo Al 995 specimens the nominal fracture stress of the notched specimens is even higher than those of the smooth specimens at a number of cycles greater than 10^7. In order to draw conclusions from these introductory tests, these observations should be substantiated by more test results.

In Figs.35 and 36 some fractured fatigue specimens are shown. Viewed from bottom to top the first specimen is a typical static test, then the numbers of cycles increase.

The fracture surfaces in the fatigued Alumina are characteristic in shape, being flat across most of the section but turning into a distinct breakaway lip. This shape is basically similar for the static failure only the breakaway lip tends to be a little greater.

Williams found a simple explanation to interpret the general shape of the fracture surfaces. The crack originates at the tension surface and runs straight and fast at right angles to the imposed stress until it encounters the influence of a shock wave reflected from the opposite surface. The crack then moves to left or right of its original path. It is interesting that at all fatigued specimens the crack runs into the direction of the increasing cross-section, whereas in the case of static failure the crack turned into the opposite direction which is the direction of the increased stress. Similar observations can be made with the notched specimens, where the crack of the static bend test runs perpendicular to the applied stress through the smallest cross-section and the crack of the fatigued specimens deviated from the right angle into increasing cross-section.

2.2.5. Dependency of the fracture stress, Young's modulus and fracture strain on the grainsize and the porosity

The microstructure of a brittle material affects considerably its fracture stress, Young's modulus and fracture strain.

Experience shows that the strength increases with decreasing grainsize and that, moreover, the brittle fracture of a polycrystalline material begins in one grain and then spreads to the others in the surroundings. The condition for the penetration of the crack across the boundary is probably the attainment of a critical stress at the end of a crack. Since the stress for the extension of a crack is inversely proportional to the square root of its length (Griffith /1/) one would expect the brittle strength of a polycrystalline material like Alumina to be inversely proportional to the square root of the mean grain diameter (Orowan E./8/). Another influence is exerted by the porosity. It is evident, however, that with increased porosity the strength of the resulting body will decrease. The relative loss will depend on the pore-size and pore-shape. E. Ryshkewitch /5/ has performed compression tests with porous sintered Alumina whose grainsize ranged from $1\mu m$ to $3\mu m$ and the experimental data can be represented by the following expression

$$\sigma = \sigma_0 \cdot e^{-Bp} \qquad (6)$$

σ = strength of the porous body

σ_0 = strength of the nonporous body of the same material

p = porosity expressed as a fraction

B = material constant

Statements of the coincident effects of grainsize G and porosity p on the strength of Alumina seem to be complicated as the pore-size and pore-distance is determined by the grainsize (see Fig.8). It can be

concluded therefore, that the grainsize affects the influence of the porosity on the fracture stress. On the other hand the pores prevent the crack propagation in a grain as they act as obstacles which means that the influence of the grainsize on the fracture stress is affected by the porosity.

For the determination of the influence of the grainsize and the porosity on the fracture stress, Young's modulus and the fracture strain 160 bending tests were conducted at room temperature with Degussit Al_2O_3 specimens having a diameter of 4 mm and a length of 250 mm. The specimens were manufactured in a way that the porosity and grainsize showed a variety according to Fig.2. As the bending test equipment displayed in Fig.16 has proved to be appropriate this test setup was used and the method of evaluation of the fracture stress, Young's modulus and fracture strain was carried out according to the equations given in /4/.

The test results are given in Table 16 and the dependency of the fracture stress, Young's modulus and the fracture strain from the grainsize and the porosity is shown in Fig.37 and Fig.38. The diagrams were received in the following way: For instance, the fracture stress was plotted versus the grain diameter for groups of specimens with porosities scattering by 0.5% at most, then the fracture stress was plotted versus the porosity for different groups of grainsizes where the range was kept within 1 μm. The curves received of one diagram allowed to construct the lines of the other diagrams.

The diagrams show that the grainsize affects the influence of the porosity on the fracture stress and fracture

strain not only by a linear displacement but also by the curvature. This is also true for the influence of the grainsize on the fracture stress and fracture strain at grains smaller than 20 μm , where the porosity affects the decrease rate. For grains larger than 20 μm the influence of the grainsize is very small.

Young's modulus decreases linearly with increasing porosity in the range 2.27% to 20.5%. The grainsize affects this influence only very little as the influence of the grainsize on Young's modulus is almost negligible small.

For small grains the relationship of equation (6) has been confirmed, whereas for large grains the experimental curves deviate more and more from the exponential character.

The influence of the grainsize on the strength of Alumina also shows an almost straightline relationship on a log - log scale for small porosities. For large porosities the curves deviate from a straight line, as the pores interfere with the dislocation movements.

2.2.6. Influence of the specimen volume and the stress distribution on the fracture stress of Alumina at various grainsizes and porosities

The existence of a size effect with Alumina specimens is known with certainty. Many possible explanations have been suggested. An increase of stress with decreasing specimen volume follows from statistical considerations. It is characteristical for ceramic materials, that their strength values scatter over a comparatively wide range.

The statistical theory of Weibull /2/ allowes an adequate prediction of the failure probability of simple shapes of brittle materials and takes full account of the volume effect as well as the nature of the stress distribution to which the body is subjected. For an application of this theory it becomes necessary to determine the variability of the strength for a certain material and certain environmental parameters.

The problem must therefore be attacked on a statistical basis, assigning a given probability of failure to a specified stress level. Theories based on this concept postulate that each material contains a random distribution of flaws. Fracture will occur by the most stress raising flaw which the specimen happens to contain. The specimen must be visualized as being composed of individual infinitesimal volumes, each of which carries a certain failure probability corresponding to the stress level to which it is subjected. When one of the volume elements is ruptured the whole specimen fails. Hence it follows that the strength will clearly be a function of size, as the larger the specimen is the greater will the probability be that a severe flaw will be contained in it.

Weibull took the elementary laws of probability as starting point in order to develop a theory the formulae of which may be readily brought to agree with the test results. The assumptions necessary for deriving these equations are only that a distribution curve of strength values exists, that the material is considered as a continuum and that the properties of the material are such that the probability of rupture starting at any

point is equal, that means that the material is isotropic.

With these assumptions and with the laws of probability the following general expression for the ultimate strength can be obtained

$$\sigma_F = \int_0^\infty e^{-\int n(\sigma)\,dV} \cdot d\sigma \qquad (7)$$

Here dV is the volume element and $n(\sigma) = -\log(1 - S_0)$ S_0 is the experimentally determined strength distribution curve as a function of σ .

If the material is such, that the risk of rupture is independent of the stress direction, then σ in the formula is a scalar quantity. For stresses distributed in an arbitrary way, σ is to be replaced by another scalar quantity which is definitely determined by the three principal stresses. If σ in the above equation denotes this comparison stress, the formula will be valid for any combination of stresses.

The function $n(\sigma)$ has to be determined from experimental data and can most frequently be written as

$$n(\sigma) = k \cdot \sigma^m \qquad (8)$$

By introducing (8) into (7) the ultimate strength is obtained

$$\sigma_{F_0} = \int_0^\infty e^{-k \cdot V \cdot \sigma^m} \cdot d\sigma \qquad (9)$$

Instead of k we may introduce the constant $\sigma_0 = k^{-\frac{1}{m}}$ and we may put $z = \sigma \cdot V^{\frac{1}{m}} / \sigma_0$. Then the final

formula for tension tests is

$$\sigma_{ftO} = \frac{\sigma_0}{V^{\frac{1}{m}}} \cdot \int_0^\infty e^{-z^m} dz \tag{10}$$

For bending tests with circular round. bar specimen of radius r , where M = const the stress σ can be written as

$$\sigma = \sigma_p \cdot \frac{x}{r} \tag{11}$$

and the volume element dV as

$$dV = \ell \cdot \sqrt{r^2 - x^2} \cdot dx \tag{12}$$

Consequently if σ in equation (8) is replaced by (11) we get from (7) with (8) and (12)

$$\sigma_{fbo} = \frac{k^{-\frac{1}{m}} \cdot \int_0^\infty e^{-z^m} \cdot dz}{\left(\frac{2}{\pi}\right)^{\frac{1}{m}} \cdot V^{\frac{1}{m}} \cdot \left[\int_0^1 \varrho^m \cdot \sqrt{1-\varrho^2}\, d\varrho\right]^{\frac{1}{m}}} \tag{13}$$

where $\varrho = \frac{x}{r}$

It is supposed that the power $\frac{1}{m}$ is a function of the grainsize and the porosity and can be obtained from the strength distribution curve S .

In order to avoid the enormous number of tests, which would be necessary to determine the strength distribution curve for each grainsize and porosity, bending tests were conducted with varying specimen volume for

constant grainsize and porosity. In the first test series it was examined whether there is an influence on the test results by changing the specimen diameter or the specimen length. It turned out however, that only the volume of the specimen is decisive. It was altered within the range from 180 mm^3 to 3750 mm^3. An example of a test diagram is given in Fig.39, where the fracture stress of specimens from a certain group of grainsize and porosity is plotted versus the specimen volume on a double logarithmic scale. According to equation (7) it is possible to determine the power $\frac{1}{m}$ from the inclination angle of the straight line given by

$$\frac{1}{m} = \frac{\ln(\sigma_{fb1}/\sigma_{fb2})}{\ln(V_2/V_1)} \qquad (14)$$

As the values $\frac{1}{m}$ scattered very much a great number of tests were performed at the volume of approximately 780 mm^3 with 4 mm diameter Degussit Al_2O_3 round bar specimens where the grainsize and porosity again showed a variety as in Fig.2. The usual bending test setup was maintained and the influence of grainsize and porosity on the fracture stress was determined in the same manner as described in chapter 2.2.5. The volume of the test specimens of this mentioned section was approximately 2390 mm^3 and it was possible to calculate the value according to equation (14) by comparing the diagrams.

The results of the bending tests are given in Table 17 and the dependency of the fracture stress from the porosity at a volume of 780 mm^3 is given for several grainsizes in Fig.40.

The diagram again shows that the fracture stress decreases monotonously with increasing porosity. However, the grainsize affects the influence of the porosity by a linear displacement and also by the curvature.

The values $\frac{1}{m}$ are given in Table 18 and the influence of the porosity on the exponent $\frac{1}{m}$ is plotted in Fig.41 for several grainsizes.

The preliminary results show that the exponent $\frac{1}{m}$ is very low for instance for grainsizes smaller than 6 μm and for porosities below 2% and also for large grainsizes beyond 20 μm in connection with porosities above 15%. The highest exponent $\frac{1}{m}$ was determined in the range of 5 to 10% porosity and at grainsizes of approximately 10 μm

From Fig.41 an empirical equation can be established for $\frac{1}{m}$ with respect to the grainsize and the porosity. If this relation is inserted into equation (13) and if k is replaced by the grainsize G in μm which was done in order to harmonize with the results of other investigations (/9/,/10/,/11/,/12/ and /13/) then this expression renders the size effect caused from the distribution curve. Equation (13), however, does not include the reduction of the effective cross-sectional area by increasing porosity and the stress-concentration created by the pores. Both factors $(1-p)$ and α , where the stressconcentration α can be determined empirically from Fig.38 or 40 with respect to the grainsize and porosity, must be incorporated in equation (13). This leads to the following expression for the influence of the grainsize, porosity

and the specimen volume on the fracture stress for a fourpoint loaded bending test of a round bar Alumina specimen:

$$\sigma_{fb} = \sigma_{fbo} \cdot \frac{1-p}{\alpha} \cdot \frac{G^{-\frac{1}{m}} \cdot \int_0^{\infty} e^{-z^m} \cdot dz}{\left(\frac{2}{\pi}\right)^{\frac{1}{m}} \cdot V^{\frac{1}{m}} \cdot \left[\int_0^1 \varrho^{\frac{1}{m}} \cdot \sqrt{1-\varrho^2}\, d\varrho\right]^{\frac{1}{m}}} \qquad (15)$$

where σ_{fbo} = 48 kp/mm^2

G = grainsize in

p = porosity in volumefraction

V = specimen volume in mm^3

α = empirical factor caused by the stressconcentration

$$= \left[0{,}416 \cdot \left(\frac{G}{G_0}\right)^{2.92} + 0.05\right] \cdot p^{\left(\frac{G}{G_0}\right)^{0.42}} \qquad G_0 \approx 5.8\,\mu m$$

$\frac{1}{m}$ = Weibull exponent

$$= (1-ap)(bp^c + 0.05)$$

$$a = 1.6\,(G/G_0)^{0.608}$$

$$b = 0.322\,(G/G_0 - 1)^{0.75} \cdot e^{-0.64\,(G/G_0 - 1)} + 0.4$$

$$c = 0.0214\,(G/G_0 - 1)^{0.78} - 0.0355\,(G/G_0 - 1) + 0.737$$

Equation (15) can also be written in terms of Gamma-functions which are tabulated and facilitate the evaluation.

$$\sigma_{fbo} = \sigma_{fbo} \cdot \frac{1-p}{\alpha} \cdot \frac{G^{-\frac{1}{m}} \cdot \Gamma\left(\frac{1}{m}+1\right)}{\left(\frac{2}{\pi}\right)^{\frac{1}{m}} \cdot V^{\frac{1}{m}} \cdot \left[0.443 \cdot \frac{\Gamma\left(\frac{m+1}{2}\right)}{\Gamma\left(\frac{m}{2}+2\right)}\right]^{\frac{1}{m}}} \qquad (16)$$

As the bending tests were only conducted in the ranges covered with dots in Fig.2, equation (16) is valid in a porosity range from p = 2.27% to p = 19.5% and in a range of grainsize from G = 6.0 μm to G = 40.5 μm.

2.2.7. Tension tests

According to equations (10) and (13) the relation between the fracture stress from a tension test and from a bending test with specimens of equal volumes and equal microstructure is:

$$\sigma_{fto} = \sigma_{fbo} \cdot \frac{1}{\left(\frac{2}{\pi}\right)^{\frac{1}{m}} \cdot \left[\int_0^1 \varrho^m \sqrt{1-\varrho^2}\, d\varrho\right]^{\frac{1}{m}}} \qquad (17)$$

As $\frac{1}{m}$ was always positive in the tested region the fracture stress for tension must be smaller than that for bending. The results from bending tests therefore can give an estimate for the results of tension tests and this should give the starting point for further investigation.

In testing of materials the tension test is a very important basis of research and engineering. However, it is well known that one of the main problems associated with tensile testing of brittle materials is the difficulty of applying a true axial load to obtain a uniform stress field in the test area.

Considerable effort was applied in designing a tension test specimen which achieves an almost uniform stress field in the test area. For instance for a tension specimen with circular cross-section it can be shown from the simple beam theory that the percentage of increase in stress resulting from eccentricity is 8 times the ratio of the eccentricity to the diameter of the rod. As only small specimens can be manufactured an eccentricity of a few thousands of a millimetre can produce an appreciable stress increase on one side of a tensile specimen which causes failure at lower loads

than those corresponding to true axial loading.

Therefore, a tension test device had to be developed which excluded the eccentricity in the specimen and the bending moments caused by the clamps and the test machine. It is known, that the most accurate symmetry can be achieved with circular ground objects. Therefore, a specimen shape and a clamping device which consisted only of circular ground parts was considered.

Fig.42 shows the proposed tension test specimen. Here it is of primary interest that the centeraxis of the ground rod coincides with a maximum discrepancy of 0,003 to 0,004 mm with the centeraxis of the drilled hole in the bushing on the front surface. This demand can easily be achieved by very careful grinding of the Alumina specimen and the bushing. Through the hole of the bushing exact fitting wires with sufficient strength will be put into the hollow spaces and fixed by filling it up with a low melting point alloy of lead, bismuth and thin. It is important that no play is allowed between the bushing and the specimen and that therefore the bushing has to be made of a material with very little temperature expansion. A normal steel would break the Alumina specimen during the preheating or the fillingup process.

The thin wires with a length of approximately 50 cm on each side are clamped in the tension test machine. No remarkable bending moments in the specimen caused by the friction in the pins or the alignment of the tension test machine and so on are possible.

Two specimens have been manufactured and tested so far. Fig.43 shows the test specimen and Fig.44 the complete test equipment.

An analysis of the stress field by means of electrical strain gages showed that the bending strain of the first specimen could be kept below 2% of the total strain during the whole test procedure. The manufacturing process can still be improved and it is expected to diminish the still existing errors further.

3. References

/1/ Griffith, A.A.: Phil.Trans.Roy.Soc. A 221 (1920) S.163-198

/2/ Weibull, W.: Ing. Vetenskaps Akad.Handl.No 151 (1939) No 153 (1939)Kungl.Tekniska Hogskolans Handl. no 27 (1949) Appl.Mech.Rev.(Nov.1952) 449

/3/ Neuber, H.: "Experimental Investigations of the Behavior of Brittle Materials at Various Ranges of Temperature", Contract AF 61/052 273 Final Report 30 April 1965

/4/ Neuber, H. a. Wimmer, A.: "Experimental Investigations of the Behavior of Brittle Materials at Various Ranges of Temperature", Technical Report AFML-TR-68-23 March 1968

/5/ Ryshkewitch,E.: Compression strength of porous sintered alumina and zirconia, 9th communication to ceramography, J.Amer.Ceram.Soc.36 S.65-68 (1953)

/6/ Sachs, G. a. Espey, G.: The measurement of residual stresses in metal, Iron Age (1941)

/7/ Williams in Kriegel, W.W. a. Palmour, H.: Mechanical Properties of engineering Ceramics, Intersc.Publ. New York, London 1961, Ch.18, 245-302

/8/ Orowan, E.: Fracture strength of solids Repts. Progr. in Phys.12 S.185-232 (1949)

/9/ Petch, N.J.: The fracture of metals, Progr. in Metal Physics 5 (1954) S.1-52

/10/ Knudsen, F.P.: Dependence of the mechanical strength of brittle polycrystalline specimens on porosity and grainsize J.Amer.Ceram.Soc.42/376-387 (1959)

/11/ Petch, N.J.: Cleavage strength of polycrystals J.Iron Steel Inst.(London) 174 Part I S.25-28 (May 1953)

/12/ Spriggs, R.M. a.Vasilos, T.: Effect of grainsize on transverse bend strength of Alumina and Magnesia, J.Amer.Ceram.Soc.46/ 224-228 (1963)

/13/ Passmore, E.M., Spriggs, R.M. a.Vasilos, T.: Strength-grainsize-porosity relations in Alumina, J.Amer. Ceram.Soc.48/S.1-7 (1965)

/14/ Neuber, H.: Stress and concentration design factors for grooved shafts. Unpublished diagrams.

4. Tables and Illustrations

Table 1

Chemical analysis of Degussit Al 23, Degussit Al 23 PT, Degussit Al 24 and Degussit test substance 2461

	Al 23	Al 23 PT	Al 24	test substance 2461
Al_2O_3	99.5%	99.5%	99.6%	99.9%
SiO_2	0.05-0.1%	0.05-0.1%	0.05-0.1%	0.00-0.02%
Fe_2O_3	0.02-0.05%	0.02-0.05%	0.02-0.05%	
MgO	0.2%	0.2%	0.01-0.02%	0.08-0.1%
CaO	0.05-0.1%	0.05-0.1%	0.05-0.1%	0
Na_2O	0.1-0.3%	0.1-0.3%	0.1-0.3%	0

Table 2

Distribution of the grainsize and the porosity over the length of Alumina rods.
(Rods with a length of 240 mm were cut into 16 pieces. The numbers represent the grainsize and the porosity of each piece. The numerical order is arranged in the same way as the parts sticked together originally.)

material and average porosity	Porosity P [%]	Grainsize G [µm]
Degussit Al 23	3.98	20.4
	3.88	19.0
P = 3.80%	3.77	19.9
	3.77	19.4
	3.85	16.7
	3.85	17.3
	3.80	19.0
	3.93	19.0
	3.95	18.0
	3.99	21.7
	3.87	19.2
	3.74	20.9
	3.93	20.2
	3.99	17.1
	4.00	19.4
	4.24	23.7
Degussit Al 23 PT	7.37	28.1
	7.71	29.9
P = 7.58%	7.55	25.9
	8.25	25.3
	7.79	27.5

continuation of Table 2

material and average porosity	Porosity P [%]	Grainsize G [µm]
	7.94	24.5
	8.07	28.4
	7.84	25.6
	7.56	26.5
	7.72	25.6
	7.06	24.2
	7.31	25.6
	7.86	25.3
	7.61	21.9
	7.65	26.2
	7.12	23.8
Degussit Al 24	18.21	71.1
	17.97	66.2
P = 17.75%	18.11	64.7
	17.97	66.9
	18.55	61.9
	17.95	54.3
	17.35	54.8
	17.48	72.9
	18.16	59.4
	17.94	60.0
	17.12	58.8
	17.86	60.0
	18.04	60.6
	18.32	58.2
	17.88	57.6
	17.31	55.9

continuation of Table 2

material and average porosity	Porosity P [%]	Grainsize G (μm)
Wesgo Al 995	3.66	11.6
	3.58	10.7
	3.59	11.5
	3.58	11.0
	3.62	11.1
	3.63	11.4
	3.73	10.5
	3.76	11.0
	3.80	10.7
	3.77	10.9
	3.80	10.9
	3.84	10.2
	3.82	10.1
	3.86	11.1
	3.94	10.7
	3.82	11.6

Table 3

Dependency of the "Rauhtiefe" R_t, "Glättungstiefe" R_p, and the Center-Line-Average CLA from the grainsize and the porosity of Degussit Al_2O_3 round bar specimens.

grainsize G [µm]	porosity P [%]	Rauhtiefe R_t [µm]	Glättungs-tiefe R_p [µm]	Center-Line-Average CLA [µm]
14.6	18.18	22.50	12.07	4.47
18.6	9.07	11.77	3.57	1.60
17.5	8.02	15.20	5.23	2.13
15.3	6.04	6.83	3.63	0.97
16.0	5.64	5.60	1.79	0.92
15.7	5.26	7.20	2.51	1.04
15.3	3.39	5.13	2.30	0.76
20.9	8.47	7.57	1.82	1.09
20.4	8.63	8.47	2.15	1.30
9.3	9.37	16.53	7.37	2.63
8.9	8.77	17.00	7.30	3.07
8.7	8.96	20.43	9.73	3.17
7.9	9.37	22.47	8.93	3.03

Table 4

Dependency of the Vickers-micro-hardness from the grainsize and the porosity of 4 mm Ø Degussit Al_2O_3 round bar specimens.

(The values of the Vickers-hardness are the arithmetic mean values of 10 hardness test on one cross-section.)

grainsize G [µm]	porosity P [%]	load P [p]	diagonal d_H [µm]	Vickers-hardness HV [kp/mm^2]
23.7	8.64	102	8.39	2687
21.0	8.55	102	7.85	3070
17.1	8.55	102	7.69	3199
13.2	8.48	102	8.01	2948
9.1	8.61	102	9.36	2159
5.6	8.37	102	9.85	1961
6.6	2.69	102	8.38	2690
6.3	4.36	102	8.71	2490
6.2	7.71	102	11.56	1418
6.2	10.96	102	10.95	1580
6.0	14.75	53*	9.71	1042
6.2	18.33	53*	8.86	1260

*) The low load was necessary, as the impression with the original load was larger than the free areas at specimens with high porosities.

Table 5

Vickers-micro-hardness measurements on single grains of different sizes. Determined on a Wesgo Al 995 rod 6 mm Ø, porosity ρ = 3.70%.

(The values for the grains and the Vickers-hardness are the arithmetic mean values of 10 tests.)

grainsize G [µm]	load P [p]	diagonal d_H [µm]	Vickers-hardness HV [kp/mm^2]
12.2	94	11.48	1333
20.4	94	10.77	1495
30.2	94	10.90	1473
41.5	94	11.13	1416
50.0	94	11.39	1355

Table 6

Variation of the damping factor of 4 mm Ø Degussit Al_2O_3 specimens with the porosity and the grainsize.

porosity P [%]	grainsize G [µm]	damping factor δ -
3.39	15.3	$0.73 \cdot 10^{-4}$
4.38	19.4	$1.05 \cdot 10^{-4}$
5.26	15.7	$0.99 \cdot 10^{-4}$
5.64	16.0	$0.71 \cdot 10^{-4}$
6.04	15.4	$1.12 \cdot 10^{-4}$
8.02	17.5	$1.22 \cdot 10^{-4}$
9.07	18.7	$0.92 \cdot 10^{-4}$
17.63	14.0	$7.05 \cdot 10^{-4}$
18.18	14.6	$10.20 \cdot 10^{-4}$
9.37	7.9	$1.49 \cdot 10^{-4}$
8.96	8.7	$1.15 \cdot 10^{-4}$
8.77	8.9	$1.08 \cdot 10^{-4}$
9.37	9.3	$1.10 \cdot 10^{-4}$
8.02	17.5	$1.22 \cdot 10^{-4}$
9.07	18.7	$0.92 \cdot 10^{-4}$
8.63	20.4	$1.05 \cdot 10^{-4}$
8.47	20.9	$1.25 \cdot 10^{-4}$

Table 7

Dependency of the fracture stress, Young's modulus and the fracture strain from the surface condition of 6 mm Ø Degussit Al_2O_3 specimens determined from a bending test at room temperature.

Rauh-tiefe R_t [µm]	Glättungs-tiefe R_p [µm]	Center-Line-Average CLA [µm]	fracture stress σ_B kp/mm^2	Young's modulus E kp/mm^2	fracture strain ε_B %
17.17	4.77	2.53	26.7	$3.68 \cdot 10^4$	0.700
14.70	4.90	3.07	23.9	$3.73 \cdot 10^4$	0.565
14.03	4.43	2.30	27.5	$3.70 \cdot 10^4$	0.725
9.77	3.10	1.43	26.5	$3.64 \cdot 10^4$	0.770
8.80	2.23	1.44	23.6	$3.65 \cdot 10^4$	0.650
8.60	2.18	1.22	23.8	$3.67 \cdot 10^4$	0.655
7.66	1.62	1.00	25.9	$3.68 \cdot 10^4$	0.685
7.13	2.02	0.90	23.0	$3.68 \cdot 10^4$	0.640
7.03	2.05	1.12	28.7	$3.70 \cdot 10^4$	0.765
7.03	1.96	1.14	27.0	$3.70 \cdot 10^4$	0.725
6.77	2.10	1.04	25.8	$3.64 \cdot 10^4$	0.690
6.43	1.26	0.85	27.6	$3.71 \cdot 10^4$	0.730
5.90	1.55	0.88	29.8	$3.70 \cdot 10^4$	0.810
5.70	0.84	0.70	24.7	$3.70 \cdot 10^4$	0.650
4.93	1.69	0.80	29.0	$3.67 \cdot 10^4$	0.805
4.87	1.77	0.79	26.2	$3.63 \cdot 10^4$	0.720
4.57	1.45	0.71	27.9	$3.71 \cdot 10^4$	0.715
4.43	0.91	0.58	29.3	$3.73 \cdot 10^4$	0.775
4.30	0.92	0.57	27.6	$3.68 \cdot 10^4$	0.760
4.27	0.46	0.42	25.3	$3.66 \cdot 10^4$	0.690
4.20	1.44	0.64	29.0	$3.70 \cdot 10^4$	0.770
2.77	0.74	0.29	25.1	$3.68 \cdot 10^4$	0.685
2.70	0.61	0.32	27.2	$3.72 \cdot 10^4$	0.690
2.07	0.80	0.20	27.2	$3.73 \cdot 10^4$	0.740

Table 8

Residual stresses of a 6 mm Ø Wesgo Al 995 specimen, grainsize G = 17.2 μm , porosity p = 3.99% (see Fig.21)

ground length ℓ [mm]	remaining area f [mm^2]	change of length $\Delta\ell$ [μm]	strain ε [‰]	residual stress σ [kp/mm^2]
199.9	28.04	0.0	0.0000	0.33
	25.29	0.1	0.0005	-0.03
	22.81	0.0	0.0000	-0.22
	20.39	-0.2	-0.0010	-0.23
	17.13	-0.3	-0.0015	-0.13
	14.32	-0.4	-0.0020	-0.03
	11.85	-0.7	-0.0035	0.02
	9.51	-0.7	-0.0035	0.07

Table 9

Residual stresses of a 6 mm Ø Wesgo Al 995 specimen, grainsize G = 16.5 μm , porosity p = 4.08% (see Fig.22)

ground length ℓ [mm]	remaining area f [mm^2]	change of length $\Delta\ell$ [μm]	strain ε [‰]	residual stress σ [kp/mm^2]
199.7	28.04	0.0	-0.0000	-0.53
	25.42	-0.3	-0.0015	-0.38
	22.98	-0.4	-0.0020	-0.26
	20.43	-0.4	-0.0020	-0.15
	17.31	-1.0	-0.0050	-0.04
	14.55	-0.8	-0.0040	0.04
	11.76	-1.2	-0.0060	0.12
	9.56	-1.3	-0.0065	0.16

Table 10

Residual stresses of a 6 mm Ø Wesgo Al 995 specimen, grainsize G = 16.4 μm , porosity p = 4.09% (see Fig.23)

ground length ℓ [mm]	remaining area φ [mm²]	change of length $\Delta\ell$ [μm]	strain ε [‰]	residual stress σ [kp/mm²]
199.9	28.04	0.0	0.0000	2.44
	25.34	1.2	0.0060	1.18
	22.90	1.8	0.0090	0.51
	20.47	1.9	0.0095	0.08
	17.31	2.0	0.0100	-0.24
	14.59	2.6	0.0130	-0.40
	11.73	2.6	0.0130	-0.47
	9.48	2.3	0.0115	-0.48

Table 11

Dependency of the fracture stress, Young's modulus and the strain at fracture from the strain rate of 6 mm Ø Wesgo Al 995 specimens at room temperature determined from a bending test.

porosity	grainsize	strain rate	fracture stress	Young's modulus	fracture strain
P [%]	G [μm]	$10^3 \dot{\varepsilon}$ [$\frac{‰}{sec}$]	σ_B [$\frac{kp}{mm^2}$]	$10^{-4} \cdot E$ [$\frac{kp}{mm^2}$]	ε_B [‰]
3.826	11.88	4.38	21.44	3.640	0.5689
3.703	11 99	4.60	23.53	3.759	0.6137
3.789	12.20	4.17	22.83	3.669	0.6156
3.593	11.94	4.38	21.57	3.729	0.5512
3.704	12.43	45.3	24.76	3.713	0.6370
3.756	12.26	49.3	25.17	3.577	0.6689
3.764	12.15	48.2	24.43	3.661	0.6470
3.807	12.49	47.8	27.17	3.690	0.7227
3.713	11.15	48.6	22.07	3.716	0.5854
3.553	11.06	46.7	21.44	3.613	0.5594
3.708	12.04	482	24.60	3.713	0.6434
3.708	11.94	450	27.65	3.680	0.7346
3.701	12.37	482	25.65	3.703	0.6891
3.543	13.02	470	26.30	3.688	0.6914
3.800	12.37	468	26.41	3.722	0.6927
3.721	12.12	452	26.72	3.622	0.7825
3.799	12.26	437	27.91	3.680	0.7203
3.865	11.48	4399	24.90	3.730	0.6628
3.778	12.78	4500	26.09	3.748	0.6857
3.709	11.63	4240	27.68	3.771	0.7218
3.691	11.78	4520	28.06	3.713	0.7362

continuation of Table 11

porosity	grainsize	strain rate	fracture stress	Young's modulus	fracture strain
P	G	$10^3\dot{\varepsilon}$	σ_B	$10^{-4}\cdot E$	ε_B
[%]	[µm]	[‰/sec]	[kp/mm²]	[kp/mm²]	[‰]
3.907	12.04	--	28.62	3.889	0.7300
3.708	12.04	4340	27.94	3.667	0.7246
3.646	12.15	4270	29.25	3.731	0.7670

Table 12

Dependency of the fracture stress of 5 mm Ø smooth Wesgo Al 995 specimens from the numbers of cycles to fracture determined from alternating bend fatigue tests at room temperature.
(Average grainsize $G = 20.5 \mu m$, average porosity $p = 3.68\%$)

diameter d [mm]	bending stress σ_B [kp/mm²]	numbers of cycles to fracture N -
4.996	25.15	static bending test
5.012	24.72	static bending test
4.993	20.00	9.800
4.993	18.00	121.500
4.978	16.00	43.300
5.010	14.00	118.200
4.915	10.00	452.500
5.008	11.00	1.110.900
4.988	8.00	2.922.300
4.979	9.00	5.478.400
5.011	7.00	5.450.300
5.003	6.50	no fatigue fracture

Table 13

Dependency of the fracture stress of notched round bar Wesgo Al 995 specimens (nominal diameter 5 mm) from the numbers of cycles to fracture determined from alternating bend fatigue tests at room temperature. (Average grainsize 20.0 μm , average porosity p = 3.68%, theoretical notch strength ratio $\bar{\alpha}$ = 1.54, according to Neuber /14/)

minimum diameter d [mm]	nominal bending stress σ_{bW} [kp/mm^2]	numbers of cycles to fracture N [-]
4.978	19.74	static bending test
4.990	18.57	static bending test
4.950	16.49	2.000
4.935	13.56	8.800
4.955	11.30	29.400
4.948	12.00	154.900
5.008	11.00	95.300
5.045	9.73	711.000
4.970	10.18	no fatigue fracture
5.013	8.92	no fatigue fracture
5.095	8.03	no fatigue fracture
5.010	9.44	no fatigue fracture

Table 14

Dependency of the fracture stress of 5 mm Ø smooth Degussit Al 23 specimens from the numbers of cycles to fracture determined from alternating bend fatigue tests at room temperature.
(Average grainsize G = 20.1 μm , average porosity p = 3.79%)

diameter d [mm]	bending stress σ_B [kp/mm^2]	numbers of cycles to fracture N -
4.970	21.24	900
4.987	21.02	1.400
4.972	17.62	18.400
4.958	13.03	50.000
5.007	11.85	147.600
4.988	9.36	117.300
5.002	6.65	1.953.800
5.022	5.47	no fatigue fracture

Table 15

Dependency of the fracture stress of notched round bar Degussit Al 23 specimens (nominal diameter 5 mm) from the numbers of cycles to fracture determined from alternating bend fatigue tests at room temperature. (Average grainsize G = 21.6 μm, average porosity p = 3.68%, theoretical notch strength ratio $\bar{\alpha}$ = 1.54, according to Neuber /14/)

minimum diameter d [mm]	nominal bending stress σ_{bW} [kp/mm^2]	numbers of cycles to fracture N [-]
5.017	18.38	1.300
4.995	15.77	3.900
5.135	13.24	28.500
5.022	11.10	109.600
4.850	9.29	112.000
5.103	8.43	914.000
5.090	6.72	1.108.300
4.970	5.15	no fatigue fracture

Table 16

Dependency of the fracture stress, Young's modulus and the fracture strain from the porosity and grain-size of 4 mm Ø Degussit Al_2O_3 specimens determined from a bending test at room temperature.

grainsize G [µm]	porosity p [%]	fracture stress σ_B [kp/mm^2]	Young's modulus E [kp/mm^2]	fracture strain ε_B [‰]
8.2	2.33	27.0	40 210	0.672
17.9	2.21	26.5	40 125	0.661
6.6	2.69	27.0	39 730	0.679
8.2	2.89	27.8	39 745	0.699
8.8	3.31	25.9	37 732	0.686
18.0	2.87	22.5	39 800	0.564
18.4	2.93	23.0	40 032	0.574
18.8	2.87	25.2	39 718	0.635
19.4	3.29	22.7	44 300	0.525
23.1	2.67	19.2	39 948	0.481
6.3	4.36	24.7	37 641	0.656
6.8	4.92	27.3	37 580	0.727
7.4	4.29	24.1	39 038	0.617
7.9	4.02	22.5	39 230	0.574
20.7	4.35	23.7	39 200	0.604
24.3	4.38	19.6	38 455	0.509
25.0	4.33	18.4	39 100	0.468
6.9	6.02	26.6	36 578	0.725
8.4	5.10	26.2	37 427	0.699
12.7	5.45	18.6	36 055	0.517

continuation of Table 16

grainsize G [µm]	porosity p [%]	fracture stress σ_B [kp/mm^2]	Young's modulus E [kp/mm^2]	fracture strain ε_B [‰]
6.1	6.55	30.4	35 981	0.844
6.6	6.69	27.6	35 708	0.773
6.8	6.38	23.8	36 633	0.648
15.4	6.60	15.3	36 400	0.420
20.7	6.60	16.5	35 900	0.457
6.5	7.43	23.5	35 034	0.669
7.6	6.91	22.5	34 914	0.642
23.1	7.05	19.7	36 600	0.535
5.0	8.22	26.2	34 420	0.758
5.4	8.35	26.9	34 240	0.784
5.6	8.37	26.3	34 314	0.764
5.7	7.98	25.3	34 694	0.728
5.7	8.05	26.8	34 470	0.776
6.2	7.71	29.3	35 000	0.834
6.4	8.13	27.9	34 477	0.807
6.4	8.07	26.2	34 808	0.752
10.0	8.40	17.6	34 997	0.505
12.2	7.80	20.3	38 700	0.522
13.2	8.48	16.3	34 881	0.470
15.3	8.50	17.3	35 082	0.495
15.4	8.30	15.0	35 199	0.427
16.3	8.39	15.9	35 370	0.450
19.0	8.49	15.7	34 854	0.450

continuation of Table 16

grainsize G [µm]	porosity p [%]	fracture stress σ_B [kp/mm^2]	Young's modulus E [kp/mm^2]	fracture strain ε_B [‰]
5.7	8.60	29.0	34 210	0.845
9.1	8.61	16.6	34 858	0.477
9.6	8.62	17.6	34 387	0.513
10.3	8.61	14.2	35 260	0.404
12.0	8.79	15.8	35 275	0.449
13.3	8.81	12.7	35 368	0.360
13.9	8.58	15.0	34 843	0.431
14.1	8.88	15.7	35 251	0.445
14.2	8.77	13.1	35 644	0.369
14.3	8.79	16.6	34 805	0.478
14.4	8.95	14.1	34 570	0.409
14.9	8.87	15.2	34 770	0.436
15.3	8.50	17.3	35 082	0.495
15.4	8.82	14.6	34 500	0.424
16.7	8.85	13.1	35 718	0.368
17.1	8.55	17.6	34 770	0.508
18.5	8.86	12.4	34 721	0.357
18.8	8.64	14.7	34 825	0.422
19.0	8.54	15.6	35 106	0.446
19.0	8.77	15.1	34 552	0.437
19.7	8.77	14.4	35 174	0.410
19.9	8.72	16.1	35 198	0.460
19.9	8.63	16.7	34 713	0.481
20.5	8.80	14.9	34 380	0.437
21.0	8.55	11.6	34 747	0.335
21.2	8.84	16.6	34 652	0.481
23.3	8.85	11.5	34 162	0.337

continuation of Table 16

grainsize G [μm]	porosity p [%]	fracture stress σ_B [kp/mm^2]	Young's modulus E [kp/mm^2]	fracture strain ε_B [‰]
23.7	8.64	15.7	35 169	0.447
28.6	9.00	14.1	34 400	0.408
5.4	9.51	22.8	34 800	0.654
14.4	9.05	14.9	34 741	0.430
15.5	9.40	12.3	34 757	0.355
15.9	9.07	13.2	35 248	0.377
16.3	9.32	15.6	34 710	0.449
16.5	9.15	17.9	34 480	0.518
16.5	9.32	17.4	34 590	0.502
16.8	9.08	13.0	34 160	0.381
18.8	9.16	12.3	34 396	0.357
19.3	9.25	12.2	34 177	0.358
19.9	9.35	13.4	34 850	0.385
20.0	9.02	13.1	34 404	0.382
20.1	9.21	14.0	34 646	0.406
23.1	9.37	17.3	34 900	0.495
28.6	9.00	14.1	34 400	0.408
4.5	17.70	20.5	25 510	0.805
4.7	17.24	20.2	25 933	0.774
5.1	17.52	21.3	25 370	0.839
5.4	17.71	21.4	25 368	0.835
5.9	17.30	17.5	25 632	0.677
6.3	17.46	20.8	25 674	0.805
44.5	17.68	11.8		0.371
47.1	17.52	11.8	25 990	0.454
47.8	17.25	9.7	26 840	0.360
51.6	17.69	11.0	26 900	0.410

continuation of Table 16

grainsize G [µm]	porosity p [%]	fracture stress σ_B [kp/mm^2]	Young's modulus E [kp/mm^2]	fracture strain ε_B [‰]
4.2	18.14	20.8	24 836	0.830
4.3	18.15	19.5	24 685	0.782
4.4	18.25	20.0	24 440	0.816
4.9	17.82	20.7	25 400	0.815
5.5	17.82	20.7	25 221	0.816
6.1	17.85	18.8	25 143	0.740
6.1	18.33	21.2	24 366	0.864
6.3	17.84	20.1	25 403	0.787
39.6	18.02	9.5	27 330	0.347
40.4	18.00	9.7	26 400	0.360
45.6	17.86	11.0	25 100	0.440
51.6	18.20	11.4	26 700	0.426
66.3	17.92	11.1	29 500	0.408
4.4	12.50	24.0	30 220	0.795
4.4	13.80	24.6	29 455	0.829
4.7	13.88	22.5	29 359	0.763
4.7	17.24	20.2	25 933	0.774
4.5	17.70	20.6	25 510	0.805
4.2	18.14	20.8	24 836	0.830
4.3	18.15	19.5	24 685	0.782
4.4	18.25	20.0	24 440	0.816
4.4	19.04	18.9	24 021	0.781
4.3	19.10	19.3	23 898	0.800
4.6	19.37	18.3	23 400	0.783
4.3	19.44	19.0	23 247	0.806
4.4	19.52	18.15	23 320	0.778
4.5	19.87	18.3	23 235	0.780

continuation of Table 16

grainsize G [µm]	porosity p [%]	fracture stress σ_B [kp/mm^2]	Young's modulus E [kp/mm^2]	fracture strain ε_B [‰]
5.0	8.22	26.2	34 420	0.758
5.4	8.35	26.9	34 240	0.784
5.6	8.37	26.3	34 314	0.764
5.1	10.83	18.7	32 026	0.581
5.4	10.91	24.1	31 619	0.758
5.0	11.15	25.7	31 700	0.810
5.0	11.33	23.9	31 539	0.755
5.4	11.48	25.2	31 513	0.794
5.5	11.51	23.7	31 661	0.745
5.0	11.52	22.3	29 141	0.758
5.0	11.63	24.0	31 493	0.759
5.1	11.68	26.8	31 315	0.852
5.5	11.69	23.1	31 449	0.731
5.1	11.70	25.7	31 100	0.825
5.1	11.75	23.9	31 167	0.762
5.5	11.89	25.1	31 288	0.778
5.0	11.99	25.0	32 170	0.773
5.4	12.10	25.6	30 770	0.831
5.4	12.21	23.5	31 039	0.754
5.4	12.74	24.1	30 213	0.793
5.6	13.28	23.3	29 650	0.782
5.5	14.27	24.0	28 486	0.838
5.3	14.31	23.7	28 492	0.828
5.0	14.45	22.2	28 645	0.772
4.9	14.82	21.5	28 130	0.765
5.1	15.07	23.6	27 660	0.852
5.1	17.52	21.3	25 370	0.839

continuation of Table 16

grainsize G [μm]	porosity p [%]	fracture stress σ_B [kp/mm^2]	Young's modulus E [kp/mm^2]	fracture strain ε_B [‰]
5.4	17.71	21.4	25 368	0.835
4.9	17.82	20.7	25 400	0.815
5.5	17.82	20.7	25 221	0.816
5.2	19.30	20.4	23 611	0.857
6.1	6.55	30.4	35 981	0.844
6.6	6.69	27.6	35 708	0.773
6.5	7.43	23.5	35 034	0.669
6.2	7.71	29.3	35 000	0.834
5.7	7.98	25.3	34 694	0.728
5.7	8.05	26.8	34 470	0.776
6.4	8.07	26.2	34 808	0.752
6.4	8.13	27.9	34 477	0.807
5.7	8.60	28.9	34 210	0.845
6.0	9.84	26.5	32 712	0.806
6.4	10.27	27.0	32 590	0.829
6.0	10.73	26.2	32 590	0.800
5.7	10.74	25.6	32 099	0.795
5.8	10.82	24.7	32 190	0.766
6.2	10.96	23.7	31 773	0.743
5.7	10.97	26.6	31 770	0.835
6.0	11.54	24.32	31 331	0.772
5.8	11.65	23.9	31 267	0.759
5.7	12.38	24.3	30 339	0.796
6.3	12.85	23.3	30 204	0.768
6.4	12.85	25.3	29 424	0.860

continuation of Table 16

grainsize G [µm]	porosity p [%]	fracture stress σ_B [kp/mm²]	Young's modulus E [kp/mm²]	fracture strain ε_B [‰]
6.3	13.61	24.2	29 304	0.820
6.0	14.75	23.7	28 180	0.836
5.7	15.22	24.1	27 928	0.857
5.7	15.49	21.3	27 393	0.772
5.9	17.30	17.5	25 632	0.677
6.3	17.46	20.8	25 674	0.805
6.3	17.84	20.1	25 403	0.787
6.1	17.85	18.7	25 143	0.740
6.1	18.33	21.2	24 366	0.864
5.7	19.25	20.3	23 594	0.852
5.7	20.49	18.8	22 688	0.820
6.8	4.92	27.3	37 580	0.727
6.9	6.02	26.6	36 578	0.725
6.8	6.38	23.8	36 633	0.648
7.4	10.70	20.2	32 170	0.629
8.2	2.33	27.0	40 210	0.672
8.2	2.89	27.8	39 745	0.699
8.8	3.31	25.9	37 732	0.686
8.1	3.67	26.6	38 575	0.688
8.1	3.79	23.4	38 526	0.607
7.9	4.02	22.5	39 230	0.574
7.4	4.29	24.1	39 038	0.617
7.6	6.91	22.5	34 914	0.642
8.7	9.65	20.3	34 360	0.592
7.5	9.67	21.3	33 800	0.634

continuation of Table 16

grainsize G [µm]	porosity p [%]	fracture stress σ_B [kp/mm^2]	Young's modulus E [kp/mm^2]	fracture strain ε_B [‰]
7.9	10.36	20.1	33 800	0.594
7.4	10.70	20.2	32 170	0.629
7.5	10.89	17.4	31 997	0.540
9.6	8.62	17.6	34 387	0.513
10.0	8.40	17.6	34 997	0.505
10.3	8.61	14.2	35 260	0.404
16.3	8.39	15.9	35 370	0.450
17.1	8.55	17.6	34 770	0.508
16.7	8.85	13.1	35 718	0.368
16.8	9.08	13.0	34 160	0.381
16.5	9.15	17.9	34 480	0.518
16.5	9.32	17.4	34 590	0.502
16.3	9.32	15.6	34 710	0.449
19.5	3.25	23.7	39 520	0.601
19.4	3.29	22.7	44 300	0.525
19.0	8.49	15.7	34 854	0.450
19.9	8.63	16.7	34 713	0.481
19.9	8.72	16.1	35 198	0.460
19.7	8.77	14.4	35 174	0.410
19.0	8.77	15.1	34 552	0.437
20.0	9.02	13.1	34 404	0.382
19.3	9.25	12.2	34 177	0.358
19.9	9.35	13.4	34 850	0.385
23.1	2.67	19.2	39 948	0.481
23.1	7.05	19.7	36 600	0.535

continuation of Table 16

grainsize	porosity	fracture stress	Young's modulus	fracture strain
G	p	σ_B	E	ε_B
[µm]	[%]	[kp/mm^2]	[kp/mm^2]	[‰]
23.7	8.64	15.7	35 169	0.447
23.3	8.85	11.5	34 162	0.337
23.1	9.37	17.3	34 900	0.495
28.6	9.00	14.1	34 400	0.408
27.4	9.62	13.1	34 650	0.379

Table 17

Dependency of the fracture stress from the specimen volume, the porosity and the grainsize, determined from a bending test at room temperature.

volume V (mm^3)	porosity P (%)	grainsize G (μm)	fracture stress σ_{fb} (kp/mm^2)
180	3.53	14.3	27.53
180	3.76	16.6	25.44
180	1.92	13.4	34.39
178	2.26	12.2	30.95
183	2.20	12.5	35.50
174	2.70	9.9	34.48
375	3.35	14.4	22.89
369	3.60	13.9	23.77
378	3.30	12.1	27.37
374	1.70	11.6	30.31
372	3.18	11.6	26.62
375	3.43	14.1	22.10
387	3.50	12.1	26.28
374	3.28	11.8	27.81
386	3.43	12.9	28.60
373	1.63	12.1	27.95
364	1.40	12.0	29.64
380	1.63	10.8	29.56
382	1.41	12.3	29.28
381	1.78	12.5	28.67
382	1.55	14.5	26.30
378	1.53	13.1	28.89
370	1.73	10.4	30.84
378	1.13	12.1	30.23

continuation of Table 17

volume V (mm^3)	porosity P (%)	grainsize G (μm)	fracture stress σ_{fb} (kp/mm^2)
377	3.33	14.1	21.35
409	2.25	18.2	26.22
415	2.04	16.6	25.35
407	2.70	22.2	25.42
413	1.88	16.6	23.81
419	1.78	16.6	23.39
408	2.98	9.5	34.60
409	2.64	12.5	36.41
419	3.45	20.4	25.40
416	2.80	26.4	24.35
412	3.10	16.0	28.15
408	4.20	12.4	28.05
416	2.26	22.8	25.98
422	2.35	15.2	22.25
410	3.74	18.8	24.53
413	3.58	11.2	30.15
413	3.58	11.2	29.07
410	3.30	9.5	31.11
407	3.30	9.5	35.47
729	3.00	1.8	31.93
721	8.65	5.9	26.86
710	8.99	6.2	33.00
719	9.07	6.2	29.89
714	9.07	6.2	30.15
718	8.59	6.4	26.36
724	8.61	9.1	18.37

continuation of Table 17

volume V (mm^3)	porosity p (%)	grainsize G (μm)	fracture stress σ_{fb} (kp/mm^2)
695	7.60	11.0	23.20
721	8.77	14.2	15.49
707	8.79	14.3	17.11
724	8.30	15.4	16.99
721	8.85	16.7	16.97
720	8.64	18.8	17.73
716	8.77	19.7	16.73
723	8.72	19.9	16.20
720	8.84	21.2	15.84
697	8.42	27.3	20.45
746	4.03	1.4	42.04
749	4.35	1.4	40.28
755	3.93	1.5	35.43
764	5.77	1.5	34.73
768	6.13	1.5	39.60
752	3.60	1.7	42.17
753	3.95	1.9	40.77
736	2.53	2.0	45.06
741	2.20	2.0	40.85
742	2.30	2.1	39.93
751	13.08	5.2	26.8[illegible]
730	12.85	6.4	28.34
746	4.29	7.4	26.48
730	8.62	9.6	19.12
731	8.40	10.0	
729	8.61	10.3	18.10
732	8.78	12.0	21.05

continuation of Table 17

volume V (mm^3)	porosity P (%)	grainsize G (μm)	fracture stress σ_{fb} (kp/mm^2)
748	4.15	12.0	25.11
743	7.80	12.0	21.80
748	5.45	12.7	21.51
748	4.68	12.8	27.61
758	6.50	12.8	22.13
765	6.40	13.0	19.31
730	8.48	13.2	19.32
736	8.81	13.3	15.28
732	8.58	13.9	17.53
743	8.88	14.1	20.13
746	4.88	14.3	23.01
740	9.05	14.4	16.30
762	6.20	14.6	22.39
731	8.87	14.9	15.64
743	9.40	15.5	15.10
734	8.50	15.3	16.62
743	8.82	15.4	14.86
750	6.40	15.4	22.17
735	9.07	15.9	14.09
740	9.32	16.3	17.71
734	9.32	16.3	18.84
736	9.33	16.5	15.89
762	2.07	16.6	25.70
743	9.08	16.8	16.18
747	3.20	17.1	22.84
768	6.48	17.1	21.76
732	8.55	17.1	19.65
757	6.00	17.6	21.14
757	2.88	18.0	26.38

continuation of Table 17

volume V (mm^3)	porosity p (%)	grainsize G (μm)	fracture stress σ_{fb} (kp/mm^2)
730	8.86	18.5	15.58
751	9.68	18.5	14.99
754	6.38	18.7	20.94
736	9.15	18.8	14.25
739	8.49	19.1	17.01
736	8.77	19.1	19.10
747	9.25	19.3	14.91
733	8.63	19.9	16.37
731	9.35	19.9	12.88
743	9.02	20.0	13.89
739	9.21	20.1	15.76
740	8.80	20.5	17.34
751	6.60	21.0	15.94
736	8.55	22.0	16.41
763	7.65	22.2	18.42
743	7.75	22.2	18.99
761	6.30	23.1	21.60
755	6.90	23.1	19.22
761	6.97	23.1	19.59
752	2.67	23.1	25.27
741	8.85	23.3	15.13
736	8.64	23.7	19.68
746	4.25	24.0	21.99
742	4.38	24.8	20.49
761	2.57	25.0	24.93
753	6.75	25.0	19.73
757	7.70	25.0	15.87

continuation of Table 17

volume V (mm^3)	porosity p (%)	grainsize G (μm)	fracture stress σ_{fb} (kp/mm^2)
761	8.15	26.1	19.18
749	4.00	27.3	22.98
751	6.63	27.3	18.37
760	5.75	28.6	18.93
752	7.00	28.6	19.44
737	9.00	28.6	13.91
756	5.15	33.3	19.03
758	7.25	33.3	17.98
829	13.80	4.4	25.84
826	13.88	4.7	25.34
814	10.89	4.9	23.95
815	10.83	5.0	24.97
812	11.33	5.0	24.48
806	11.74	5.1	25.56
816	14.31	5.3	26.01
801	12.30	5.3	22.92
822	12.74	5.4	25.59
816	11.48	5.4	26.03
813	11.69	5.5	24.82
826	13.28	5.6	24.24
809	10.74	5.7	27.93
797	7.98	5.7	29.01
797	8.05	5.7	29.20
820	12.38	5.7	25.13
810	11.10	5.8	26.57
804	10.56	6.0	25.63
817	11.54	6.0	27.29

continuation of Table 17

volume V (mm^3)	porosity P (%)	grainsize G (μm)	fracture stress σ_{fb} (kp/mm^2)
811	10.96	6.2	25.92
818	13.61	6.3	26.01
823	12.85	6.4	24.75
791	7.43	6.5	30.05
805	10.40	7.5	22.36
790	9.35	7.8	20.37
794	9.66	8.5	19.19
790	9.65	8.7	19.80
812	9.88	9.4	18.14
815	18.95	9.5	13.11
814	10.30	10.0	20.11
810	18.70	16.3	14.36
817	19.35	19.3	13.94
799	18.20	38.8	10.12
805	18.03	39.6	10.57
792	18.00	40.4	10.90
801	17.60	40.8	11.03
799	17.70	40.8	11.94
793	18.10	42.1	10.89
804	17.80	42.6	10.62
799	17.80	43.1	10.96
803	17.90	43.5	10.04
824	18.25	44.0	8.76
793	17.80	44.5	12.53
791	17.60	46.1	12.28
795	17.80	46.1	11.37
806	18.40	46.1	9.27

continuation of Table 17

volume V (mm^3)	porosity p (%)	grainsize G (μm)	fracture stress σ_{fb} (kp/mm^2)
799	17.70	46.7	10.70
789	17.52	47.1	11.13
808	18.30	47.2	10.03
792	17.25	47.8	11.33
802	17.80	48.4	9.90
805	17.97	48.4	10.06
790	18.00	48.4	10.60
793	17.80	49.0	12.27
797	18.20	49.0	11.19
793	18.20	49.6	10.63
802	17.80	50.2	9.73
789	18.20	51.6	10.77
794	17.70	52.3	10.35
793	17.70	53.0	10.72
795	18.30	54.4	10.72
828	17.40	60.9	10.80
829	17.92	66.0	11.11
820	17.87	69.9	11.44
844	18.14	4.2	21.43
837	18.15	4.3	19.56
870	19.10	4.4	18.95
855	19.04	4.4	22.46
871	19.52	4.4	19.08
854	18.25	4.4	20.26
857	17.70	4.5	19.31
871	19.87	4.5	19.41
862	19.37	4.6	19.29

continuation of Table 17

volume V (mm^3)	porosity p (%)	grainsize G (μm)	fracture stress σ_{fb} (kp/mm^2)
851	17.82	5.0	21.48
854	17.52	5.1	22.28
864	19.30	5.2	22.33
851	17.71	5.4	20.87
865	19.39	5.7	20.91
865	19.25	5.7	21.17
871	20.49	5.7	19.54
850	17.30	5.9	23.27
855	17.85	6.1	21.66
859	18.33	6.2	20.82
852	17.46	6.3	23.14
1205	3.19	11.8	26.93
1199	3.19	11.8	26.66
1204	3.67	12.0	24.27
1196	3.99	12.8	22.54
1193	3.50	15.0	26.30
1195	3.60	15.0	26.51
1186	3.26	12.4	31.04
1199	3.16	12.7	26.60
1204	3.65	16.0	27.32
1188	2.98	12.4	31.95
1204	2,91	14.3	27.49
1202	3.05	13.3	27.41
1187	2.66	11.1	29.04
1201	3.42	15.4	10.13
1199	3.19	16.5	25.52
1194	3.27	12.6	31.15

continuation of Table 17

volume V (mm^3)	porosity p (%)	grainsize G (μm)	fracture stress σ_{fb} (kp/mm^2)
1199	3.26	14.9	28.49
1203	3.26	14.9	25.55
1191	3.23	20.1	28.52
1599	3.22	14.6	22.66
1591	3.40	18.3	22.15
1601	3.11	14.2	22.23
1613	2.81	22.5	21.62
1605	2.48	18.2	23.05
1582	2.39	15.4	27.60
1677	4.30	13.8	20.83
1677	5.59	18.6	21.87
1672	5.59	17.0	23.49
1667	5.59	17.0	25.97
1658	4.20	10.8	27.81
1658	4.20	10.8	23.12
1670	3.89	7.1	26.56
1662	3.74	12.1	21.28
1667	3.74	12.1	25.60
1691	4.22	13.5	21.34
1682	7.79	23.3	23.66
1667	3.82	14.3	24.03
1654	3.81	18.2	25.41
1665	3.49	15.4	25.52
1657	3.94	8.0	23.78
1779	3.04	19.0	13.79
1801	2.97	23.3	18.94

continuation of Table 17

volume V (mm^3)	porosity p (%)	grainsize G (μm)	fracture stress σ_{fb} (kp/mm^2)
1793	2.48	15.2	20.14
1793	2.61	18.7	20.81
1781	2.62	18.3	18.15
1781	2.68	19.6	20.17
1808	2.79	17.8	20.89
1781	2.70	24.6	21.49
1786	3.04	18.5	19.55
3000	3.00	27.2	21.84
3022	3.46	26.4	20.56
2997	3.48	21.3	20.65
2999	3.12	25.4	16.62
3015	3.56	23.0	21.07
3010	3.56	23.0	21.71
3029	3.49	22.2	18.50
3016	3.06	20.0	21.53
3029	3.65	26.9	20.00
3036	3.65	24.8	18.25
3036	3.06	20.0	20.11
3064	3.06	22.0	23.17
3059	3.06	22.0	22.34
3049	3.73	20.0	18.07
3047	3.34	22.2	17.97
3092	3.17	22.2	21.77
3076	3.93	18.2	18.07
3091	3.57	22.9	20.17
3778	3.19	16.5	24.42
3748	3.27	12.6	28.00

continuation of Table 17

volume V (mm^3)	porosity p (%)	grainsize G (μm)	fracture stress σ_{fb} (kp/mm^2)
3777	3.26	14.9	22.25
3754	3.23	20.1	26.60

Table 18

Dependency of the exponent $\frac{1}{m}$ from the porosity and grainsize, determined at room temperature

grainsize G (μm)	porosity P (%)	$\frac{1}{m}$
6.0	6.0	0.0645
	9.0	0.0612
	12.0	0.0671
	15.0	0.0736
	18.0	0.0764
7.0	4.0	0.0839
	6.0	0.0830
	9.0	0.0786
	12.0	0.0790
7.96	2.0	0.0935
	4.0	0.0964
	6.0	0.0897
	9.0	0.1080
	12.0	0.0982
9.86	4.0	0.0982
	6.0	0.1039
	9.0	0.1188
	12.0	0.1241
	15.0	0.1384
	18.0	0.1384
16.6	2.0	0.0691
	4.0	0.1072
	6.0	0.1155

continuation of Table 18

grainsize G (μm)	porosity p (%)	$\frac{1}{m}$
	9.0	0.1108
	12.0	0.1141
	15.0	0.0975
	18.0	0.1150
19.5	4.0	0.1146
	6.0	0.1139
	9.0	0.1195
	12.0	0.1110
	15.0	0.1060
	18.0	0.1108
23.3	2.0	0.0652
	4.0	0.1080
	6.0	0.1070
	9.0	0.1045
28.0	4.0	0.1130
	6.0	0.1130
	9.0	0.1120
40.5	17.5	0.0125
	4.5	0.0937
	8.8	0.0952
	9.3	0.0791
	5.6	0.1125
	7.3	0.0424
	18.5	0.0085

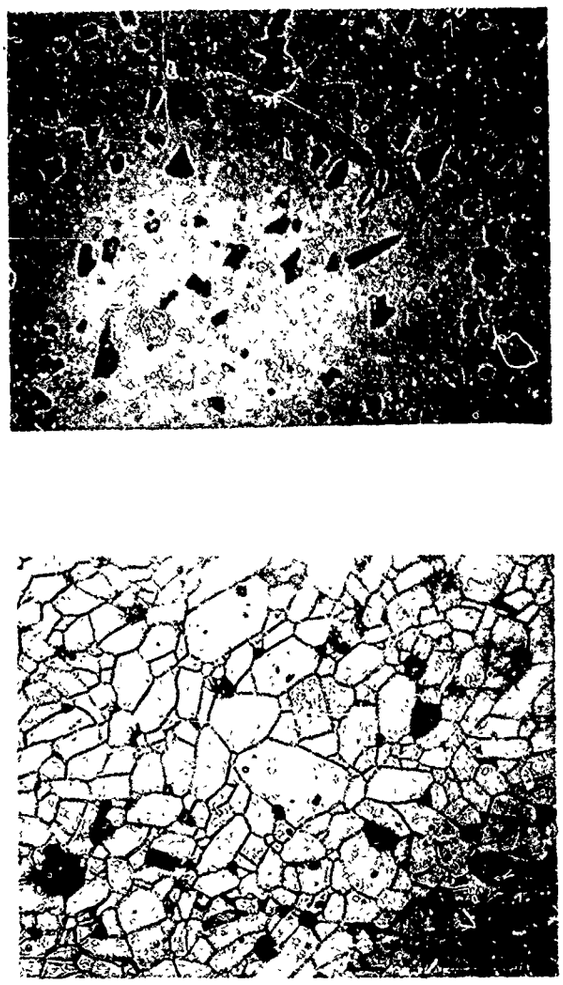

Fig.1 Polished and etched Alumina specimens
(grainsize G = 6.2 μm ; porosity p = 2.33%;
magnification 500-times)

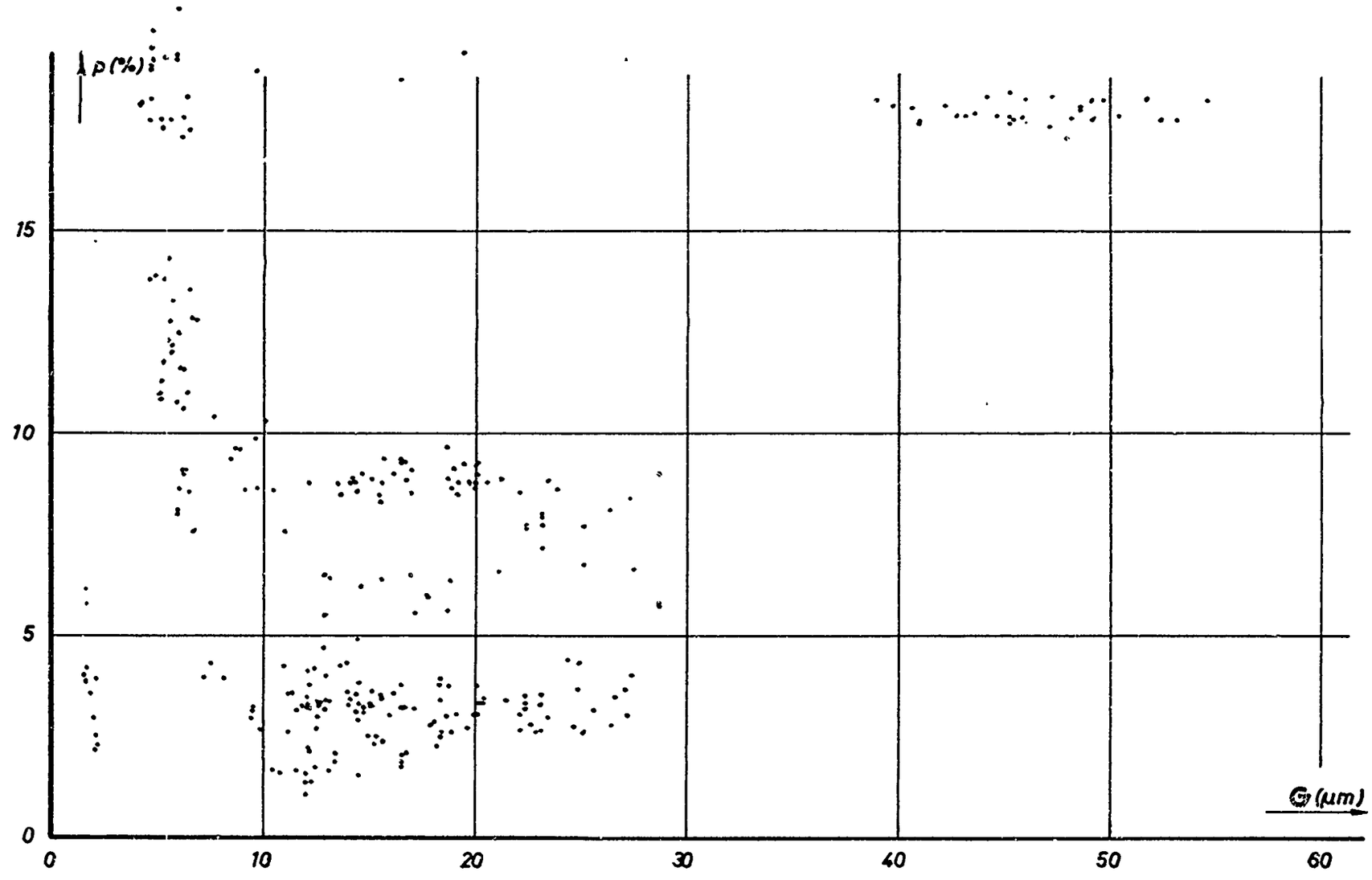

Fig.2 Distribution of the grainsize and the porosity of the round bar Alumina specimens delivered by Degussa

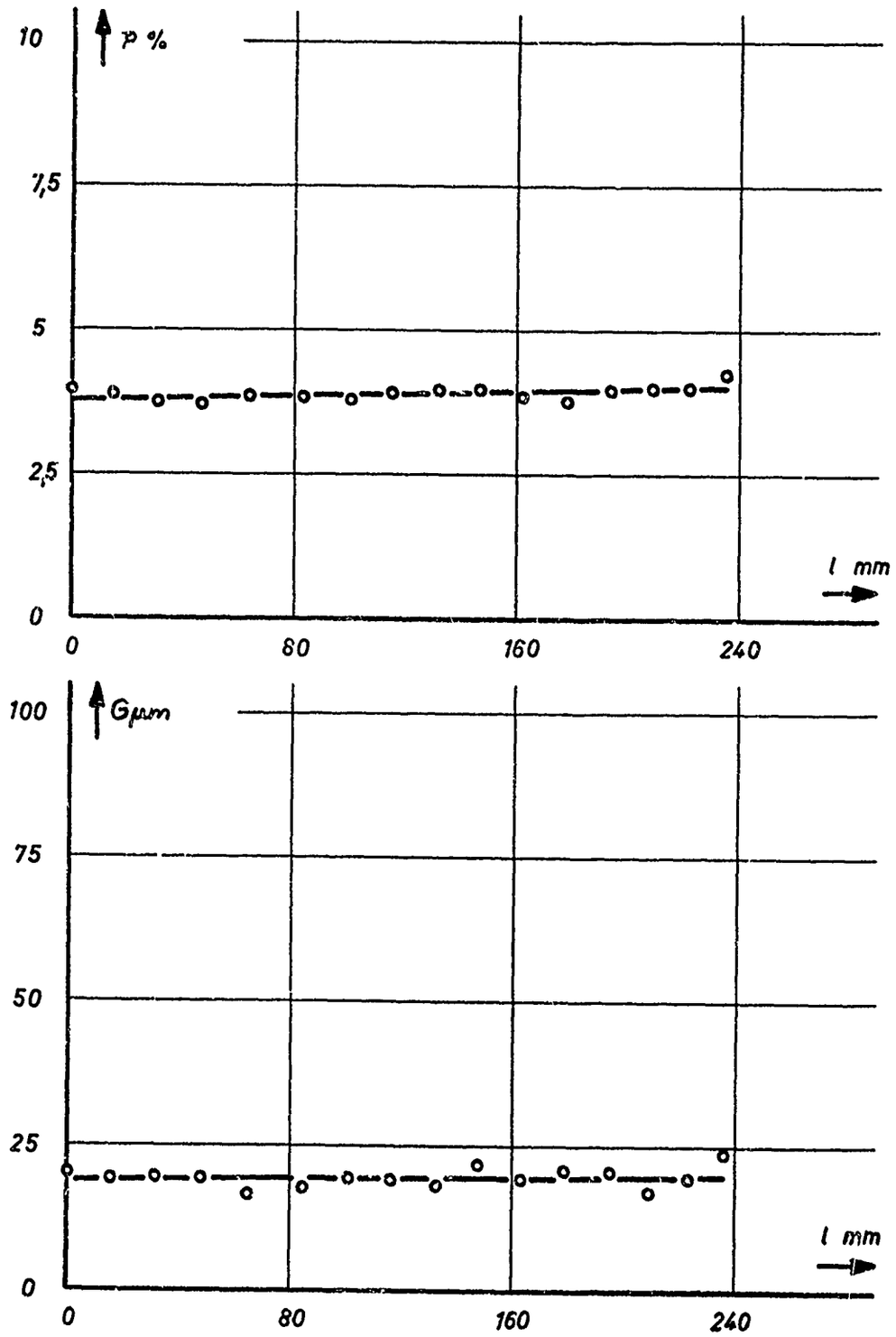

Fig.3 Distribution of the porosity and the grainsize over the length of a 4 mm diameter Degussit Al 23 specimen

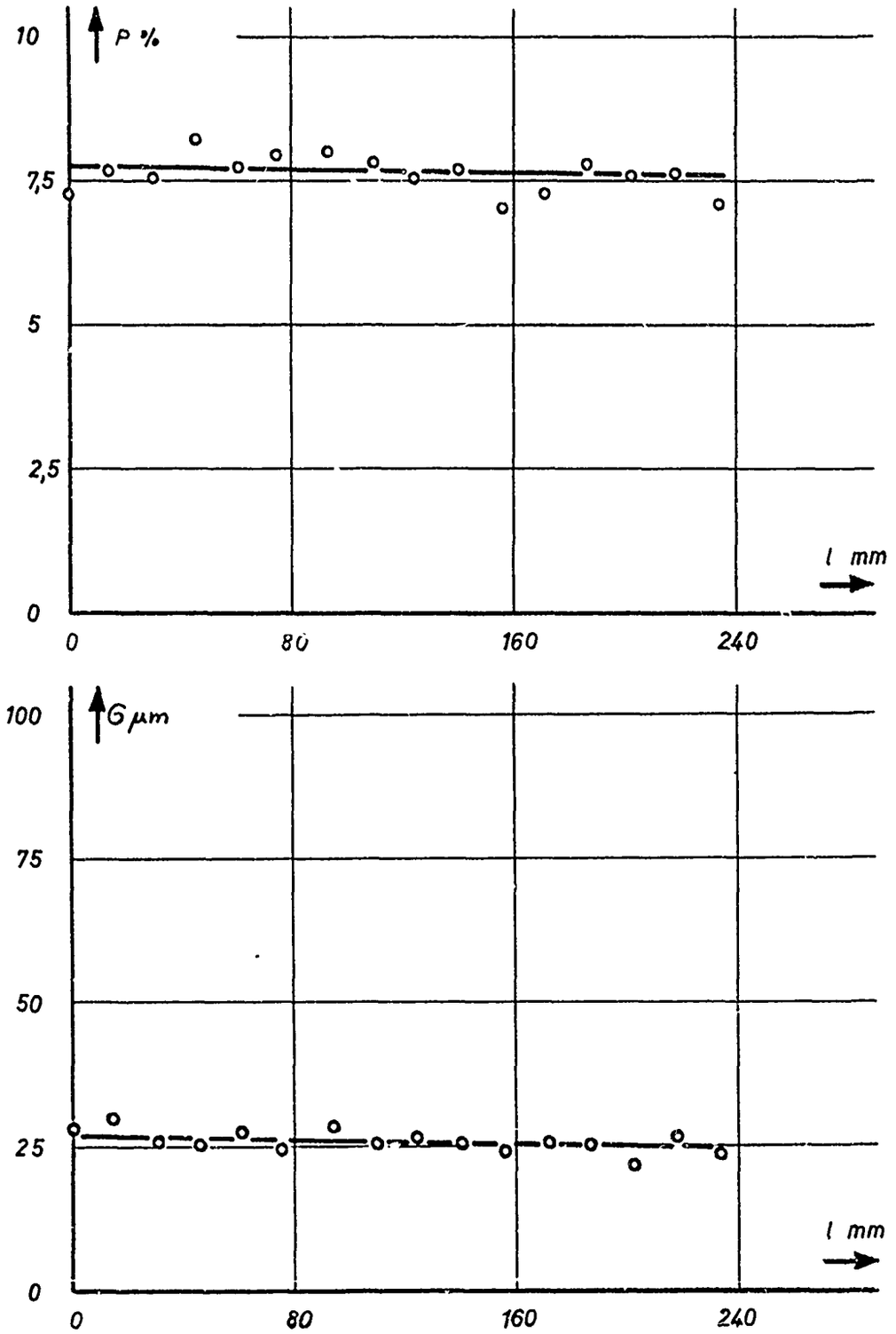

Fig.4 Distribution of the porosity and the grainsize over the length of a 4 mm diameter Degussit Al 23 PT specimen

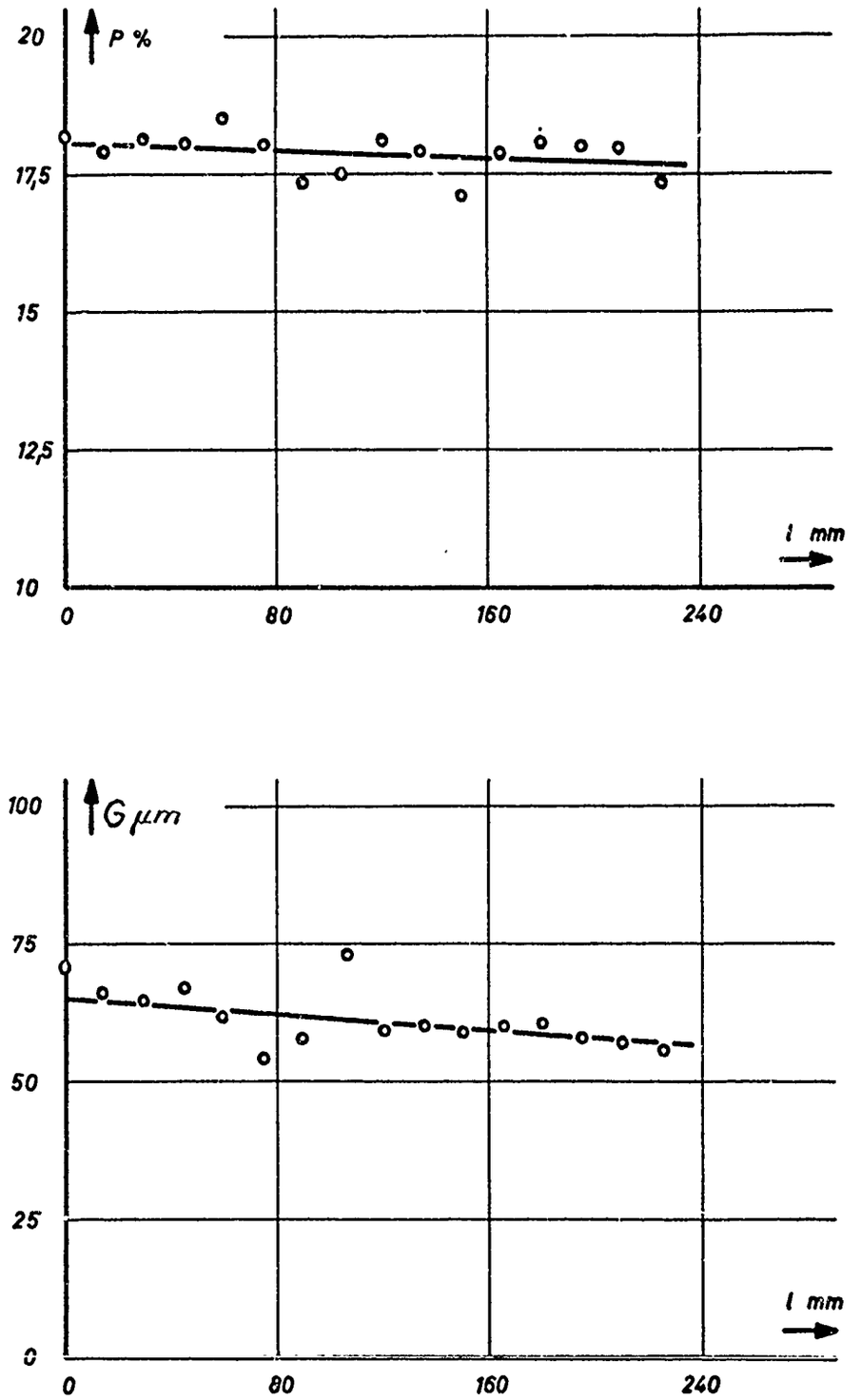

Fig.5 Distribution of the porosity and the grainsize over the length of a 4 mm diameter Degussit Al 24 specimen

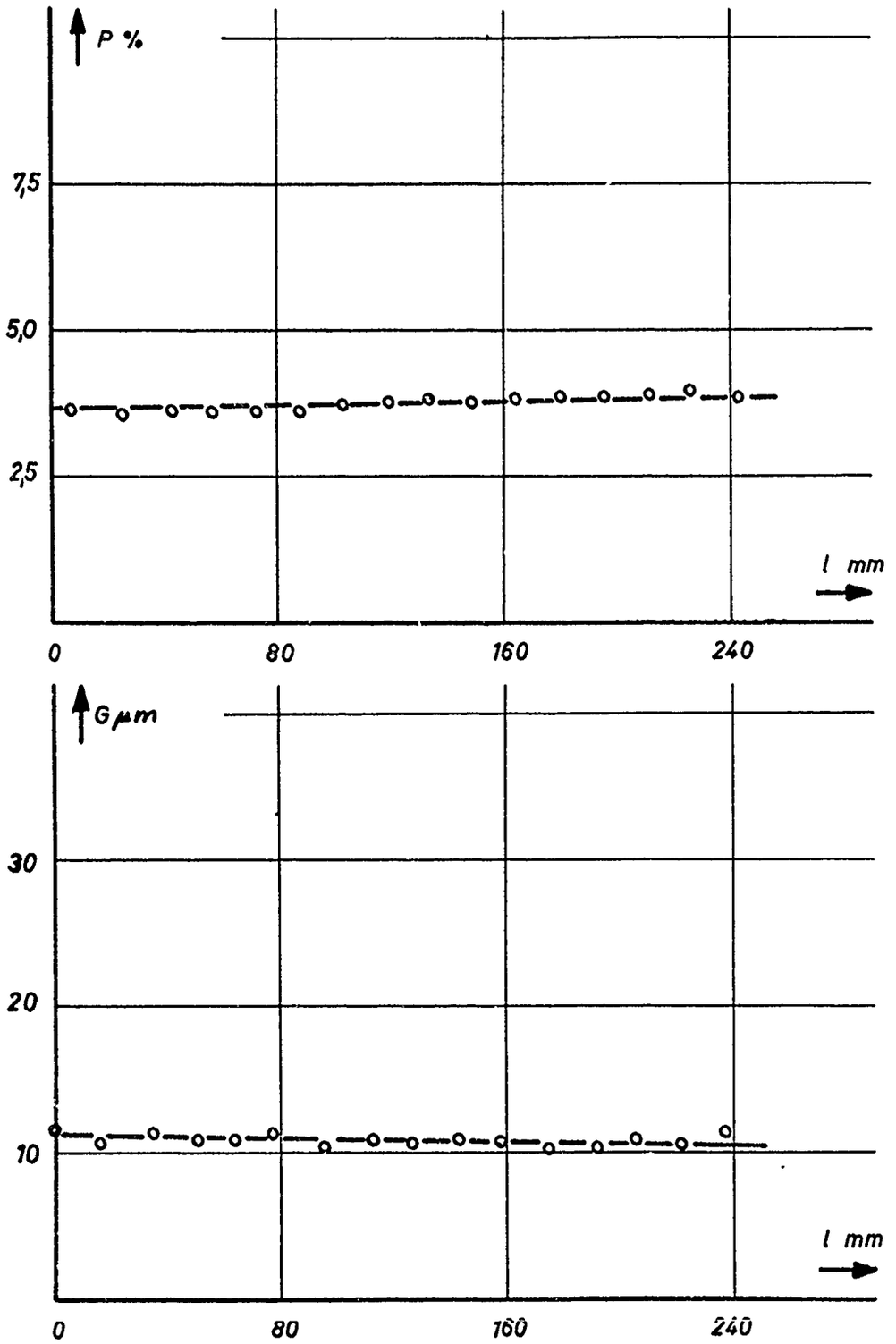

Fig.6 Distribution of the porosity and the grainsize over the length of a 6 mm diameter Wesgo Al 995 specimen

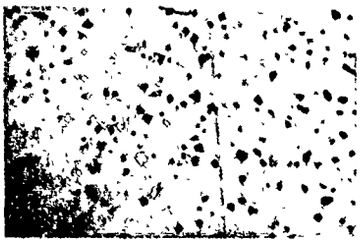

p = 2.69%

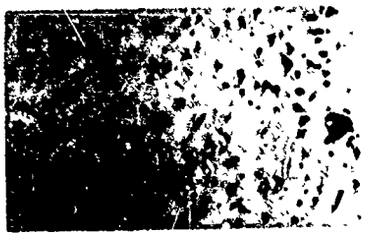

p = 4.36%

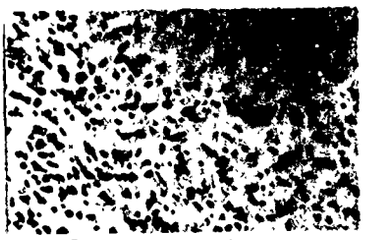

p = 6.55%

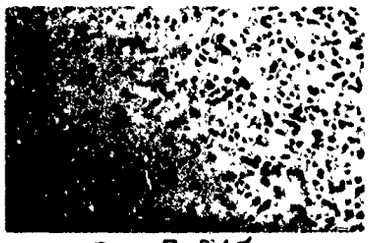

p = 7.71%

p = 8.37%

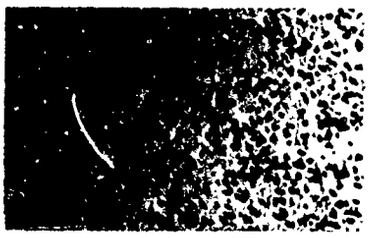

p = 10.7%

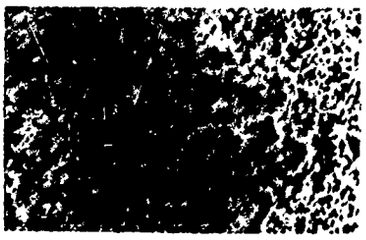

p = 14.75%

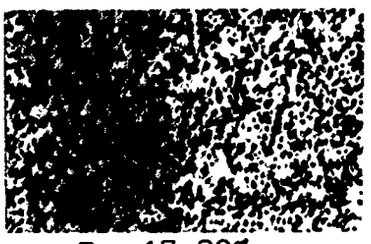

p = 17.80%

For comparison

p = 17.4%
G = 60.9 μm

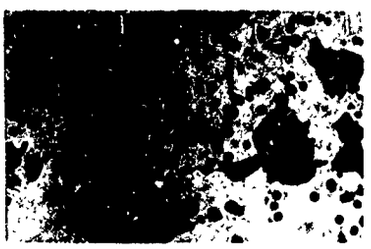

Fig.7 Dependency of the poresize and poredistance from the porosity at constant grainsize $G \sim 6.1 \mu m$

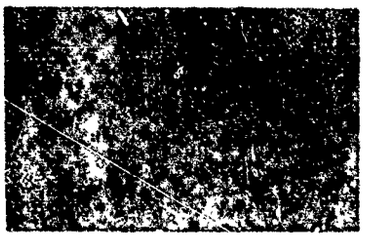

$G = 1.54\ \mu m$

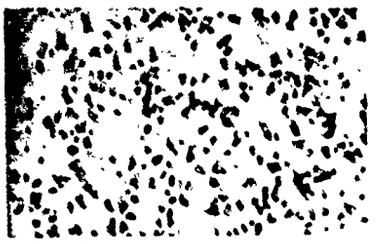

$G = 6.03\ \mu m$

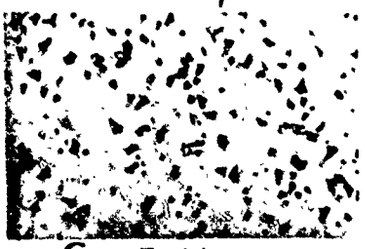

$G = 7.44\ \mu m$

$G = 10.97\ \mu m$

$G = 12.7\ \mu m$

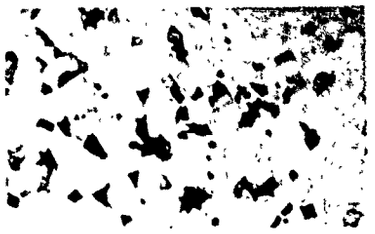

$G = 17.1\ \mu m$

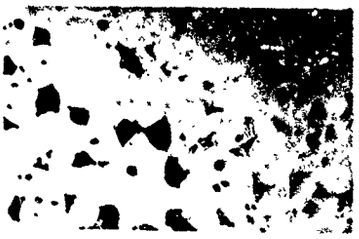

$G = 20.0\ \mu m$

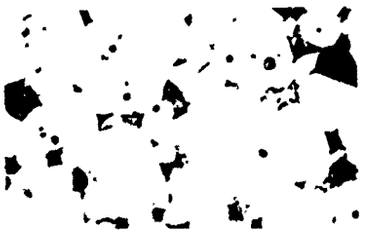

$G = 33.3\ \mu m$

For comparison $G = 12.3\ \mu m$
$= 1.27\%$

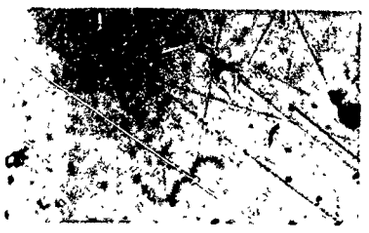

Fig.8 Dependency of the poresize and poredistance from the grainsize at constant porosity $p \sim 5.6\%$

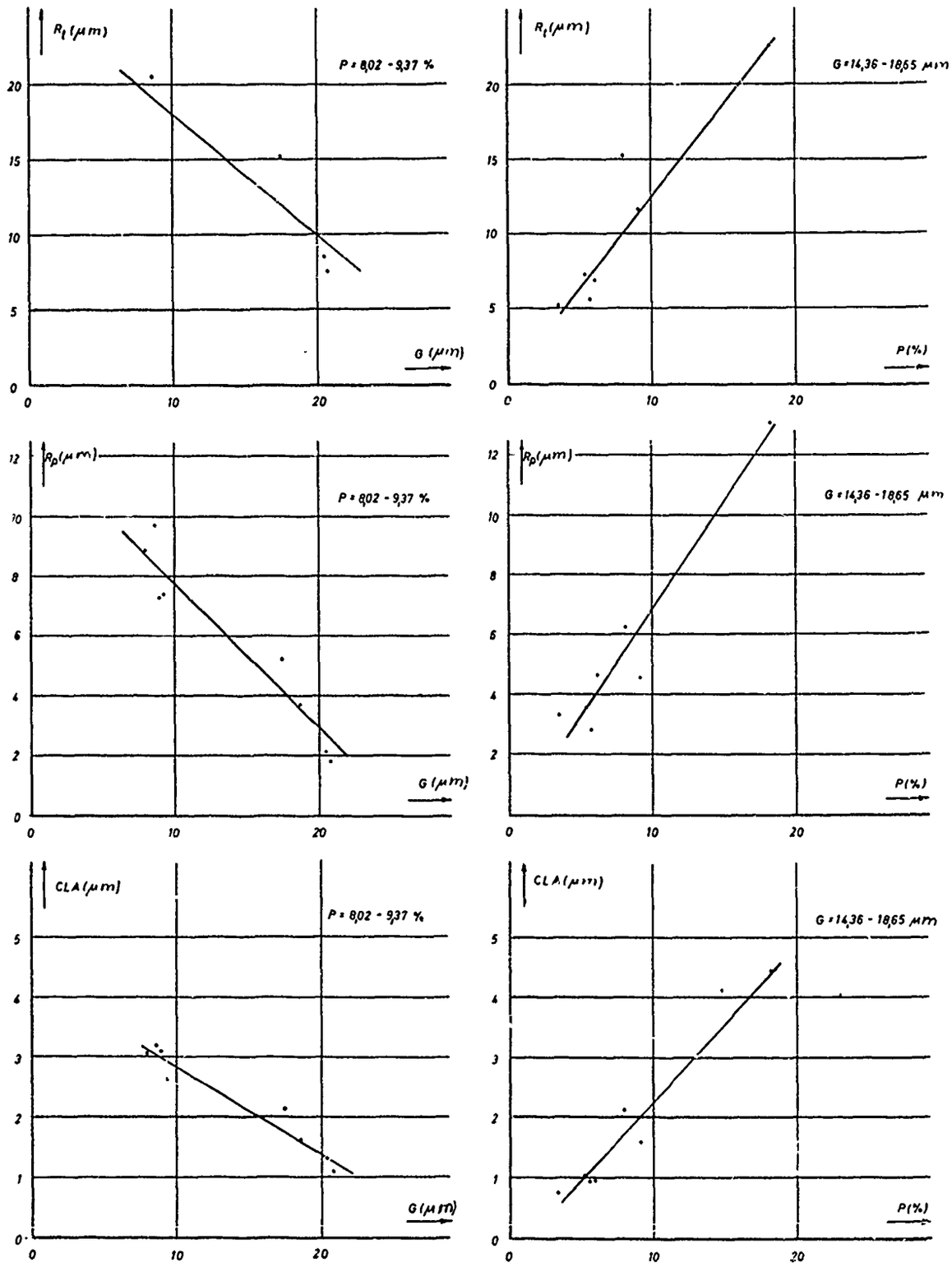

Fig.9 Dependency of the "Rauhtiefe" R_t, "Glättungstiefe" R_p and the Center-Line-Average CLA from the grainsize and the porosity of 4 mm diameter Degussit Al_2O_3 specimens

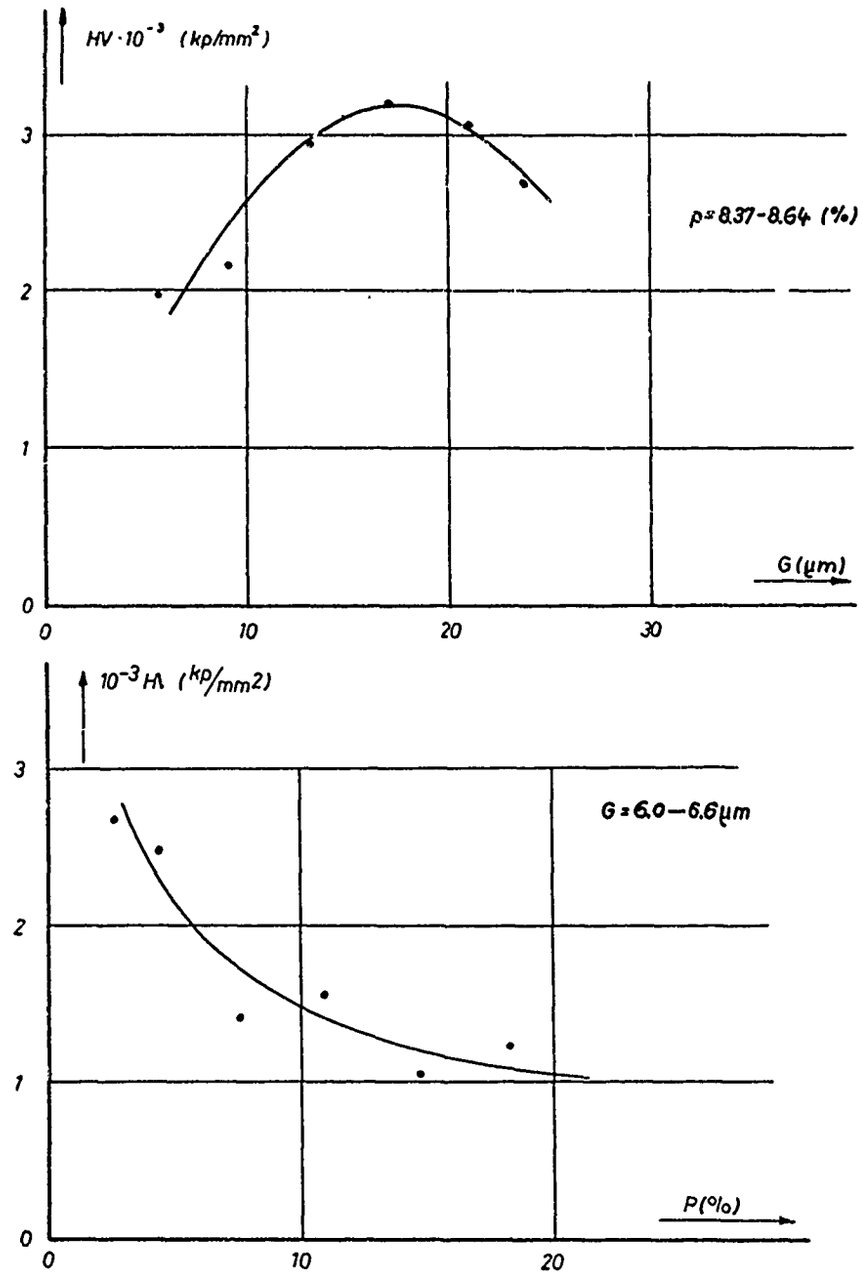

Fig.10 Dependency of the Vickers-micro-hardness on the grainsize and the porosity of 4 mm Ø Degussit Al_2O_3 round bar specimens.
(The points are the arithmetic mean values of 10 hardness tests on one cross-section)

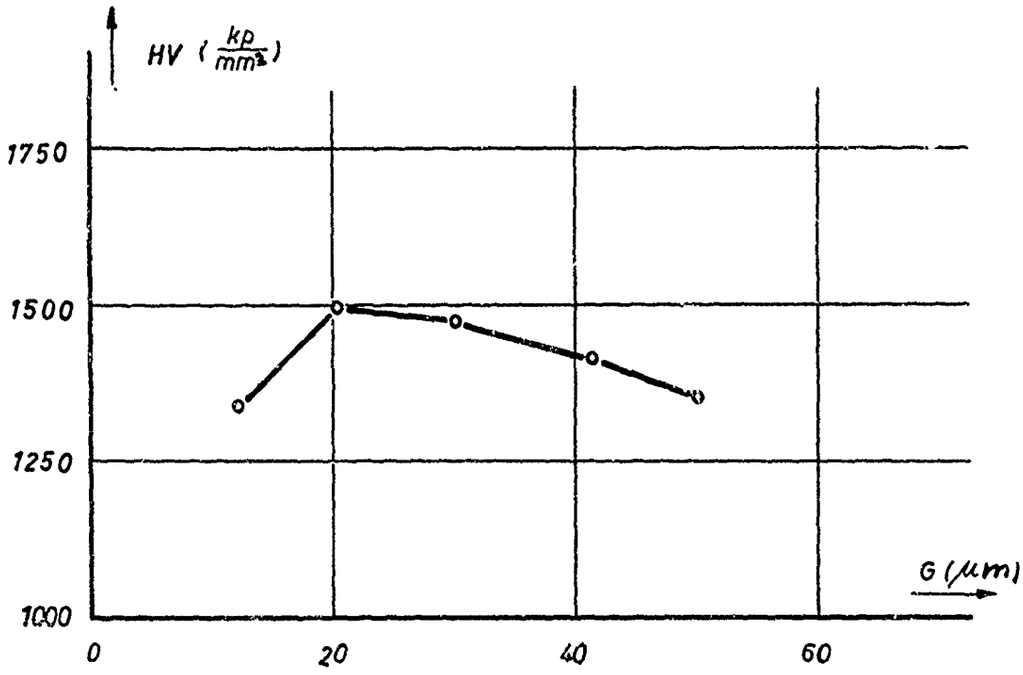

Fig.11 Dependency of the Vickers-hardness from the size of single grains of a Wesgo Al 995 rod 6 mm Ø, porosity 3.7%. (The points are the arithmetic mean values of 10 tests)

Fig.12 Vickers-impression on an Alumina specimen. Pressure of the diamond pyramid 94 p. Magnification 1400 x

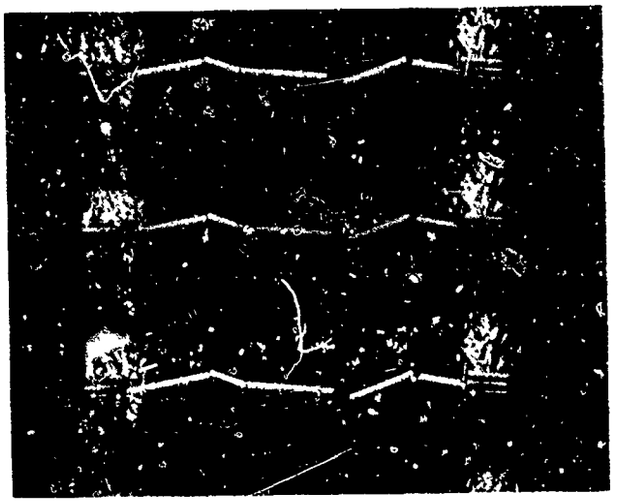

Fig.13 Broken pieces of an Alumina rod photographed shortly after a bending test with a Hitachi high speed motion camera (Picture taking rate: 10 000 pictures per second)

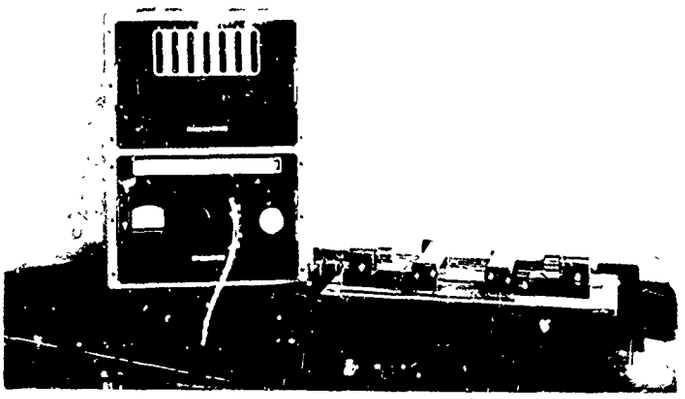

Fig.14 Förster elastomat for the determination of the damping constant δ

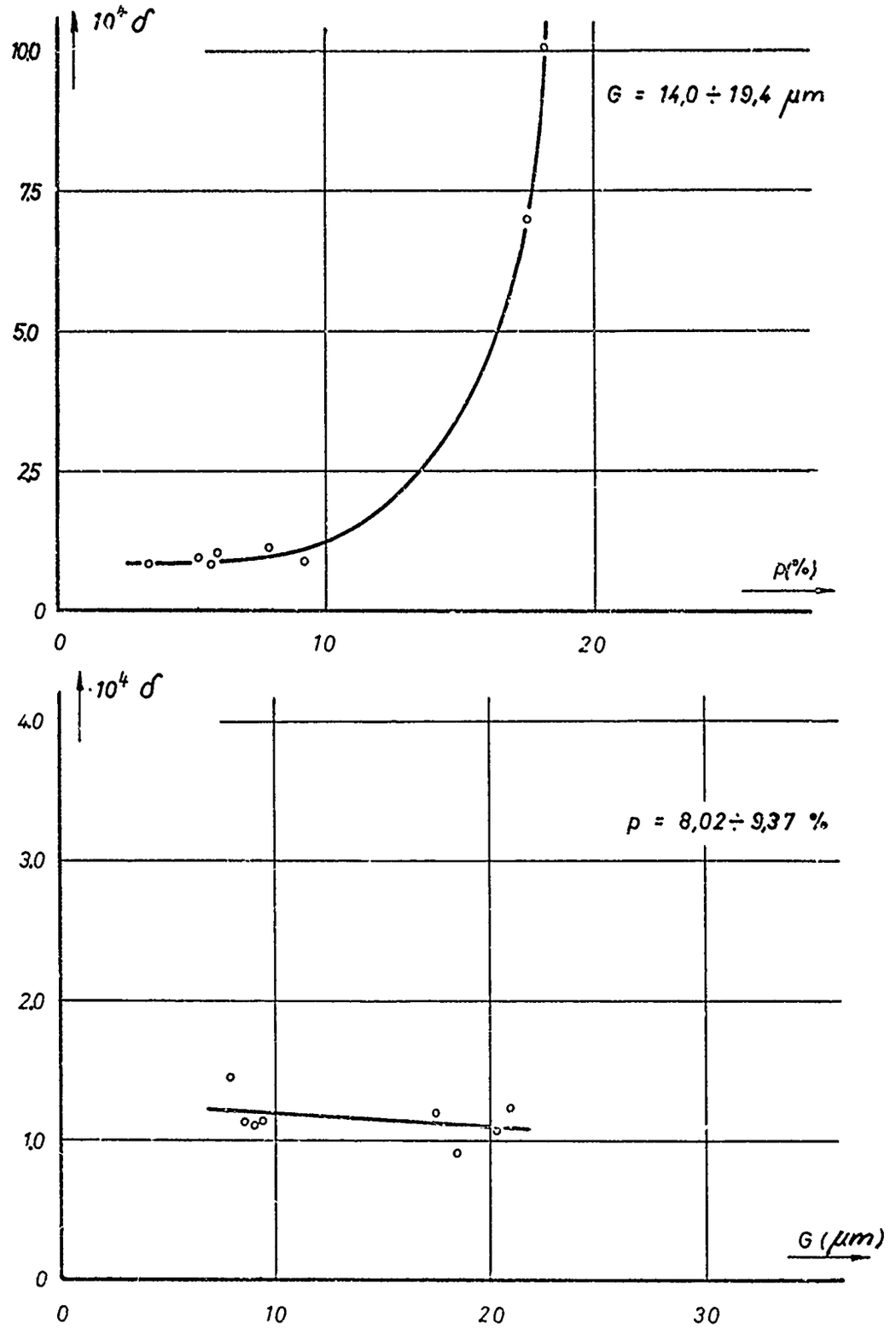

Fig.15 Variation of the damping factor of 4 mm diameter Degussit Al_2O_3 specimens with the porosity and the grainsize

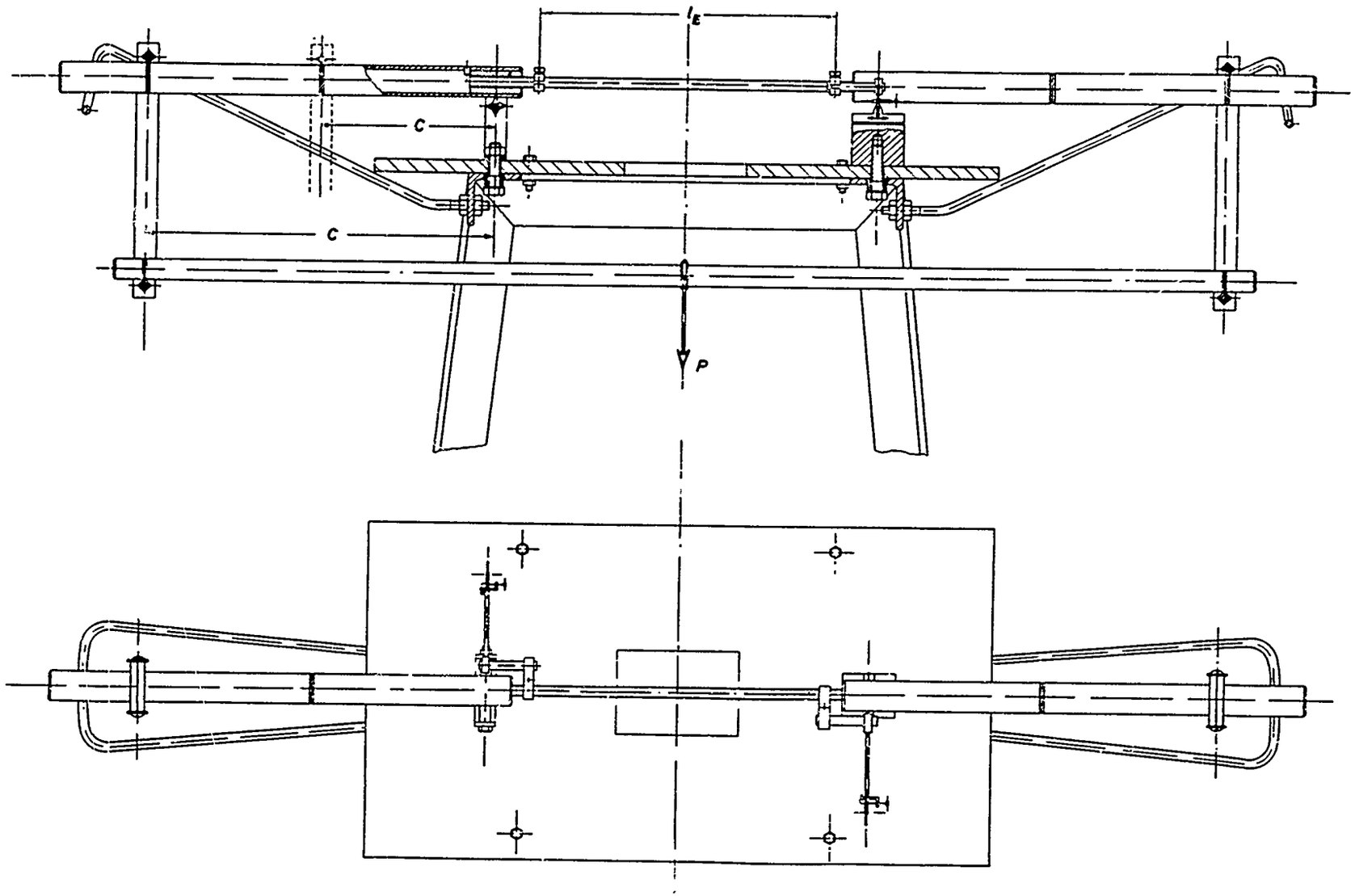

Fig.16 Bending test equipment for the determination of the fracture stress, Young's modulus and the fracture strain of Alumina at room temperature.

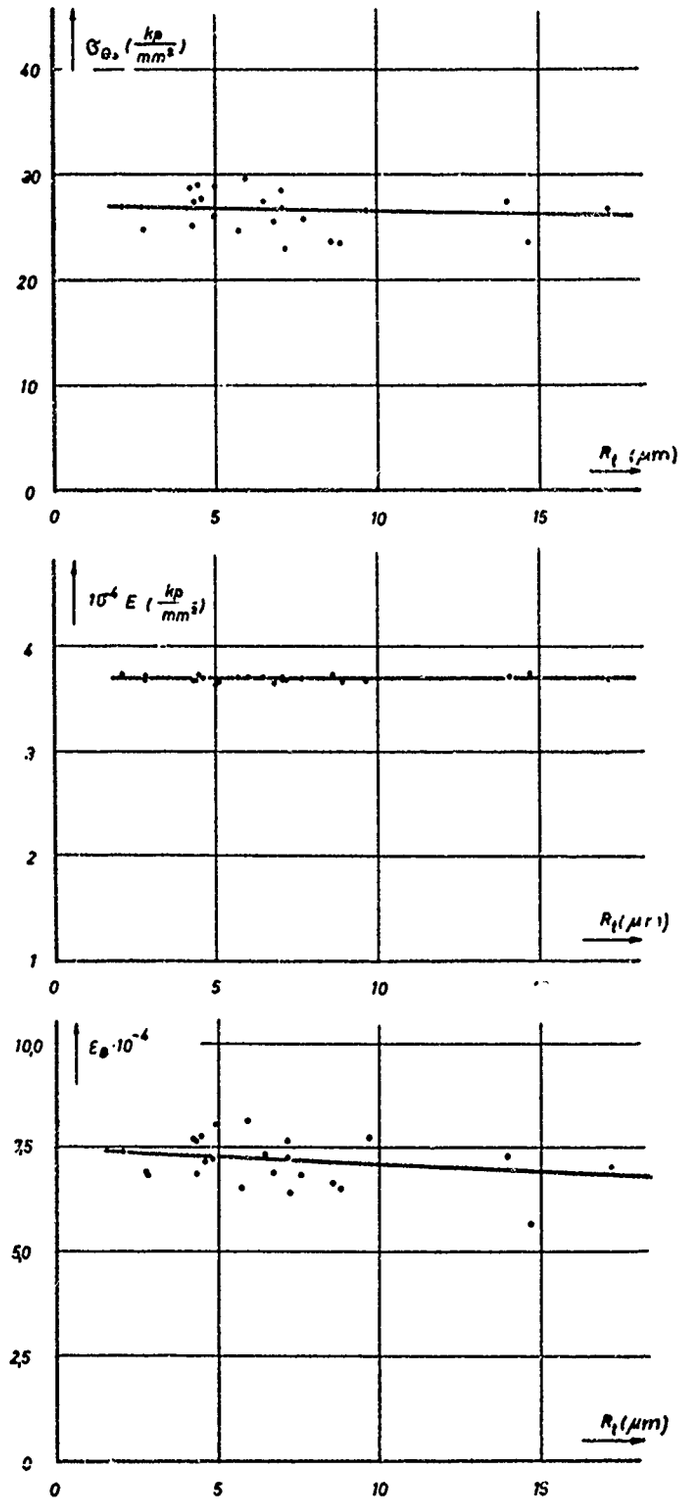

Fig.17 Dependency of the fracture stress, Young's modulus and the fracture strain from the Rauhtiefe R_t of 6 mm diameter Degussit Al_2O_3 specimens determined from a bending test (grainsize G = 9.0 µm , porosity p = 5.37%)

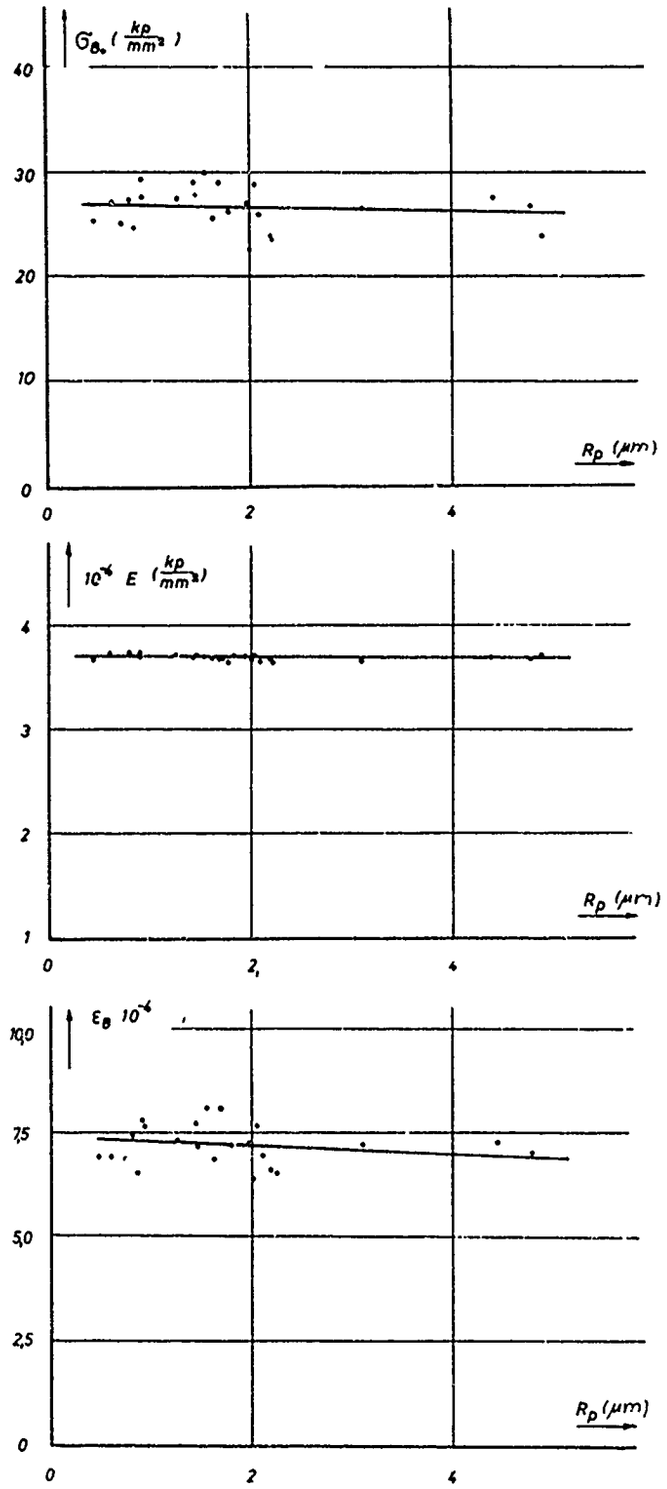

Fig.18 Dependency of the fracture stress, Young's modulus and the fracture strain from the Glättungstiefe R_p of a 6 mm diameter Degussit Al_2O_3 specimens determined from a bending test (grainsize G = 9.0 µm , porosity p = 5.37%)

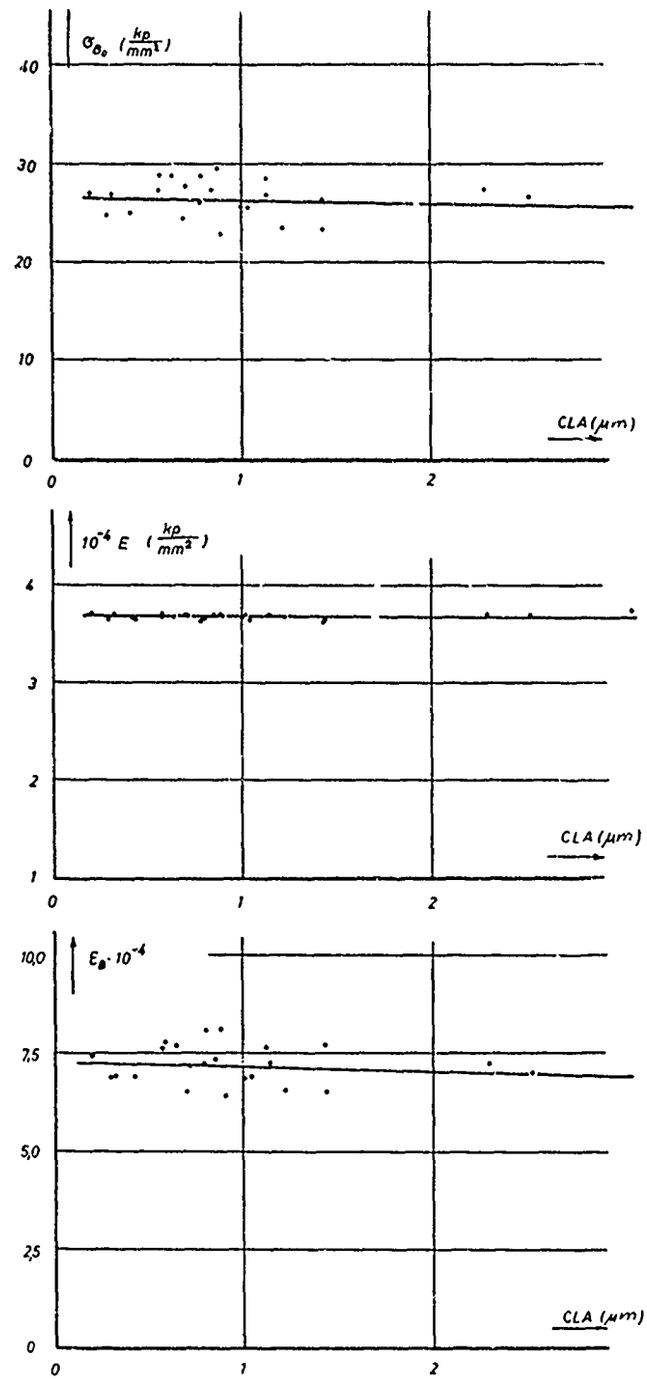

Fig.19 Dependency of the fracture stress, Young's modulus and the fracture strain from the Center-Line-Average CLA of 6 mm diameter Degussit Al_2O_3 specimens, determined from a bending test (grainsize G = 9.0 μm , porosity p = 5.37%)

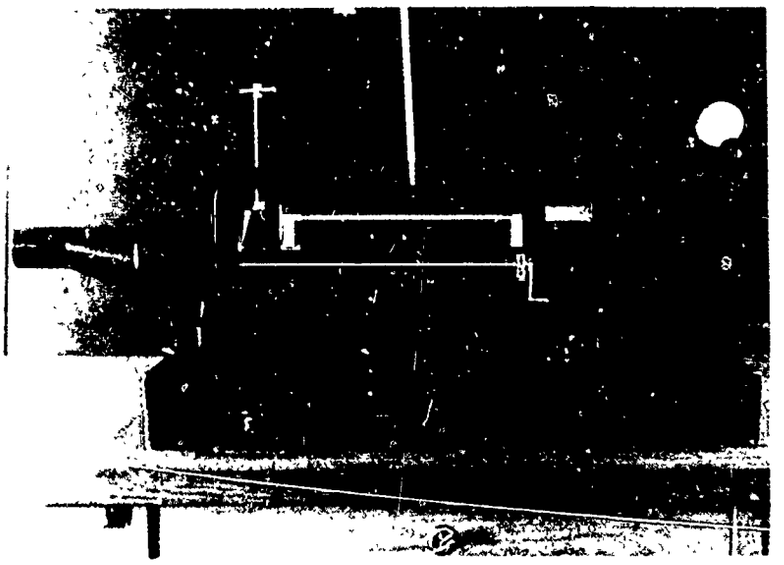

Fig.20 Measuring equipment for the determination of the residual stresses on 6 mm diameter Wesgo Al 995 specimens

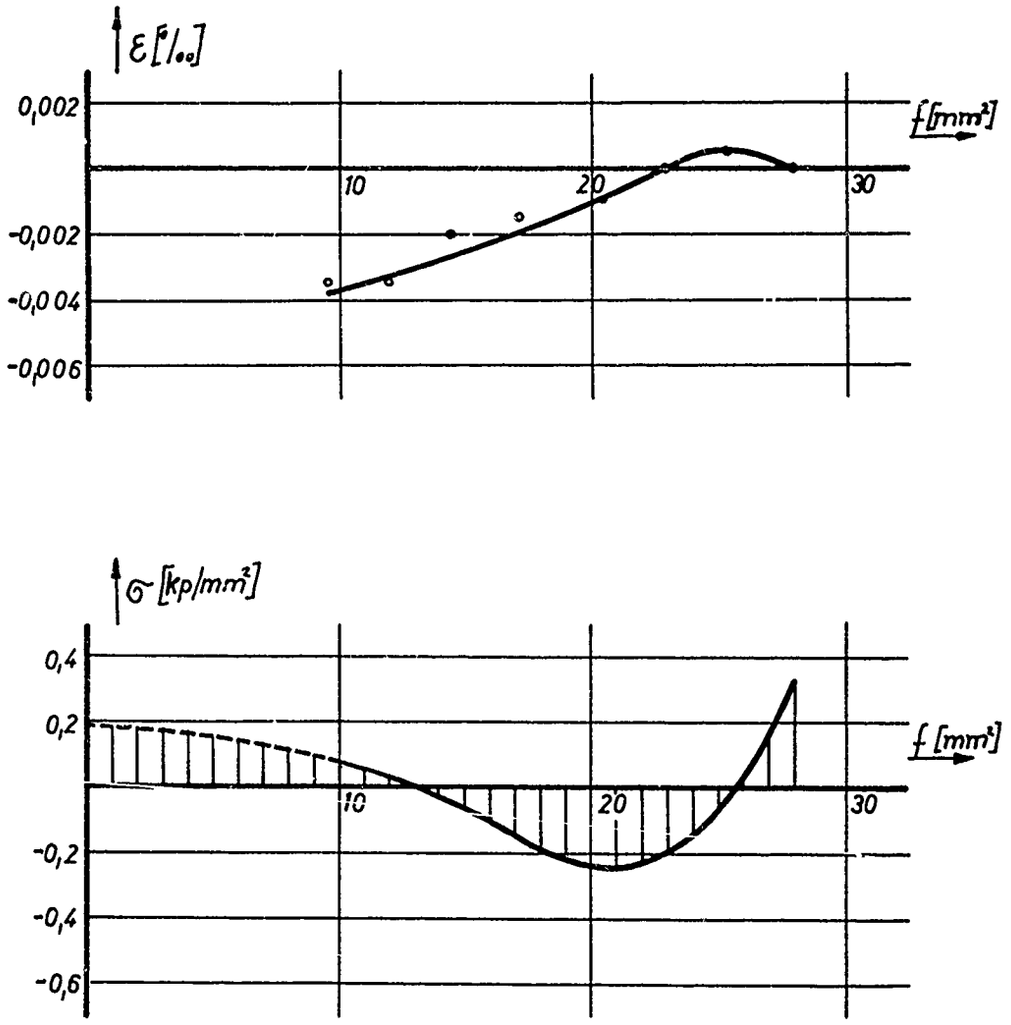

Fig.21 Strains ε plotted versus the remaining area received from the grinding off process of a 6 mm diameter Wesgo Al 995 specimen and distribution of the residual stress over the cross-section f determined from the above diagram (grainsize σ = 17.2 μm , porosity p = 3.99%)

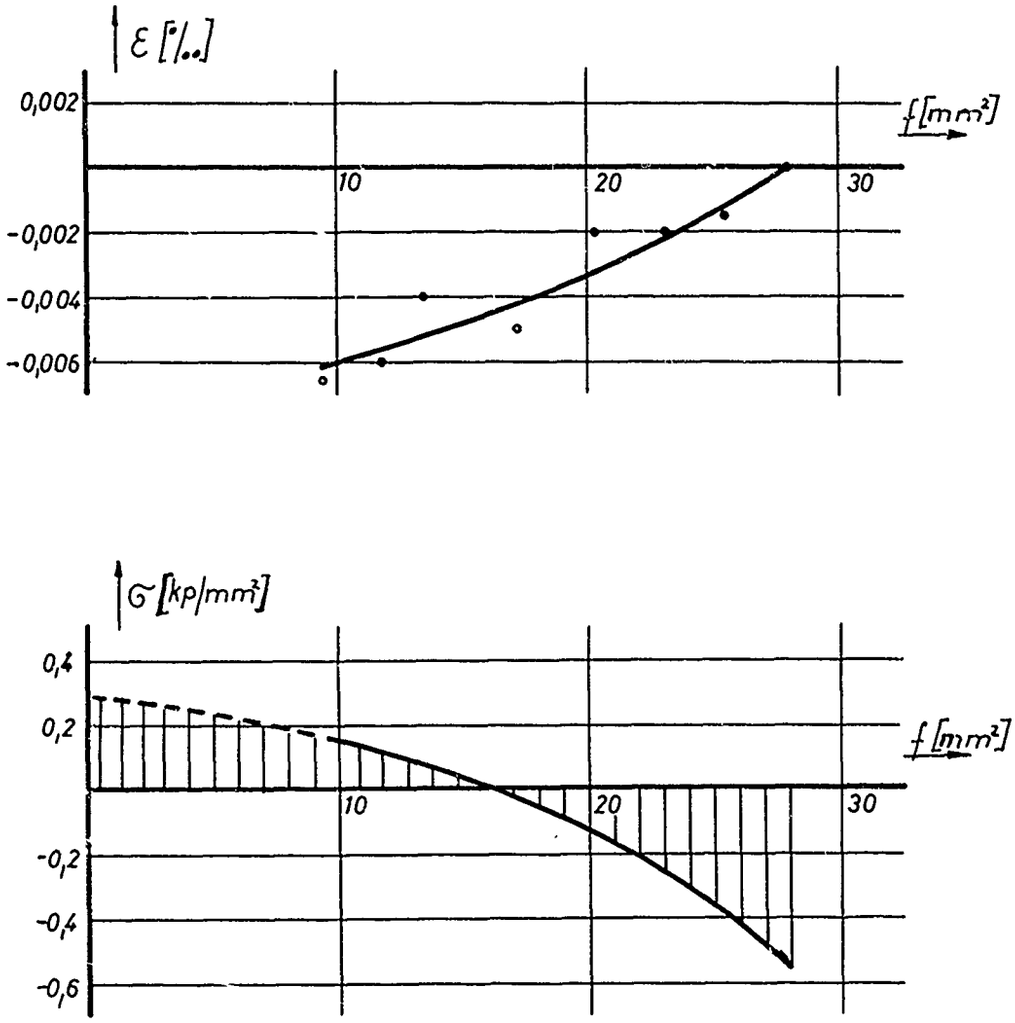

Fig.22 Strains ε plotted versus the remaining area received from the grinding off process of a 6 mm diameter Wesgo Al 995 specimen and distribution of the residual stress over the cross-section f determined from the above diagram (grainsize G = 16.5 μm , porosity p = 4.08%)

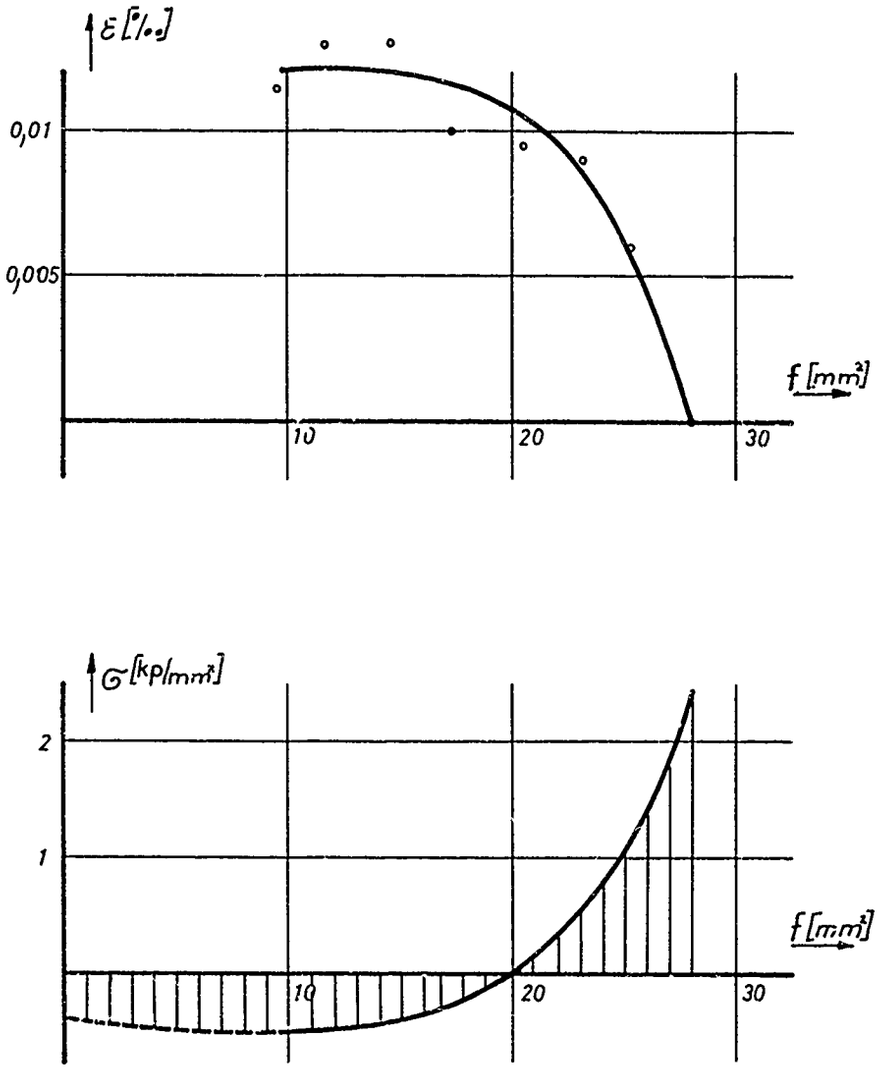

Fig.23 Strains ε plotted versus the remaining area received from the grinding off process of a 6 mm diameter Wesgo Al 995 specimen and distribution of the residual stress over the cross-section f determined from the above diagram (grainsize G = 16.4 μm , porosity p = 4.09%)

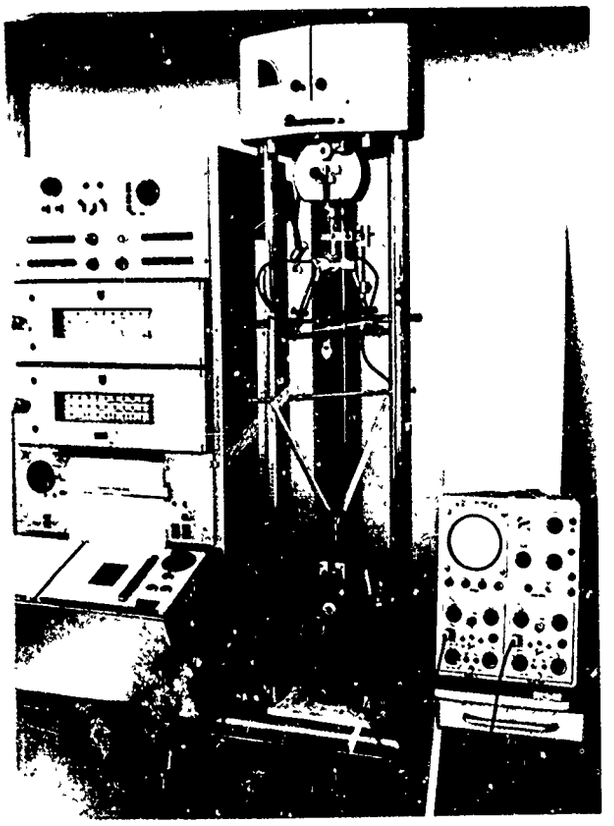

Fig.24 Test equipment for the determination of the influence of the loading speed on the fracture stress, Young's modulus and the strain at fracture

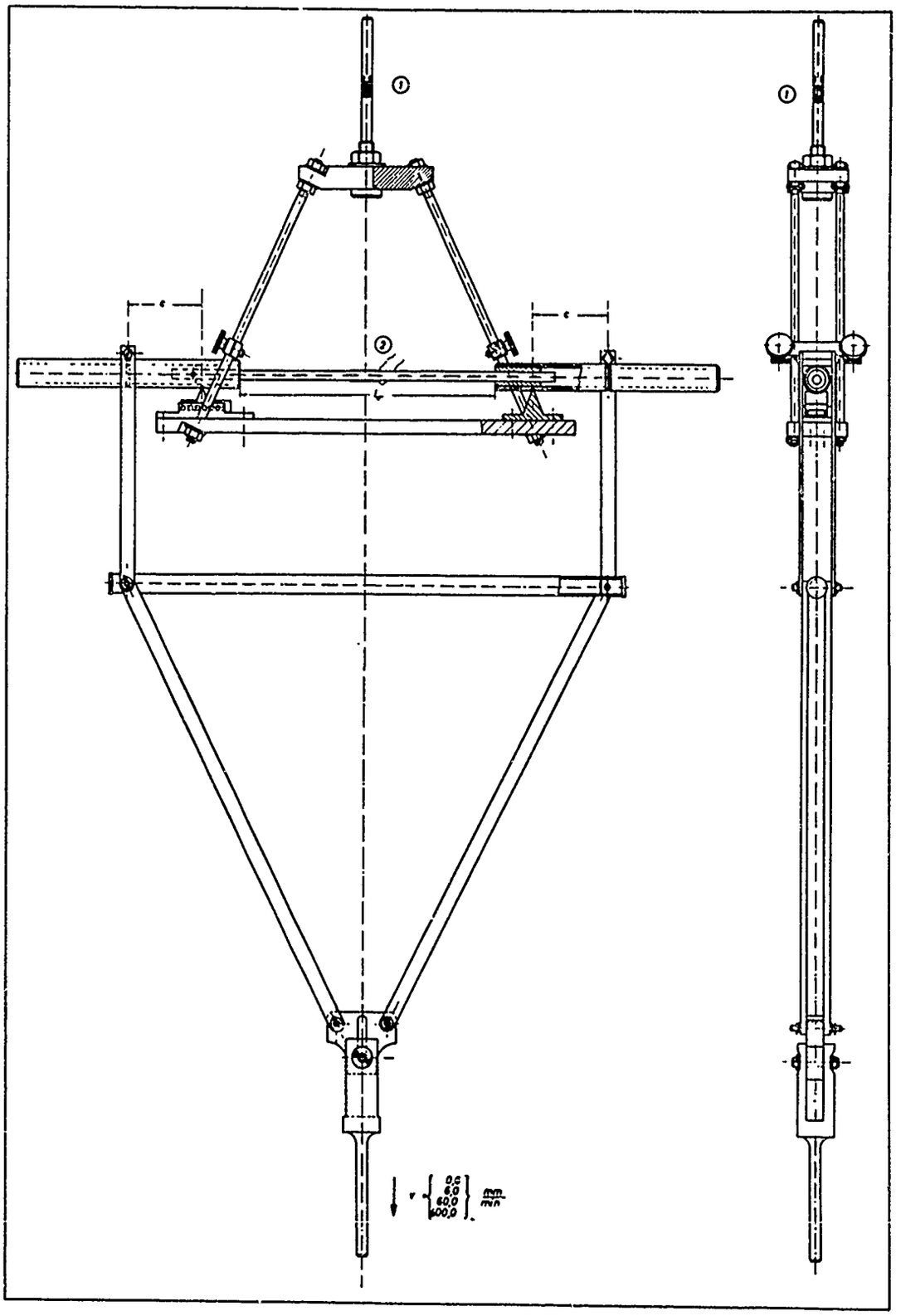

Fig.25. Bending test equipment for the determination of the influence of the loading speed on the fracture stress, Young's modulus and the strain of fracture

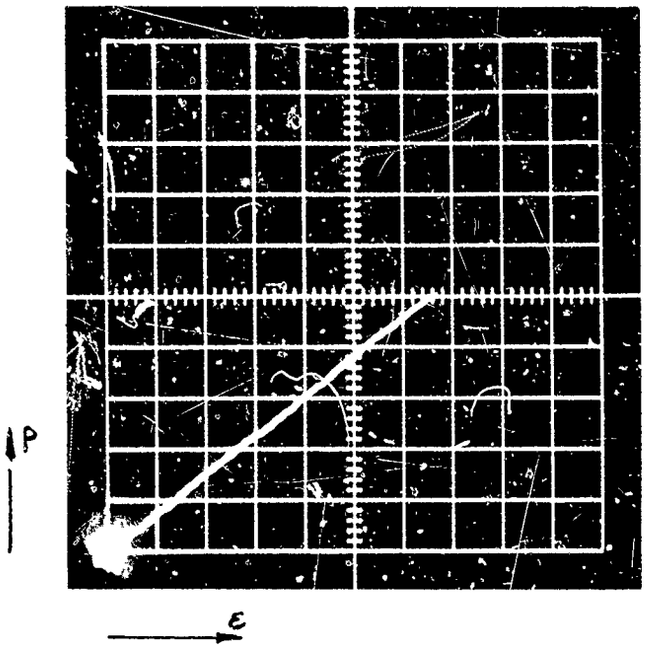

Fig.26a Load-strain diagram

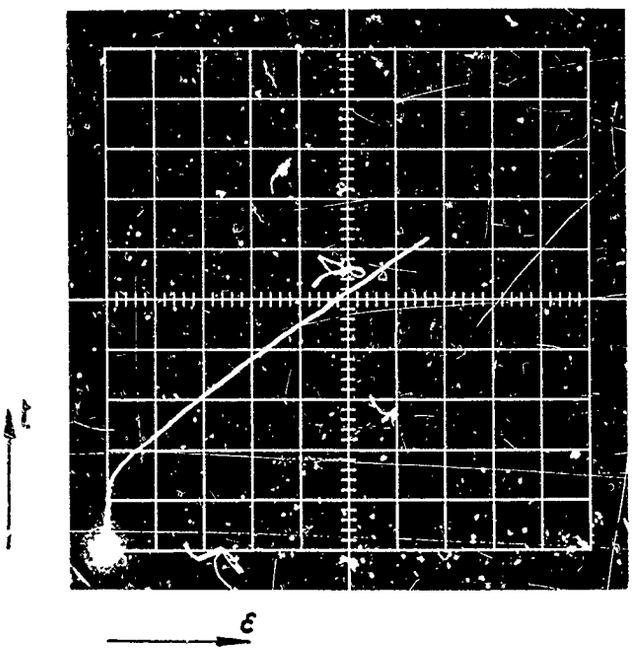

Fig.26b Time-strain diagram

Photographs of a bending test taken on Tektronix cathode ray oscillographs. Crosshead speed of the Zwick electronic tension test machine 600 mm/minute.

Fracture load P = 21.92 kp, fracture strain ε_B = 0.686‰, time t = 0.0345 sec. per unit.

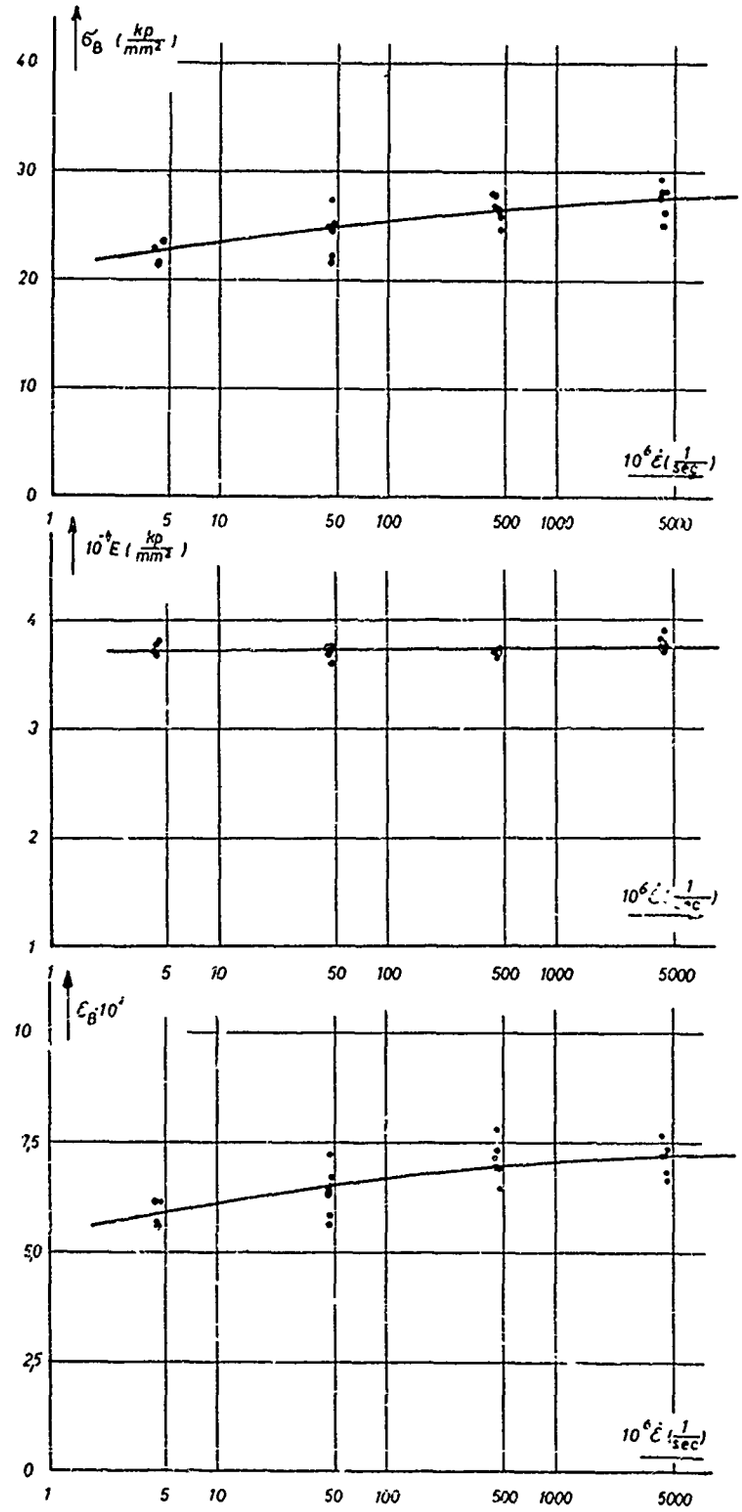

Fig.27 Dependency of the fracture stress, Young's modulus and the strain at fracture from the strain rate of 6 mm diameter Wesgo Al 995 specimens determined from a bending test at room temperature

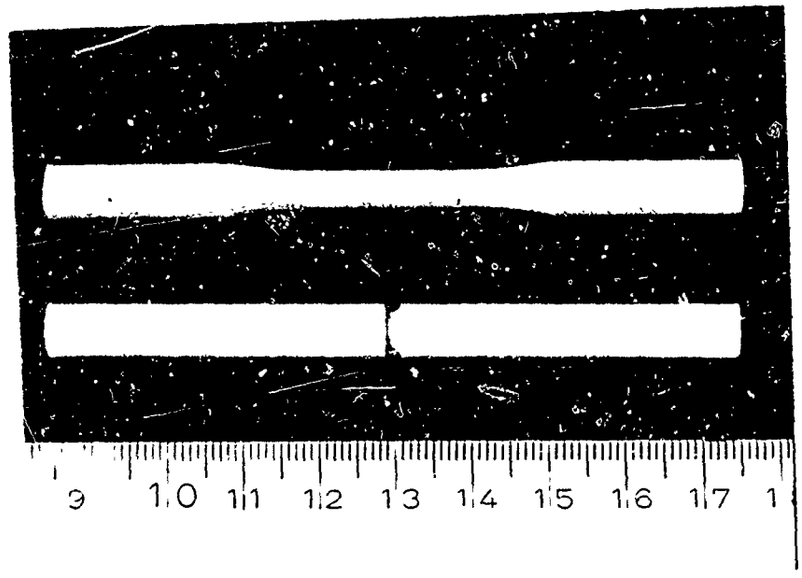

Fig.28 Degussit Al_2O_3 specimen for alternating bend fatigue tests (residual diameter 5 mm, notch root radius 1 mm)

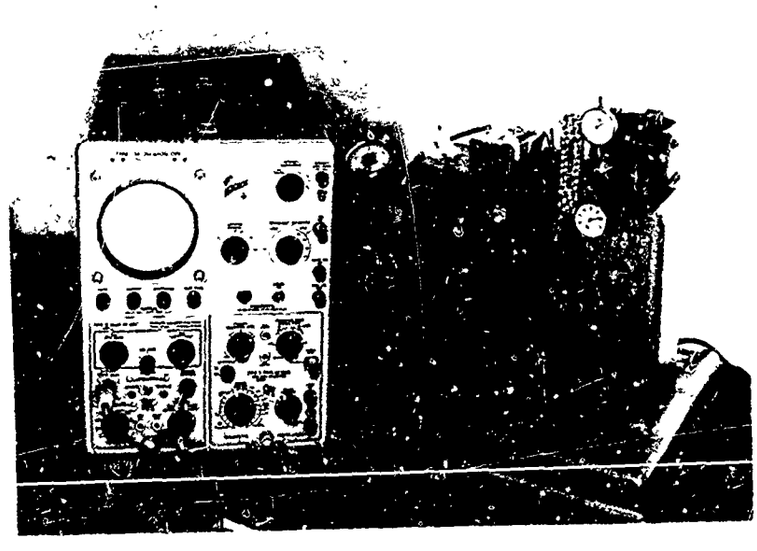

Fig.29 Schenck-Webi fatigue test machine and Tektronix cathode ray oscilloscope

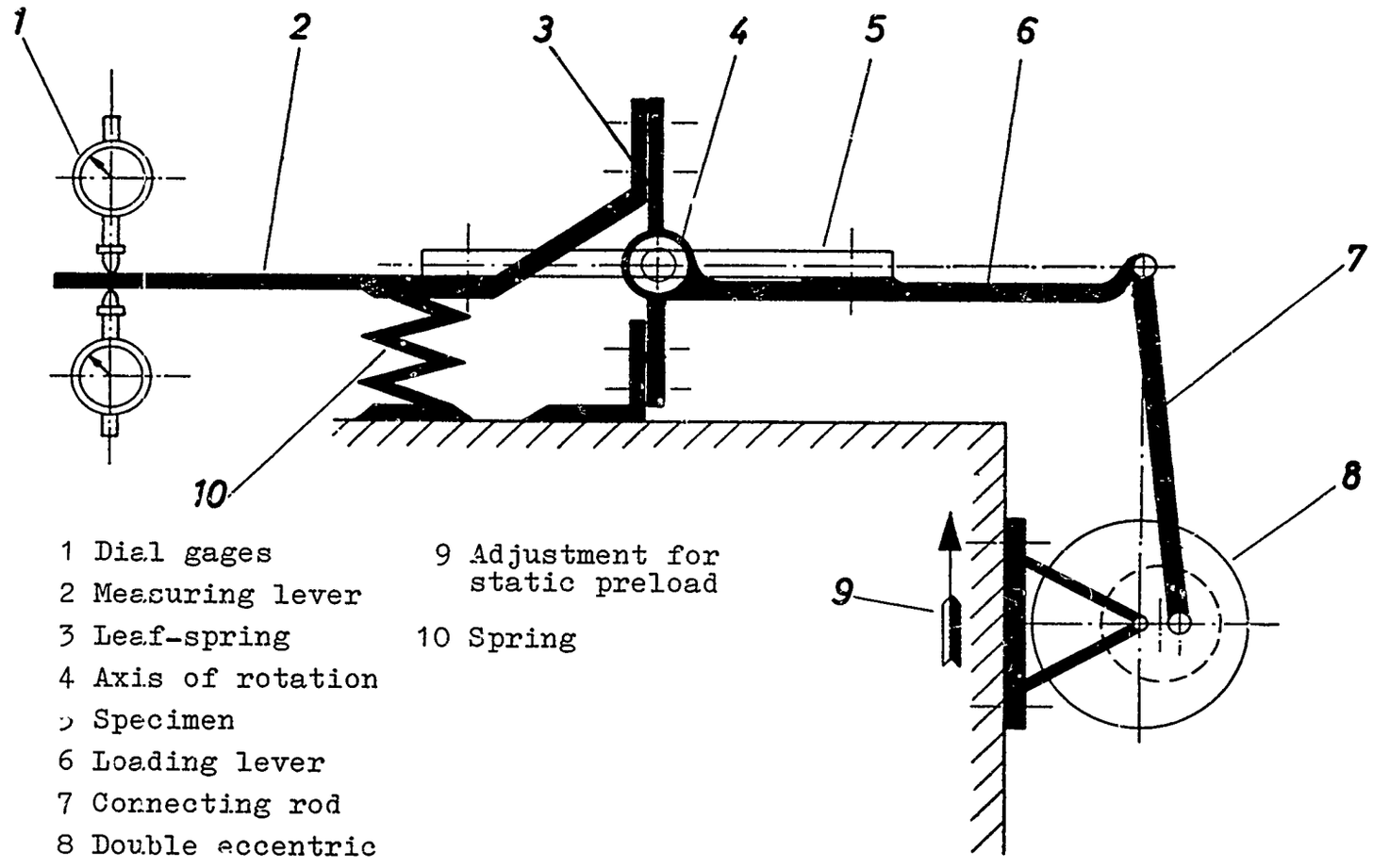

Fig.30 Scheme of the Schenck-Webi fatigue test machine

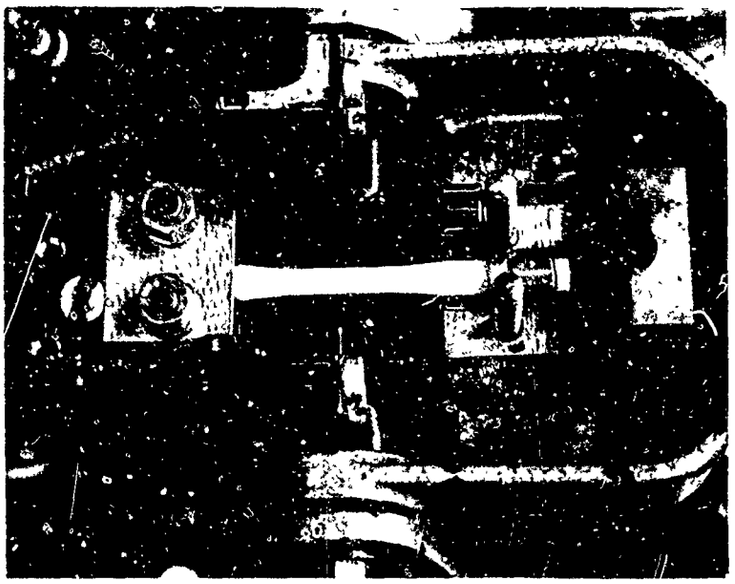

Fig.31 Clamping device for alternating bend fatigue tests

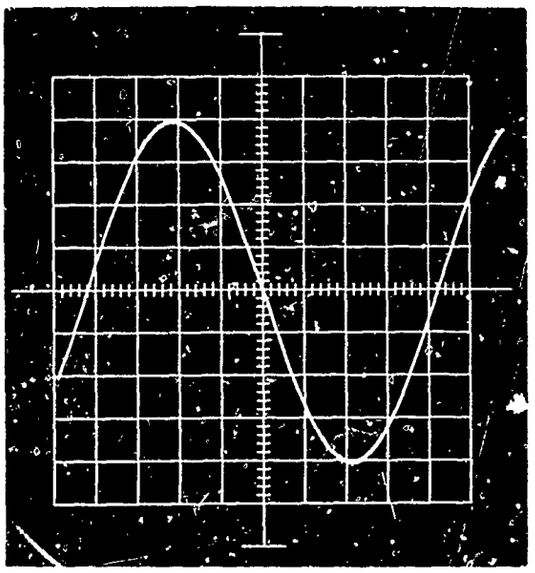

Fig.32 Vibration of a specimen mounted in a Schenck-Webi fatigue test machine (strain amplitude ~ 0.41‰, frequency 1495 cpm)

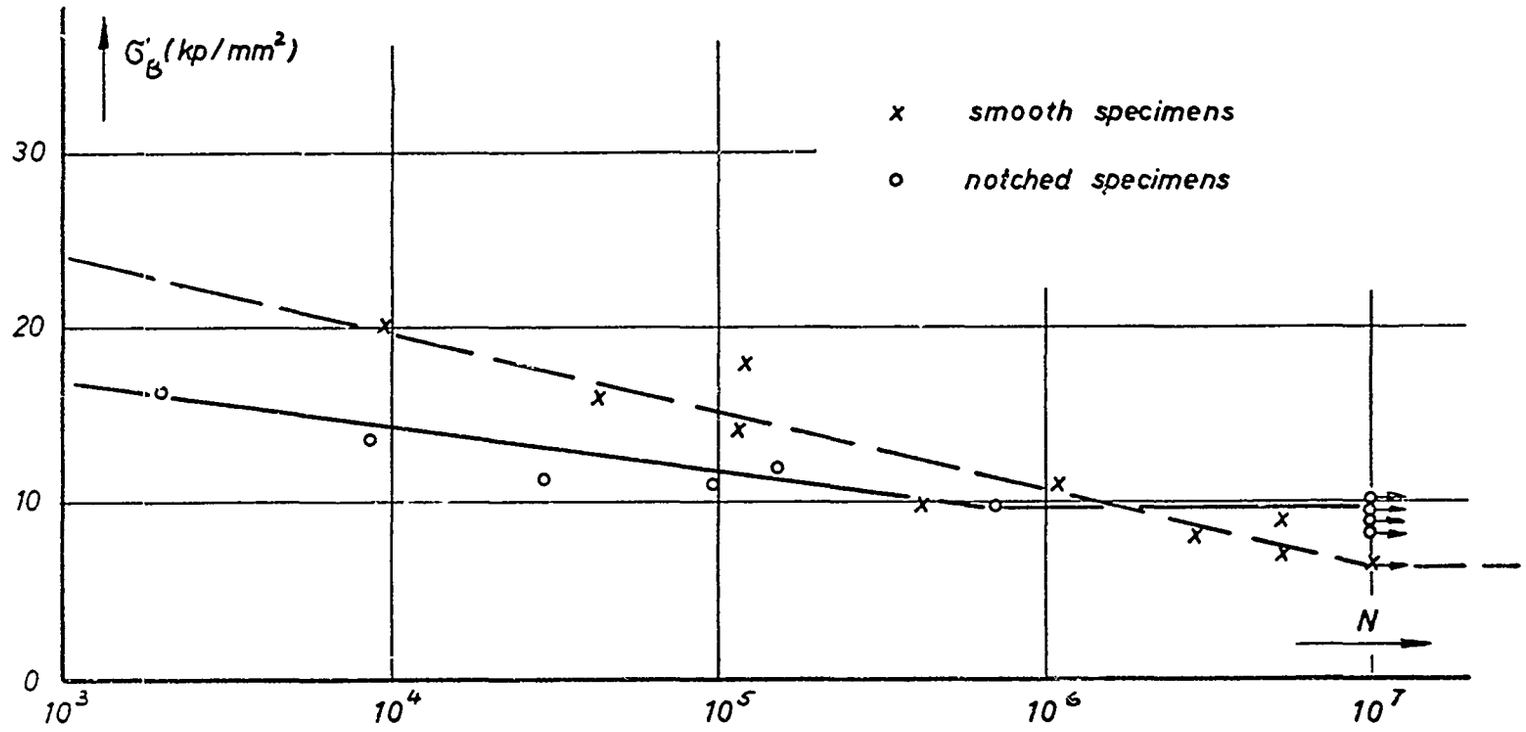

Fig.33 Dependency of the fracture stress of smooth and notched Wesgo Al 995 specimens from the numbers of cycles to fracture, determined from an alternating bend fatigue test at room temperature (diameter d = 5 mm, notch root radius ϱ = 1mm, theoretical notch strength ratio $\bar{\alpha}$ = 1.54, average grainsize $G \sim 20.3\,\mu m$, average porosity p = 3.68%)

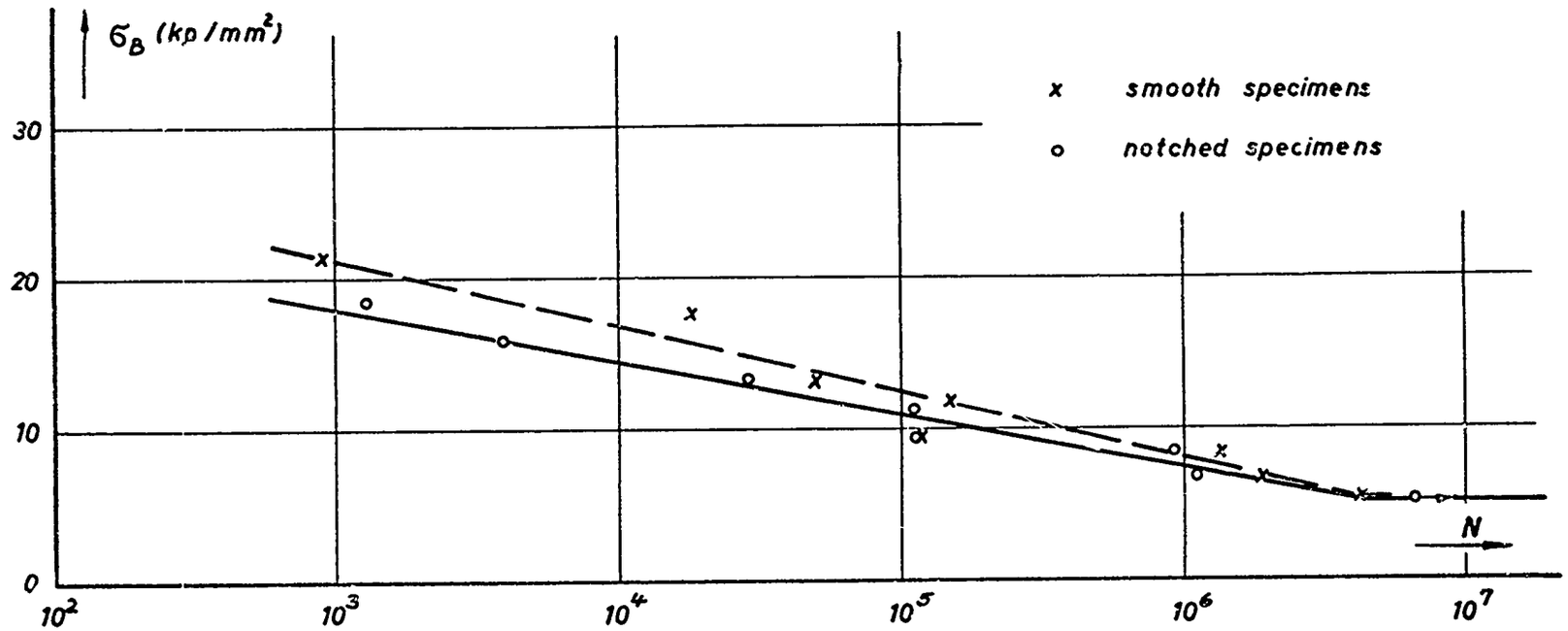

Fig.34 Dependency of the fracture stress of smooth and notched Degussit Al 23 specimens from the numbers of cycles to fracture, determined from an alternating bend fatigue test at room temperature (diameter d = 5 mm, notch root radius ϱ = 1 mm, theoretical notch strength ratio $\bar{\alpha}$ = 1.54, average grainsize $G \sim 21\,\mu m$, average porosity $p \sim 3.90\%$)

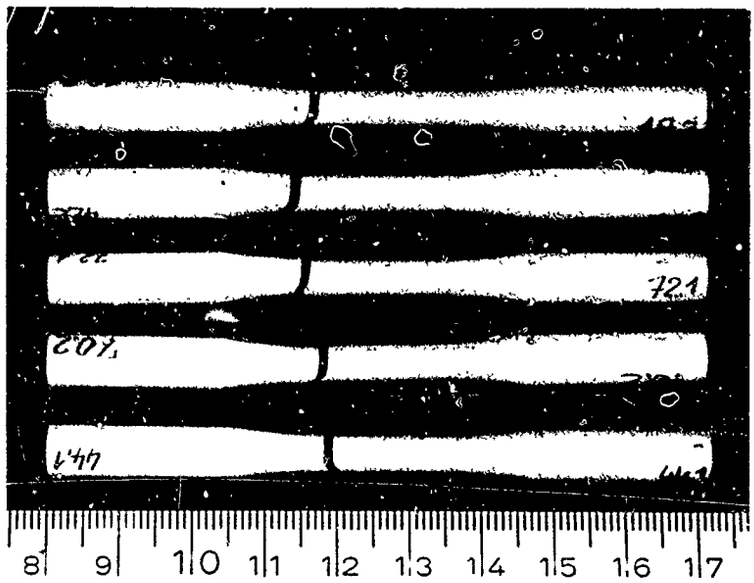

Numbers of cycles to fracture

5,478,000

2,922,000

452,000

43,000

static failure

Fig.35 Fracture shapes of smooth Wesgo Al 995 specimens broken under static and cyclic loads

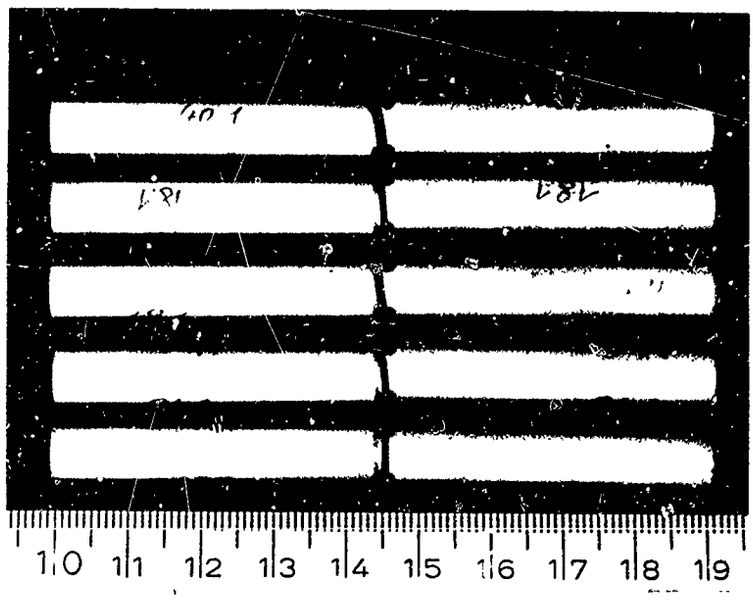

Numbers of cycles to fracture

1,162,000

155,000

29,000

2,000

static failure

Fig.36 Fracture shapes of notched Wesgo Al 995 specimens broken under static and cyclic loads

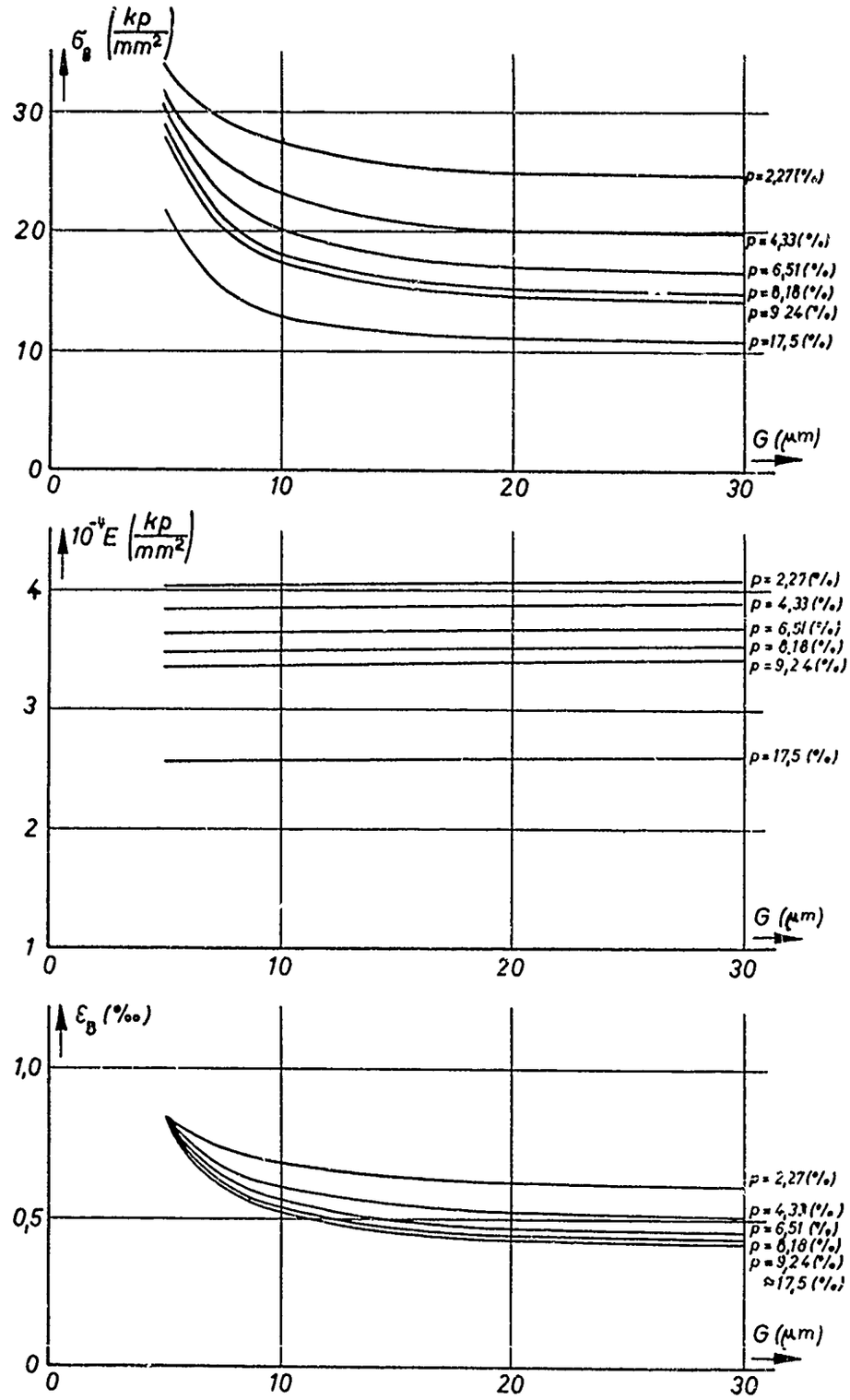

Fig.37 Dependency of the fracture stress, Young's modulus and the fracture strain from the grainsize of 4 mm diameter Degussit Al_2O_3 specimens determined from a bending test at room temperature

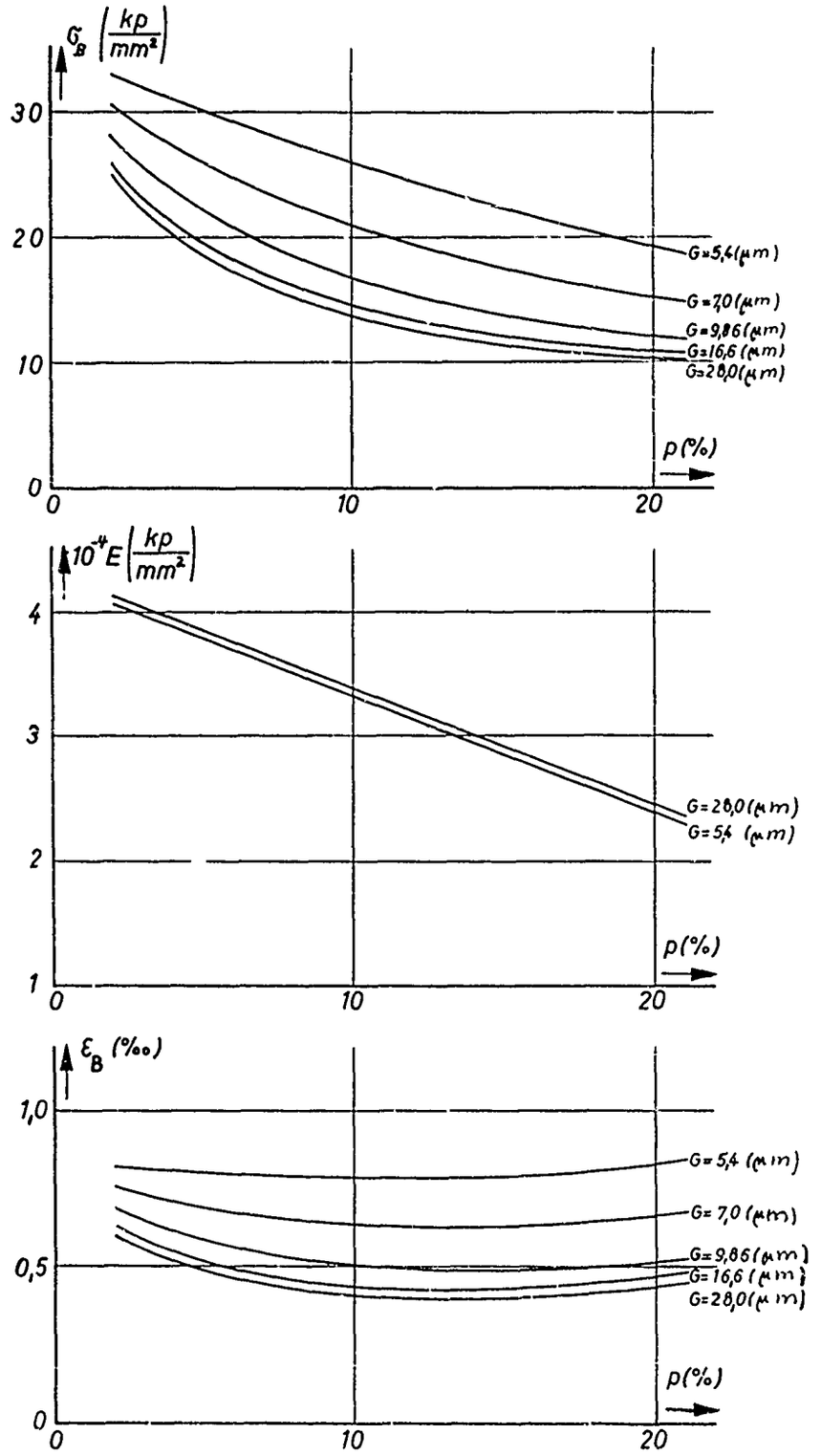

Fig.38 Dependency of the fracture stress, Young's modulus and the fracture strain from the porosity of 4 mm diameter Degussit Al_2O_3 specimens determined from a bending test at room temperature

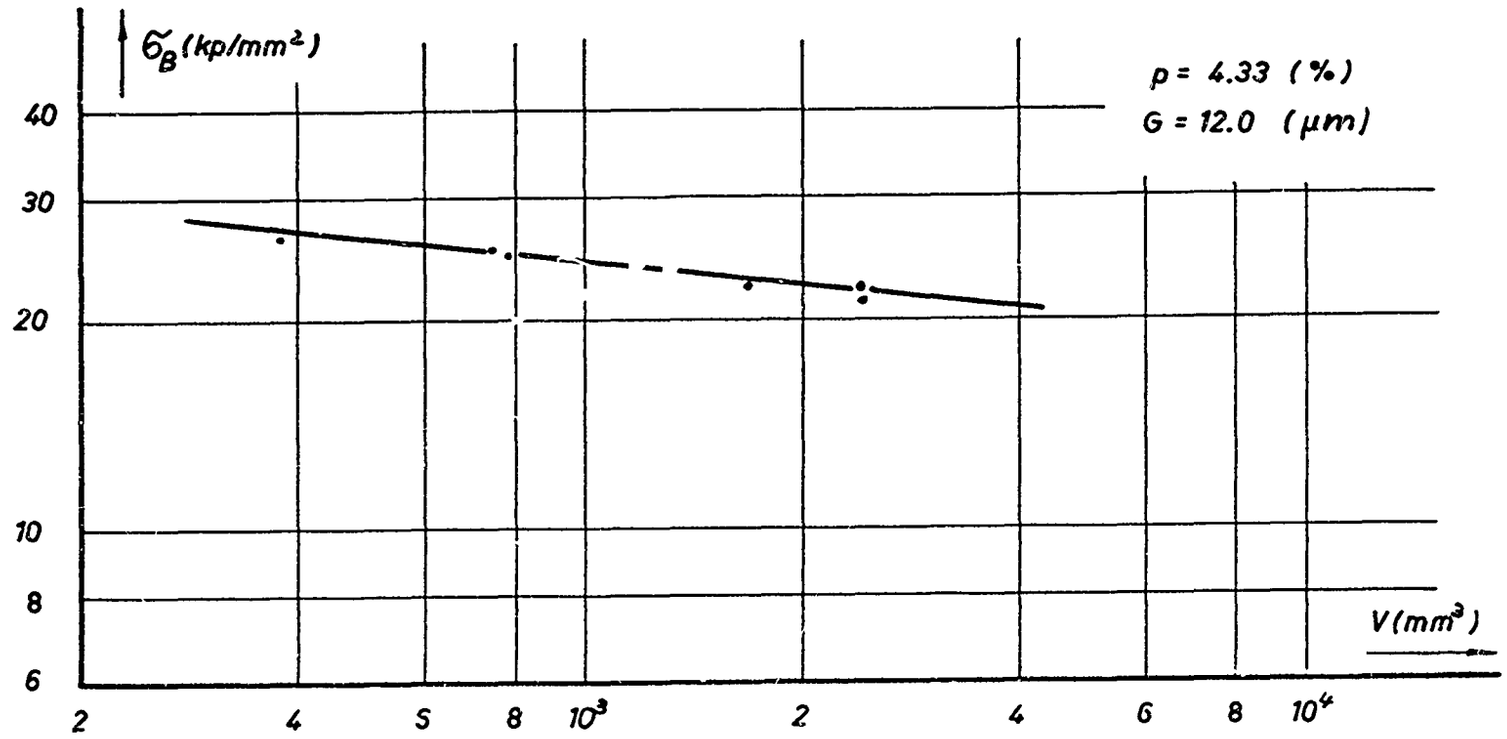

Fig.39 Dependency of the fracture stress of round bar Alumina specimens from the specimen volume, determined from a bending test at room temperature (grainsize 12.0 μm , porosity 4.33%)

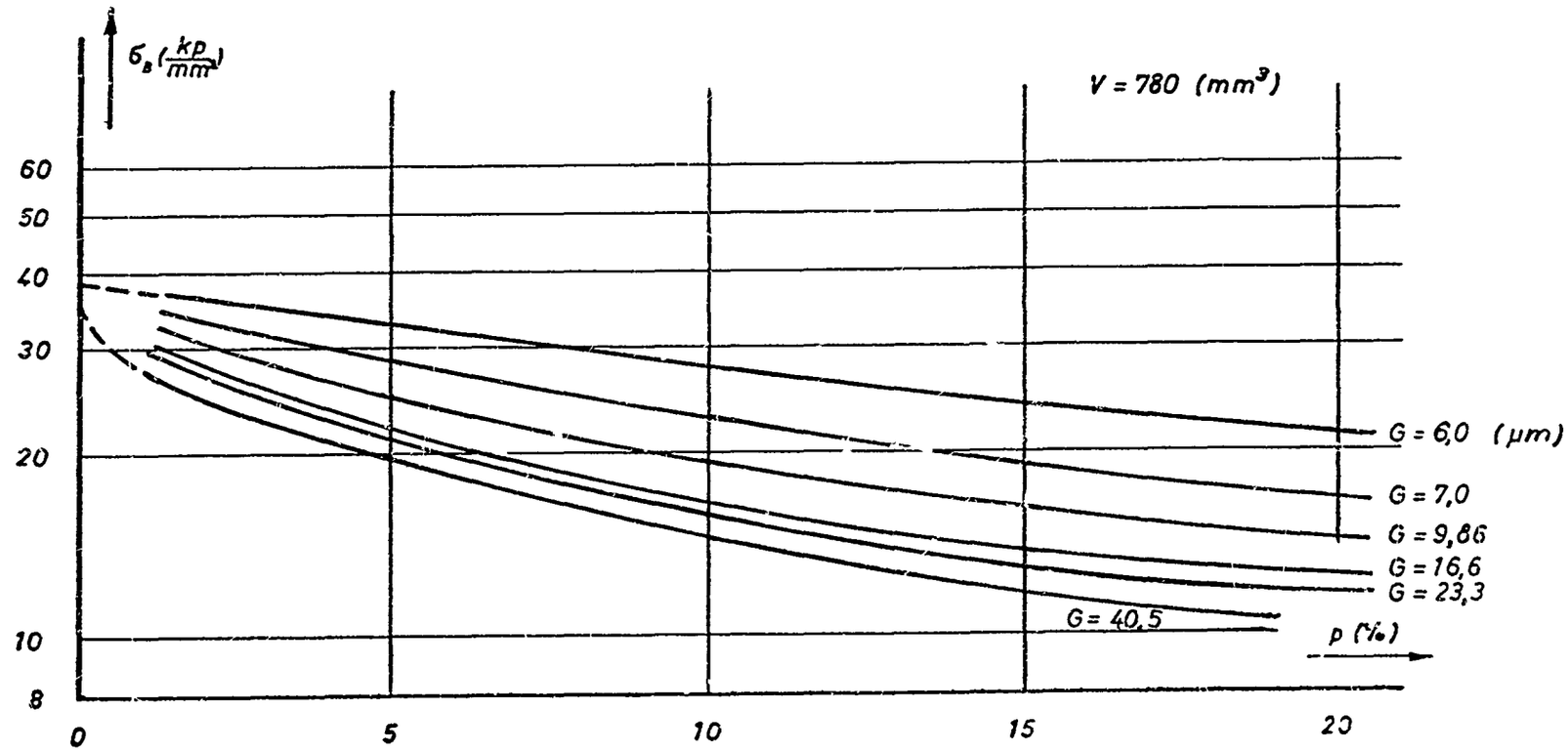

Fig.40 Dependency of the fracture stress of 4 mm Ø round bar Degussit Al_2O_3 specimens from the porosity with the grainsize as parameter. The values were determined from bending tests at room temperature

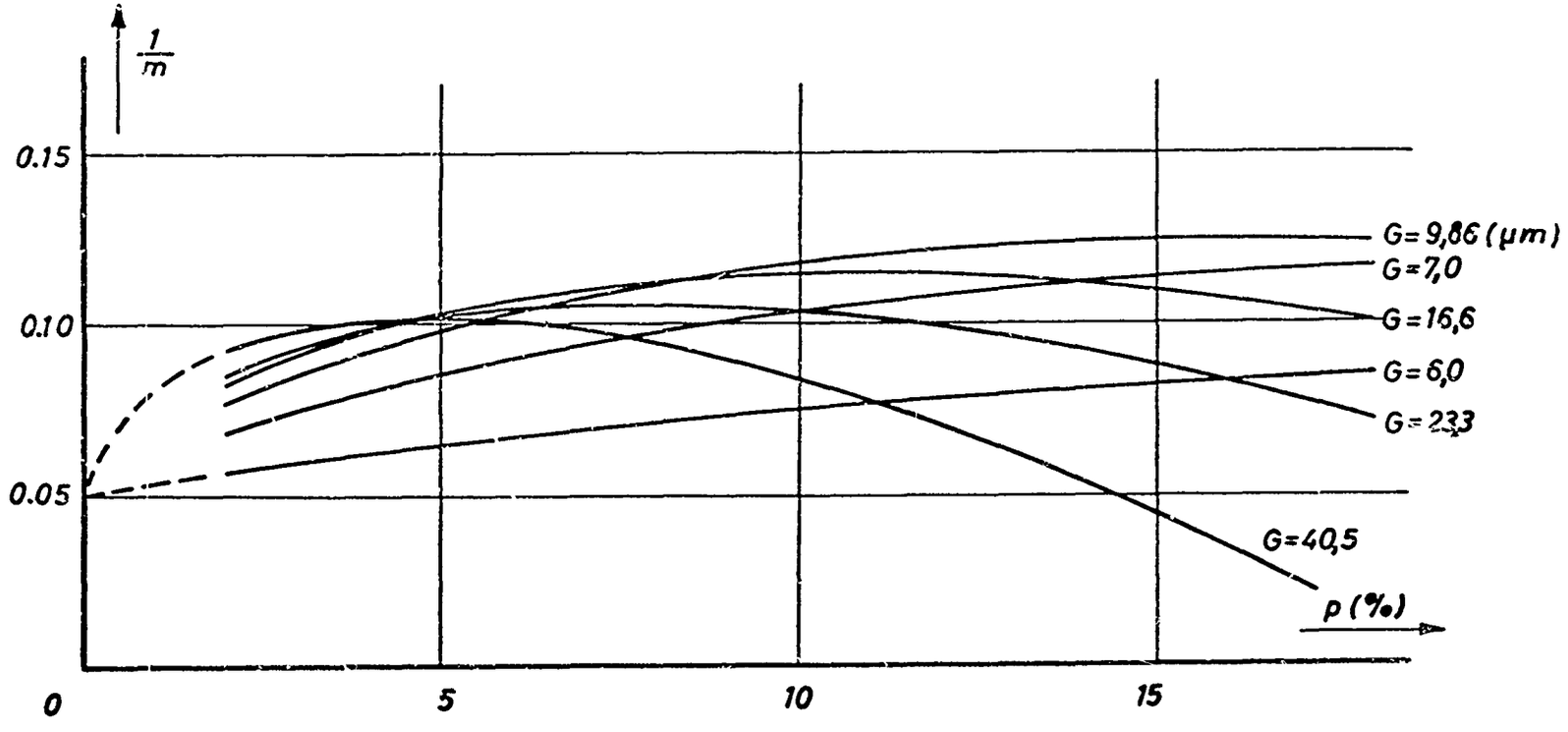

Fig.41 Dependency of the Weibull exponent $\frac{1}{m}$ from the porosity for various grainsizes

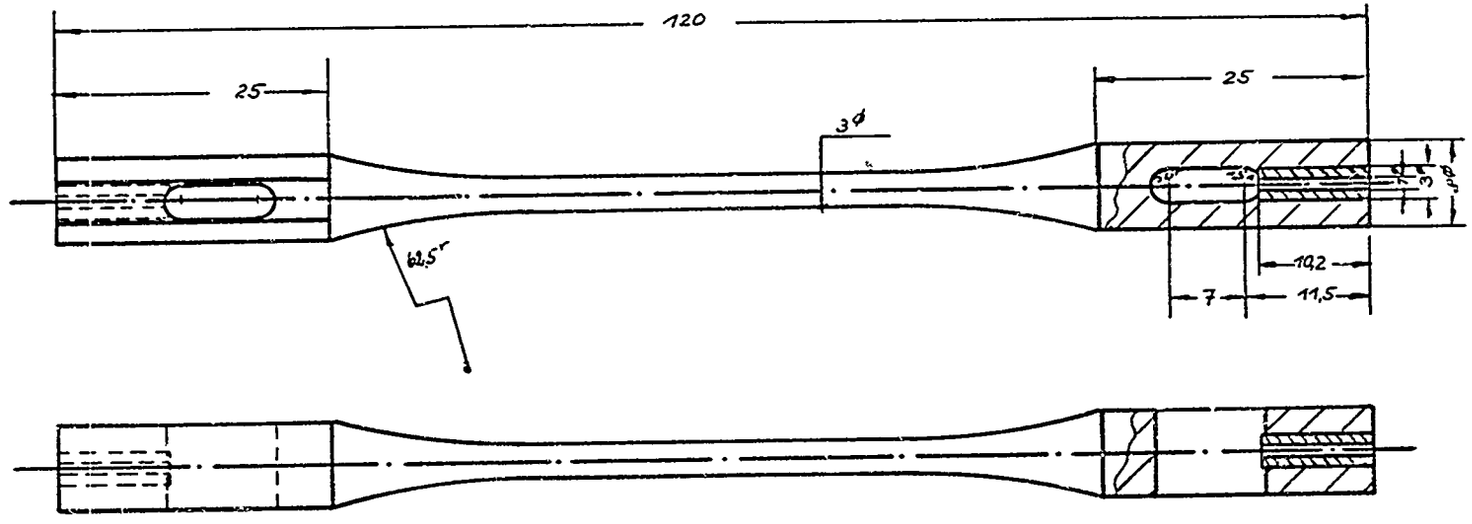

Fig.42 Specimen shape for tension tests with Alumina

Fig.43 Tension test specimen of Alumina

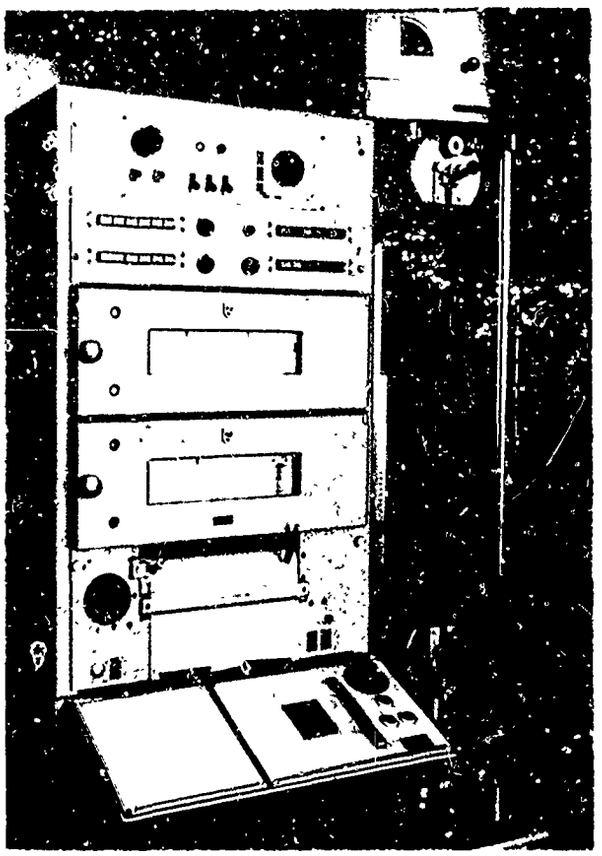

Fig.44 Complete test setup for a tension test on Alumina